

**ZERO-VOLTAGE SWITCHING BI-DIRECTIONAL  
ISOLATED LLC RESONANT DC/DC CONVERTER FOR  
WIDE VOLTAGE GAIN AND LOAD RANGE**

**S.M. SHOWYBUL ISLAM SHAKIB**

**FACULTY OF ENGINEERING  
UNIVERSITY OF MALAYA  
KUALA LUMPUR**

**2017**

**ZERO-VOLTAGE SWITCHING BI-DIRECTIONAL  
ISOLATED LLC RESONANT DC/DC CONVERTER FOR  
WIDE VOLTAGE GAIN AND LOAD RANGE**

**S.M. SHOWYBUL ISLAM SHAKIB**

**DISSERTATION SUBMITTED IN FULFILMENT OF  
THE REQUIREMENTS FOR THE DEGREE OF MASTER  
OF ENGINEERING SCIENCE**

**FACULTY OF ENGINEERING  
UNIVERSITY OF MALAYA  
KUALA LUMPUR**

**2017**

**UNIVERSITY OF MALAYA**  
**ORIGINAL LITERARY WORK DECLARATION**

Name of Candidate: S.M. Showybul Islam Shakib

Matric No: KGA 150009

Name of Degree: Master of Engineering Science

Title of Dissertation:

ZERO-VOLTAGE SWITCHING BI-DIRECTIONAL ISOLATED LLC  
RESONANT DC/DC CONVERTER FOR WIDE VOLTAGE GAIN AND LOAD  
RANGE

Field of Study: Power Electronics

I do solemnly and sincerely declare that:

- (1) I am the sole author/writer of this Work;
- (2) This Work is original;
- (3) Any use of any work in which copyright exists was done by way of fair dealing and for permitted purposes and any excerpt or extract from, or reference to or reproduction of any copyright work has been disclosed expressly and sufficiently and the title of the Work and its authorship have been acknowledged in this Work;
- (4) I do not have any actual knowledge nor do I ought reasonably to know that the making of this work constitutes an infringement of any copyright work;
- (5) I hereby assign all and every rights in the copyright to this Work to the University of Malaya ("UM"), who henceforth shall be owner of the copyright in this Work and that any reproduction or use in any form or by any means whatsoever is prohibited without the written consent of UM having been first had and obtained;
- (6) I am fully aware that if in the course of making this Work I have infringed any copyright whether intentionally or otherwise, I may be subject to legal action or any other action as may be determined by UM.

Candidate's Signature

Date: 20<sup>th</sup> September , 2017

Subscribed and solemnly declared before,

Witness's Signature

Date:

Name:

Designation:

## ABSTRACT

Bi-directional DC/DC converters (BDCs) are widely used in many electric power applications such as automobiles, electric vehicles, renewable energy sources, uninterrupted power supplies (UPS), DC micro grid with energy storage systems (ESSs) and so on. Among all the BDCs, Bi-directional resonant DC/DC converters (BDRDCs) are considered as the best suitable for minimizing the switching losses, reducing electromagnetic interference and achieving high frequency operation ability. However, BDRDCs have the inherent limitation of zero voltage switching (ZVS) operation for a wide variation of load and input voltages. This study presents an isolated bi-directional LLC series resonant DC/DC converter with novel frequency adaptive phase shift modulation (FAPSM) control, which is capable of maintaining ZVS for wide variation of load and input voltages. This topology is composed of a stacked structure where four switches are connected in series but sharing the same resonance tank and high frequency transformer. The voltage stress across each switch is reduced to half of the input voltage due to the series combination of four switches. It also uses an active rectifier in the secondary side of the transformer and becomes the key component of an energy storage system (ESS) to enable the bi-directional power flow. The proposed control is composed of two control variables: switching frequency and phase shift angle of the secondary switches. The Switching frequency changes with the load in such a way that, it is secured ZVS to the primary side switches for all phase shift angles. Automatically, it maintains the converter gain characteristics identical regardless of load conditions for all phase shift angles. On the other hand, the phase shift changes according to the input variations only. Thus the converter maintains ZVS to all switches for wide voltage gain and load range. The control also makes the converter voltage gain independent of the loaded quality factor. The simultaneous use of two control variables also reduces the circulating current (or reactive power), especially at light load

conditions. In addition, Frequency selection for each load condition helps to minimize the series RMS resonance current as compared to fixed frequency operation which improves the light load efficiency significantly. Furthermore, high value of magnetizing inductance is designed (which has no effects on voltage gain) in this converter, which reduces the conduction losses as well as increases the efficiency of the converter. Experimental results of a 1kW prototype converter with 200-400V input and 48V output are presented to verify the performance of the proposed converter. The measured efficiency of the converter at full load condition is 96.5% and 92% for maximum and minimum input voltage respectively during power flow in forward direction.

University of Malaya

## ABSTRAK

Penukar DC / DC dwi-arah (BDC) digunakan secara meluas dalam pelbagai aplikasi kuasa elektrik seperti kereta, kenderaan elektrik, sumber tenaga boleh diperbaharui, bekalan kuasa tanpa gangguan (UPS), DC-grid dengan sistem penyimpanan tenaga (SMEA) dan sebagainya. Di antara semua BDC, dwi-arah salunan penukar DC / DC (BDRDCs) adalah dianggap sebagai yang terbaik untuk menghapuskan kehilangan pensuisan, mengurangkan gangguan elektromagnet dan mencapai keupayaan operasi frekuensi tinggi. Walau bagaimanapun, BDRDCs mempunyai had yang wujud semasa operasi ZVS untuk variasi beban tinggi dan voltan masukan. Kajian ini membentangkan satu siri LLC dua arah salunan DC/DC penukar terpicil dengan kekerapan novel fasa penyesuaian kawalan anjakan modulasi, yang sesuai untuk voltan input yang luas aplikasinya (200-400V). Topologi ini terdiri daripada struktur yang disusun di mana empat suis disambung secara siri tetapi berkongsi tangki resonansi dan pengubah berfrekuensi tinggi yang sama. Gabungan siri empat suis mengurangkan tekanan voltan merentasi setiap penukar sama dengan separuh daripada voltan input. Ia juga digunakan penerus aktif dalam bahagian sekunder pengubah dan menjadi komponen utama sistem penyimpanan tenaga (ESS) bagi membolehkan aliran kuasa dua arah. Kawalan yang dicadangkan untuk litar ini berdasarkan dua pemboleh ubah kawalan seperti kekerapan penukaran dan sudut anjakan fasa suis menengah. Perubahan kekerapan pensuisan dan beban dengan cara yang seperti itu, dicadangkan agar ZVS dianjak fasa ke sisi utama untuk semua sudut. Secara automatik, ia mengekalkan ciri-ciri kelebihan penukar yang sama tanpa mengira keadaan beban untuk semua sudut anjakan fasa. Sebaliknya, fasa beralih perubahan mengikut variasi masukan sahaja. Ia boleh dikawal selia voltan keluaran ketat dan kekal malar di bawah semua voltan input. Oleh itu, penukar yang dicadangkan mampu beroperasi pada pelbagai keadaan dengan ZVS di bawah semua keadaan beban. Oleh itu, kawalan ini mengatasi masalah ketidakseimbangan

konvensional DAB LLC penukar salunan. Ia juga membuat gandaan voltan penukar bebas daripada faktor kualiti muatan. Tidak seperti DAB LLC penukar salunan konvensional, kawalan yang dicadangkan meningkatkan pelbagai kelebihan dan membuat penukar yang terbaik sesuai untuk sistem penjanaan tenaga boleh diperbaharui. Di samping itu, penggunaan serentak bagi dua pembolehubah juga mengurangkan peredaran arus (atau kuasa reaktif), terutama pada keadaan beban rendah. Tambahan pula, reka bentuk yang betul dengan nisbah induktor (yang tidak mempunyai kesan ke atas keuntungan voltan), mengurangkan kehilangan pengaliran serta meningkatkan kecekapan penukar. Keputusan eksperimen prototaip penukar 1kW dengan masukan 200-400V dan keluaran 48V dibentangkan untuk mengesahkan semua analisis teori dan ciri-ciri. Kecekapan penukar yang dicadangkan pada keadaan beban penuh adalah 96.5% dan 92% untuk masukan voltan maksimum dan minimum masing-masing semasa aliran kuasa ke hadapan.

## ACKNOWLEDGEMENTS

First and foremost, I would like to thank Almighty God for giving me the strength, knowledge, ability and opportunity to undertake this research study and to persevere and complete it satisfactorily. Without his blessings, this achievement would not have been possible.

In my journey towards this degree, I have found a supervisor, a mentor, an inspiration, a role model and a pillar of support in my Guide, Dr. Saad Mekhilef. He has provided his heartfelt support and guidance at all times and has given me invaluable guidance, inspiration, and suggestions in my quest for knowledge. Without his able guidance, this thesis would not have been possible and I shall eternally be grateful to him for his assistance.

I would like to express my deep appreciation to Dr. Mutsuo Nakaoka, who introduced me to the area of the resonant converter and kindly gave me insightful suggestions for my academic research. I also appreciate the generous help of Nadir Boutasseta in learning about DSP controller.

I am grateful to my father MD. Nazrul Islam Talukder and mother Dilowara Begum, who provided me unconditional love in my life and showed me the right way towards goal. Their continuous support and motivations gave me strength to accomplish the whole work successfully in time. I am also thankful to my brother and sister, for their faith and emotional support on me.

It is a great honor for me to be the part of the Power Electronics and Renewable Energy Research Laboratory (PEARL) at the University of Malaya. My study and research were full of joy and hard work, which are really unforgettable and precious memories to me. I would like to thank all lab members including alumni of PEARL for

their continuous support throughout the journey. Special gratitude to the administrative staffs in the Department of Electrical Engineering, Faculty of Engineering and Institute of Graduate Studies for their quick responses and facilities. I would also like to acknowledge the Ministry of Higher Education Malaysia and University of Malaya for providing financial support through HIR-MOHE project UM.C/HIR/MOHE/ENG/17 and Postgraduate Research Grant (PPP) project PG269-2016A.

University of Malaya

## TABLE OF CONTENTS

Abstract .....	iii
Abstrak .....	v
Acknowledgements .....	vii
Table of Contents .....	ix
List of Figures .....	xiii
List of Tables.....	xvii
List of Symbols and Abbreviations.....	xviii
<b>CHAPTER 1: INTRODUCTION.....</b>	<b>1</b>
1.1 Background.....	1
1.2 Problem Statement.....	3
1.3 Objectives of the study .....	4
1.4 Thesis Outline.....	4
<b>CHAPTER 2: LITERATURE REVIEW.....</b>	<b>6</b>
2.1 Introduction.....	6
2.2 Classification of Single Phase Bi-directional DC/DC Converter .....	6
2.2.1 Non-isolated Bi-directional DC/DC Converter .....	7
2.2.2 Isolated Bi-directional DC/DC Converter .....	8
2.2.3 Dual Half Bridge Converter .....	9
2.2.4 Dual Full Bridge Converter .....	10
2.2.5 Stacked Bridge Converter.....	10
2.2.6 Three-Level Converter .....	11
2.2.7 Resonant Converter .....	12
2.2.7.1 Series Resonant Converter (SRC).....	13

2.2.7.2	Parallel Resonant Converter .....	15
2.2.7.3	Series-Parallel Resonant Converter (SPRC) .....	17
2.2.7.4	LLC Resonant Converter (LLC RC) .....	19
2.2.7.5	CLLLC Resonant Converter (CLLLC RC).....	21
2.2.7.6	CLLC Resonant Converter (CLLC-RC) .....	22
2.3	Bi-directional Resonant Converter Hardware .....	24
2.3.1	Semiconductors .....	25
2.3.2	High Frequency (HF) Transformer .....	28
2.4	Control of the Bi-directional Resonant Converter.....	30
2.4.1	Variable Frequency Control .....	31
2.4.2	Constant Frequency Control.....	34
2.5	Comparison of Bi-directional Resonant Converter Topologies and Control Techniques.....	39
2.6	Summary.....	41

**CHAPTER 3: OPERATION ANALYSIS OF PROPOSED LLC RESONANT  
CONVERTER .....43**

3.1	Introduction.....	43
3.2	LLC Resonant Converter Topology .....	43
3.2.1	Forward Mode of Operation.....	44
3.2.2	Backward Mode of Operation .....	50
3.3	Steady State Analysis .....	56
3.4	Converter Voltage Gain.....	60
3.5	Reverse Power .....	61
3.6	Summary.....	62

## **CHAPTER 4: DESIGN OF THE PROPOSED LLC RESONANT CONVERTER**

.....	<b>64</b>
4.1 Introduction.....	64
4.2 ZVS in the Primary Side Switches .....	64
4.3 Selection of Quality Factor at Full Load .....	67
4.4 Gain Selection.....	68
4.5 ZVS in the Secondary Side Switches .....	69
4.6 Selection of Inductor Ratio K.....	70
4.7 Design of Resonance Tank Components.....	70
4.8 Modified SPM Control Scheme .....	72
4.9 Converter Power Losses .....	73
4.9.1 Conduction Power Losses .....	74
4.9.2 Switching Power Losses.....	75
4.9.3 Gate Driver Losses .....	75
4.9.4 Core Losses of Magnetic Components.....	76
4.10 Light Load Efficiency Evaluation .....	78
4.11 Summary.....	79

## **CHAPTER 5: SIMULATION AND EXPERIMENT RESULTS..... 80**

5.1 Introduction.....	80
5.2 Simulation Results .....	80
5.3 Experimental Results .....	84
5.4 Loss breakdown .....	88
5.5 Measured Efficiency .....	90
5.6 Comparison Studies .....	91
5.7 Summary.....	94

<b>CHAPTER 6: CONCLUSION AND FUTURE WORK .....</b>	<b>95</b>
6.1 Conclusion .....	95
6.2 Future Work.....	96
References .....	98
List of Publications and Papers Presented .....	106

University of Malaya

## LIST OF FIGURES

Figure 1.1: Percentage of global energy consumption, (a) 2014 (b) 2015.....	1
Figure 1.2: DC grid with energy storage system .....	2
Figure 2.1: Classification of bi-directional DC/DC power converter .....	7
Figure 2.2: Non-isolated Bi-directional DC/DC converter topology.....	8
Figure 2.3: Isolated Bi-directional DC/DC converter topology.....	8
Figure 2.4: Half bridge structure (a) and (b) .....	9
Figure 2.5: Full bridge structure.....	10
Figure 2.6: Stacked-bridge structure .....	11
Figure 2.7: Three-level structure.....	12
Figure 2.8: LC series resonant DC/DC converter .....	14
Figure 2.9: DC characteristics of SRC over normalized frequency (Li & Bhat, 2010).	14
Figure 2.10: LC parallel resonant DC/DC converter .....	16
Figure 2.11: Symmetrical bi-directional Parallel resonant DC/DC converter .....	16
Figure 2.12: DC characteristics of PRC over normalized frequency (Steigerwald, 1987) .....	17
Figure 2.13: LCC resonant DC/DC converter.....	19
Figure 2.14: DC characteristics of LCC resonant converter over normalized frequency (Khalil-Abaker, Shi, & Kalam, 2016).....	19
Figure 2.15: LLC resonant DC/DC converter.....	20
Figure 2.16: DC characteristics of LLC resonant converter over normalized frequency (Bo, Rengang, & Lee, 2002; Choi, 2007) .....	21
Figure 2.17: CLLLC resonant DC/DC converter.....	22
Figure 2.18: DC characteristics of CLLLC resonant converter over normalized frequency (Jung et al., 2013).....	22
Figure 2.19: CLLC resonant DC/DC converter (Type-1).....	23

Figure 2.20: CLLC resonant DC/DC converter (Type-2).....	23
Figure 2.21: DC characteristics of CLLC resonant converter (Type-1) over normalized frequency (Wei et al., 2010).....	24
Figure 2.22: DC characteristics of CLLC (Type-2) resonant converter over normalized frequency (Wei et al., 2010).....	24
Figure 2.23: Classification of control schemes of bi-directional resonant converter .....	31
Figure 2.24: Block diagram of a variable frequency control for resonant converter.....	32
Figure 2.25: Block diagram of a constant frequency phase shift control for resonant converter.....	35
Figure 3.1: Proposed LLC resonant converter .....	43
Figure 3.2: Key operating waveforms of LLC resonant converter in forward mode of operation.....	45
Figure 3.3: Operation in forward mode during interval 1 ( $t_0 \sim t_1$ ) .....	46
Figure 3.4: Operation in forward mode during interval 2 ( $t_1 \sim t_2$ ) .....	46
Figure 3.5: Operation in forward mode during interval 3 ( $t_2 \sim t_3$ ) .....	47
Figure 3.6: Operation in forward mode during Interval 4 ( $t_3 \sim t_4$ ).....	47
Figure 3.7: Operation in forward mode during Interval 5 ( $t_4 \sim t_5$ ).....	48
Figure 3.8: Operation in forward mode during interval 6 ( $t_5 \sim t_6$ ) .....	48
Figure 3.9: Operation in forward mode during interval 7 ( $t_6 \sim t_7$ ) .....	49
Figure 3.10: Operation in forward mode during interval 8 ( $t_7 \sim t_8$ ) .....	49
Figure 3.11: Backward power flow operation.....	50
Figure 3.12: Key operating waveforms of LLC resonant converter in backward mode of operation.....	51
Figure 3.13: Operation in backward mode during interval ( $t_0 \sim t_1$ ) .....	52
Figure 3.14: Operation in backward mode during interval ( $t_1 \sim t_2$ ) .....	52
Figure 3.15: Operation in backward mode during interval ( $t_2 \sim t_3$ ) .....	53
Figure 3.16: Operation in backward mode during interval ( $t_3 \sim t_4$ ) .....	53

Figure 3.17 : Operation in backward mode during interval ( $t_4 \sim t_5$ ) .....	54
Figure 3.18: Operation in backward mode during interval ( $t_5 \sim t_6$ ) .....	54
Figure 3.19: Operation in backward mode during interval ( $t_6 \sim t_7$ ) .....	55
Figure 3.20: Operation in backward mode during interval ( $t_7 \sim t_8$ ) .....	55
Figure 3.21: AC equivalent circuit of LLC resonant converter .....	57
Figure 3.22: Plots of voltage gain with regards to F at $K=0.2, Q=2.5$ .....	61
Figure 3.23: Plots of power ratio with regards to $\Theta$ and $\psi$ ( $K=0.1, F=1.11, Q=2.5$ ) .....	62
Figure 4.1: Plots of $\Phi$ and G with respect to $\psi$ for the fixed switching frequency ( $F = 1.2$ ), and K ( $K=0.6$ ) .....	66
Figure 4.2: Plots of $\Phi$ and G with respect to $\psi$ at different Q and F values respectively .....	67
Figure 4.3: Plots of $\Theta$ and G with respect to Phase-shift $\psi$ at different Q, F, and K values respectively .....	68
Figure 4.4: Plots of $\Phi, \Theta$ and G with respect to $\psi$ .....	71
Figure 4.5: Simplified block diagram of the proposed FAPSM control .....	72
Figure 4.6: Flow chart of Output regulation method using the proposed control scheme .....	73
Figure 4.7: Plot of core loss density versus AC field flux density ( <a href="http://www.epcos.com/material">www.epcos.com/material</a> ) .....	77
Figure 4.8: Plot of core loss density versus frequency ( <a href="http://www.epcos.com/material">www.epcos.com/material</a> ) .....	77
Figure 4.9: Plots of RMS resonance current with respect to the voltage gain. ....	79
Figure 5.1: Voltage and current waveforms of proposed converter under 400V input, 48V output and full load condition .....	81
Figure 5.2: Voltage and current waveforms of proposed converter under 200V input, 48V output and full load condition .....	82
Figure 5.3: Voltage and current waveforms of proposed converter under 400V input, 48V output and 20% load condition .....	83
Figure 5.4: Voltage and current waveforms of proposed converter under 200V input, 48V output and 20% load condition .....	84

Figure 5.5: LLC resonant converter hardware .....	85
Figure 5.6: Measured voltage and current waveforms under 400V input , 48V output and full load condition .....	86
Figure 5.7: Measured voltage and current waveforms under 200V input, 48V output and full load condition .....	86
Figure 5.8: Measured voltage and current waveforms under 400V input , 48V output and 20% load condition.....	87
Figure 5.9: Measured voltage and current waveforms under 200V input , 48V output and 20% load condition.....	87
Figure 5.10: Measured Switching waveforms of 400V and full load condition.....	88
Figure 5.11: Measured voltage and current waveforms of reverse power flow at 48 V input, 400 V output, full load condition.....	88
Figure 5.12: Loss breakdown for (a) 400V input (b) 200V input.....	90
Figure 5.13: Measured efficiency of the proposed LLC resonant converter .....	91

## LIST OF TABLES

Table 2.1: Components Comparison of three DAB converters (Wang et al., 2009) .....	27
Table 2.2: Comparison of Bi-directional Resonant Converter Topologies and Control Techniques .....	40
Table 3.1: Summary of forward mode of operation.....	50
Table 3.2: Summary of backward mode of operation.....	56
Table 4.1: Specifications of the Designed Converter.....	72
Table 5.1: Comparison of Different Angles.....	91
Table 5.2: Comparison of LLC Resonant converter topologies .....	93

University of Malaya

## LIST OF SYMBOLS AND ABBREVIATIONS

$V_{in}$	:	Input Voltage
$L_r$	:	Resonance Inductor
$C_r$	:	Resonance Capacitor
$L_m$	:	Magnetizing Inductance
$K$	:	Inductor Ratio
$Q$	:	Quality Factor
$R_L$	:	Load Resistance
$C_1, C_2$	:	DC link Capacitors
$C_o$	:	Filter Capacitor
$f_s$	:	Switching Frequency
$f_r$	:	Resonance Frequency
$f_o$	:	Open Circuit Resonance Frequency
$R_{DS}$	:	Switch Drain to Source Resistance
$n$	:	Transformer Turns Ratio
$I_r$	:	Resonance Current
$I_t$	:	Transformer Current
$I_{Lm}$	:	Magnetizing Current
$V_t$	:	Transformer Voltage
$I_o$	:	Output Current
$I_{in}$	:	Input Current
$V_{cr}$	:	Resonance Capacitor Voltage
$P_{in}$	:	Input Power
$P_{out}$	:	Output Power
$F$	:	Normalized Frequency

$\phi$	:	Input Impedance Angle
$\psi$	:	Controlled Phase-Shift
DB	:	Dual Bridge
DAB	:	Dual Active Bridge
RC	:	Resonance Converter
SRC	:	Series Resonant Converter
PRC	:	Parallel Resonant Converter
SPRC	:	Series Parallel Resonant Converter
BDC	:	Bi-directional Converter
PWM	:	Pulse Width Modulation
PFM	:	Pulse Frequency Modulation
SPM	:	Single Phase-shift Modulation
FAPSM	:	Frequency Adaptive Phase Shift Modulation
EMI	:	Electromagnetic Interference
ZVS	:	Zero Voltage Switching
ZCS	:	Zero Current Switching
RMS	:	Root of Mean Square
ZVZCS	:	Zero Voltage Zero Current Switching
ESR	:	Equivalent Series Resistance
BDCs	:	Bi-directional DC/DC converters

## CHAPTER 1: INTRODUCTION

### 1.1 Background

Nowadays, the traditional fossil fuels based energy sources like oil, gas, and coal are providing the large percentage of electricity in the world. The energy conversion processes from these sources become the major cause of environment pollution. As energy saving and environmental protections become more and more important, people are seeking renewable energy sources such as photovoltaic, wind and fuel cell. to utilize in a clean and efficient way. In addition, these renewable sources are highly promising to mitigate the upcoming energy crisis throughout the world. As shown in Figure 1.1, ("Renewables, Global status report, 2016, REN21 (Renewable energy policy network for the 21st century),") the use of renewable energy is increasing annually.

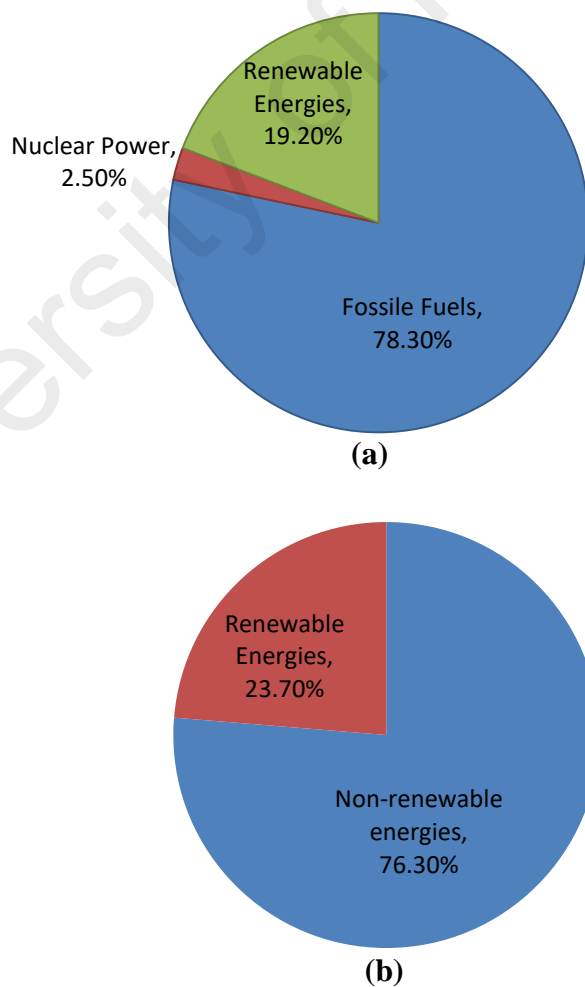


**Figure 1.1: Percentage of global energy consumption, (a) 2014 (b) 2015**

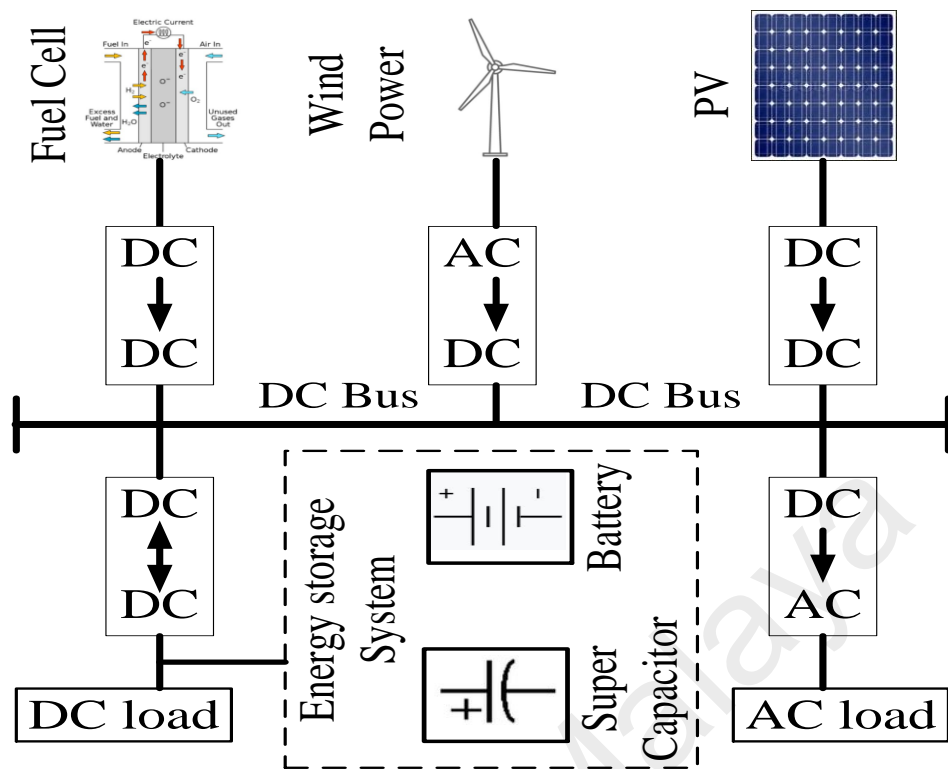


**Figure 1.2: DC grid with energy storage system**

However, the renewable energy sources are not steady in nature and it is a challenging task to supply stable and continuous power from the DC grid system. There is a fluctuation in the power generation due to the intermittent nature of renewable energy sources (Huang, Crow, Heydt, Zheng, & Dale, 2011; Kakigano, Miura, Ise, & Uchida, 2007). Energy storage elements are required to integrate with DC grid for making the system more efficient, reliable and stable (Liserre, Sauter, & Hung, 2010). Electric vehicles can also be integrated with renewable energy sources to stabilize the grid through the vehicle-to-grid (V2G) system (Hu & Liaw, 2016; Monteiro, Pinto, & Afonso, 2016; Weearsinghe, Thrimawithana, & Madawala, 2015). Figure 1.2 shows the typical DC grid system with renewable energy sources and energy storage elements. The output of the renewable energy sources is fed into the DC bus through AC/DC and DC/DC converter. The energy storage elements can be charged or discharged from the DC bus through the bi-directional DC/DC converters. Besides, the DC bus is also connected to the AC loads through the DC/AC converters.

The Energy storage systems (ESSs) should have bi-directional DC/DC converter to store the excess energy and release it when the renewable energy sources unable to generate sufficient energy or during the peak demand of energy consumption. A number of applications like motor drives, uninterruptible power supplies, alternate energy systems battery charger-dischargers, telecommunications and space systems, electric aircraft's require bi-directional power transfer in between loads to variable sources. Besides, voltage variation in the DC bus is wide, so the voltage gain range of bidirectional DC/DC converter should be as wide as possible.

## 1.2 Problem Statement

Dual bridge converter (DBC) has drawn lots of interest in the energy storage systems due to its bi-directional capability with high-efficiency, high-power density, and reliability (Costinett, Maksimovic, & Zane, 2013; Engel, Soltau, Stagge, & De Doncker, 2013; Inoue & Akagi, 2007a; Krismer & Kolar, 2012; Peng, Hui, Gui-Jia, & Lawler, 2004; Qin & Kimball, 2012; B. Zhao, Song, Liu, Liu, & Zhao, 2015). The main problem of Dual Bridge type converter is that the voltage gain is limited to unity to maintain ZVS for all load variations (Jain & Ayyanar, 2008; Zhou & Khambadkone, 2009). It also suffers from high circulating current and high turn-off losses. The circulating current increases rapidly when the converter is operated in boost mode. In order to extend the operating voltage gain range with ZVS and minimize the circulating energy further, some control strategies are proposed in (Costinett et al., 2013; Hua & Mi, 2008; Krismer & Kolar, 2012; Oggier, Garc, x00Ed, & Oliva, 2011; B. Zhao, Song, & Liu, 2012, 2013). However, these control strategies cannot overcome all the disadvantages at a time.

The resonant version of DBC is called the dual bridge resonance converter (DBRC) which is increased the power density further but still has the limited ZVS range for wide

loads and input voltage variations. (Beiranvand, Rashidian, Zolghadri, & Alavi, 2012; Fang, Hu, Shen, & Batarseh, 2012; Li & Bhat, 2010; R. Severns, 1990; Tianyang, Junming, Xinke, Kuang, & Yousheng, 2015, 2016; H. Wu, Mu, Gao, & Xing, 2015; G. Yang, Dubus, & Sadarnac, 2015). Like DBC, the efficiency at light loads is degraded due to high circulating current. The main challenge of DBC is to maintain the suitable efficiency even at higher voltage gain condition by controlling both conduction and switching losses. Hence, a bi-directional DC/DC converter needs to be designed to operate efficiently for wide voltage gain and load range.

### **1.3 Objectives of the study**

The main goal of this study is to increase the voltage gain range of bi-directional isolated LLC resonant converter with zero voltage switching (ZVS) which can be suitable for wide input voltage applications. The focus also lies on efficient operation throughout the voltage gain range and light load efficiency improvement. The specific objectives of this study are as follows:

1. To propose a new topology of an isolated bi-directional LLC resonant converter with a new control scheme that maintains ZVS to all switches for wide voltage gain and load conditions.
2. To implement the proposed topology and control scheme of the isolated bi-directional LLC resonant converter.
3. To analyze the performance of the proposed converter for wide input and load conditions.

### **1.4 Thesis Outline**

This study introduces a new topology and control scheme for isolated bi-directional LLC resonant DC/DC converter which is suitable for wide input voltage applications. It organized as follows:

Chapter 2 presents the detail literature review on the bi-directional resonant converter. The DC characteristics of different resonant tanks are explained in terms of switching frequency. Besides, all control schemes which are reported in the previous literature are classified and explained in detail. Finally, a comparison of different topologies is described the soft-switching ranges and characteristics due to the variation of resonant tank parameters and control strategies.

Chapter 3 presents the detail operation of selected topology. It also represents the steady-state analysis and graphical representations of key characteristics in terms of control variables.

Chapter 4 explains the detail design procedure and modified secondary side phase shift control scheme for the bi-directional isolated LLC resonant converter. It also presents the ZVS range, voltage gain range and mathematical modeling of control laws.

Chapter 5 represents the simulation and experiment results of the proposed converter for the wide load and input variations. The organization of this chapter is such as that; firstly, each part of simulation and experiment results is explained separately. After that, a comparison is drawn among theoretical, simulation and experimental results to validate the steady-state analysis. Then the estimated loss breakdown and measured efficiencies for the entire operating range are explained. Finally, a comparison of the designed converter is drawn with the state-of-the-art work.

Chapter 6 summarizes and concludes the main contributions of the thesis and presents an outlook on possible future research work.

## CHAPTER 2: LITERATURE REVIEW

### 2.1 Introduction

This chapter presents a comprehensive literature review of bi-directional resonant DC/DC power converters. The classifications based on electrical isolation, switching networks, and resonant tank topologies are performed in detail. The main hardware components and their advantages and disadvantages are also presented in this chapter. Besides that the control schemes which are reported in the literature, are classified and critically reviewed in details. Finally, a comparison is drawn based on their characteristics and reported efficiencies.

### 2.2 Classification of Single Phase Bi-directional DC/DC Converter

DC/DC converters are useful to convert the system DC voltages from one DC level to another DC level. Bi-directional DC/DC converters are the branch of DC/DC families where it can maintain the power flow in either direction while needed. Generally, bi-directional DC/DC converters can be classified as either non-isolated or isolated converter depending on whether transformers are added between the input and output. Besides, the switching networks for the DC/DC topologies are varied according to the desired voltage and power levels. The choice of topological structures is substantially dependent on the converter ratings, i.e upon the required voltage range and desired power level. Thus, the bi-directional DC/DC converters can also be classified by the selected switching networks like dual half bridge topology, dual full bridge topology, three level topology and stacked-bridge topology. Integrating resonant circuits in these topologies turn into the resonant converters which can be classified as a series resonant converter (SRC), parallel resonant converter (PRC) and series-parallel resonant converter (SPRC). Figure 2.1 is given an overview of state-of-the-art single phase bi-directional DC/DC converter topologies which are further described in this chapter.

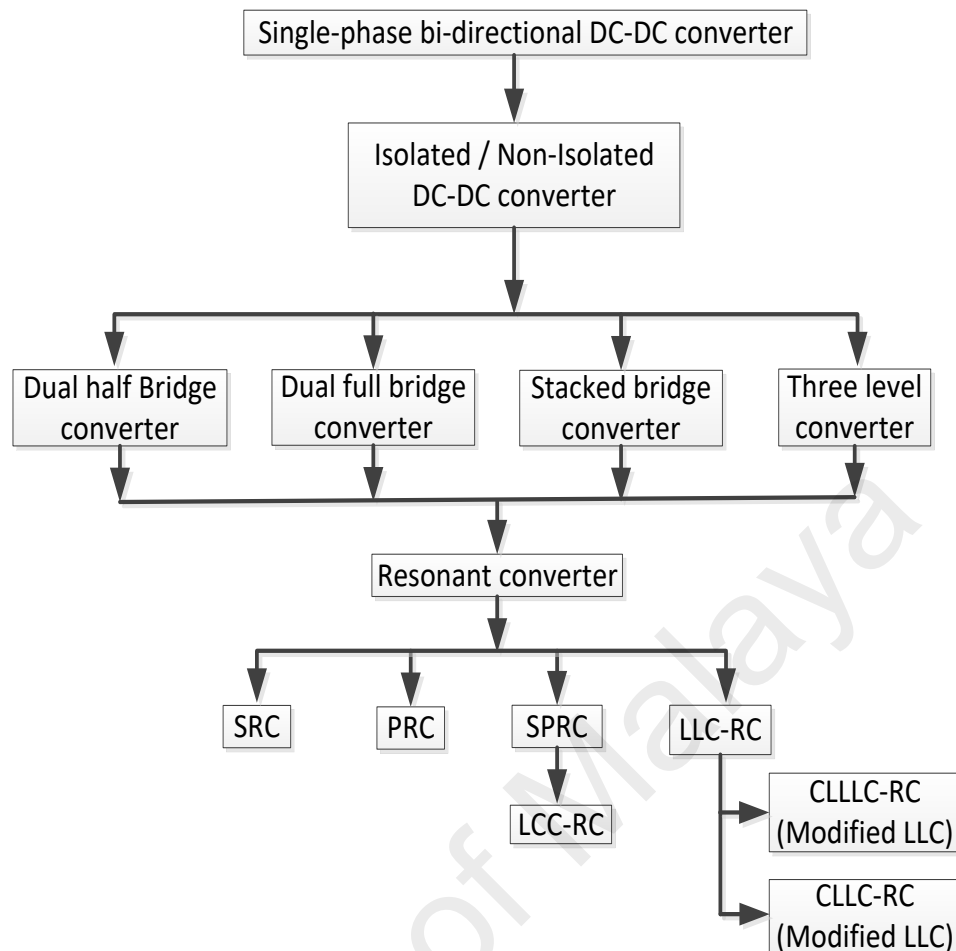


**Figure 2.1: Classification of bi-directional DC/DC power converter**

### 2.2.1 Non-isolated Bi-directional DC/DC Converter

Non-isolated converters are performed the power conversion process without galvanic isolation (Das, Mousavi, & Moschopoulos, 2010). These can be operated as a buck, boost or buck boost converters which are attractive in the power conversion system in terms of efficiency, size, weight and cost. However, non-isolated topology is very popular only for unidirectional power flow rather than the bi-directional system. The resonant version of the non-isolated bi-directional DC/DC converter has a resonant tank in between two switching networks as shown in Figure 2.2 (Rathore, Patil, & Srinivasan, 2016). It has obvious merits of lower cost and magnetic size, higher efficiency, and compactness (Lin, Yang, & Wu, 2013). But, the whole system will be failed if a short circuit happened in one side of switching networks. Thus, a galvanic

isolation in between switching networks has drawn much more attention as compared to the non-isolated converter.

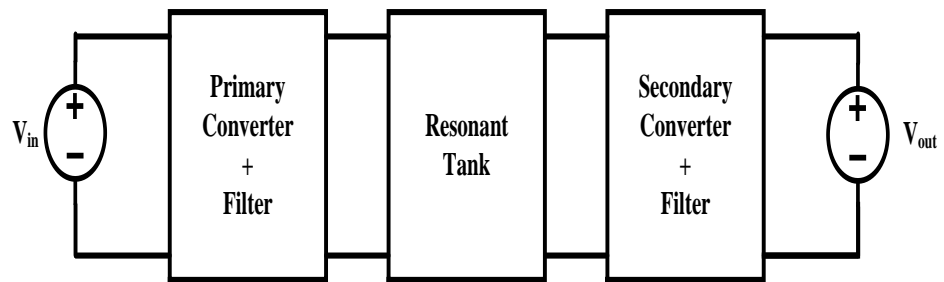


**Figure 2.2: Non-isolated Bi-directional DC/DC converter topology**

### 2.2.2 Isolated Bi-directional DC/DC Converter

A transformer is used in between switching networks as shown in Figure 2.3 to isolate the input and output. While the transformer are adding extra cost with the other components cost; however it is the only component which facilitates isolation by providing impedance matching between two sides. Thus it can protect the entire converter system from the short circuit occurred in one side of the converter. The resonant version of isolated bi-directional converters is advantageous over isolated PWM based converter (Rani, 2015) in terms of magnetics size, losses, and high-frequency operation. As resonance converter allows the high-frequency operation rather than common PWM converter, the size of the transformer can be minimized by employing the high operating frequency. The parasitic components of the high-frequency transformer can also be used as the resonance tank components.

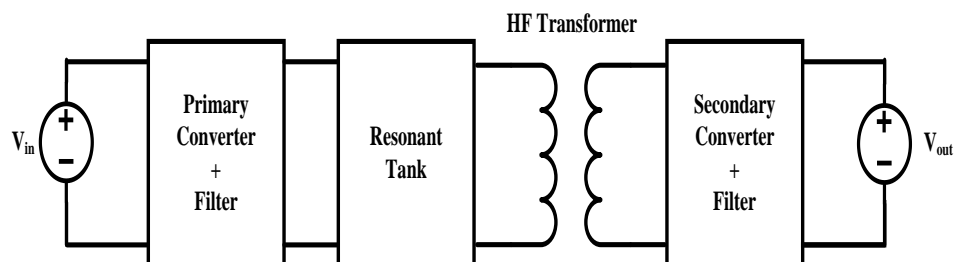


**Figure 2.3: Isolated Bi-directional DC/DC converter topology**

### 2.2.3 Dual Half Bridge Converter

Half bridge converters consist of a converter leg in parallel with a split capacitors bus as shown in Figure 2.4(a). The semiconductor switches are driven in a complementary manner where small dead time is used to prevent short circuit and also to charge and discharge the junction capacitors of the switches to provide soft-switching. The switches in a half-bridge are controlled in such a way that it can produce an alternating voltage pulse and the input voltage equally divided into DC-link capacitors. A separate control is required if the voltage imbalance exists in between split capacitors. Although it has a small number of switches, but the primary drawback is the size and cost of DC-link capacitors required. Another type of half bridge structure is used in resonant converter where converter leg in parallel with one DC-link capacitor as shown in Figure 2.4(b). Unlike the half-bridge with split capacitors, the bridge output voltage is unipolar, stepping between zeros to positive level. But, the resonance capacitor normally connected on the primary side can absorb the DC values and provide pure AC waves for the operation of the resonant tank. Although, it increases the resonant capacitor voltage stress due to DC bias voltage but reduces the number of capacitor and voltage imbalance complexity in the split capacitors type structure mentioned in Figure 2.4(a). Due to high voltage and current stress across the switches, the half bridge structure becomes best suitable for low voltage and low power applications.

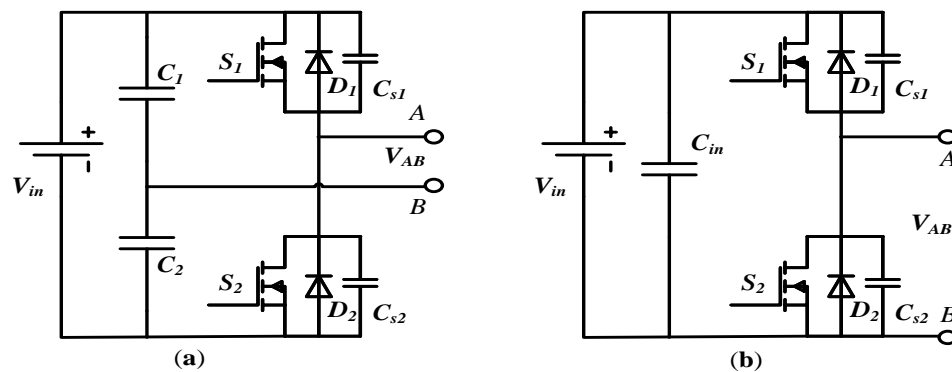


Figure 2.4: Half bridge structure (a) and (b)

### 2.2.4 Dual Full Bridge Converter

A Full bridge converter is composed of two switching legs in parallel with DC-link capacitor. Figure 2.5 shows the single phase full bridge converter structure consists of two switching legs. The current in the full bridge converter is shared between two legs which reduced the current stress on the devices as compared to half bridge converter. It is also known as DAB (Dual Active Bridge) converter which is generally used for high power applications.

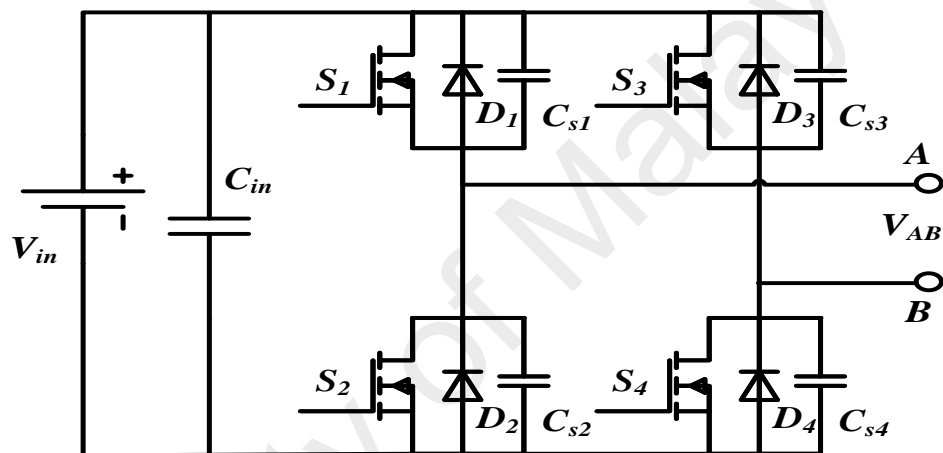
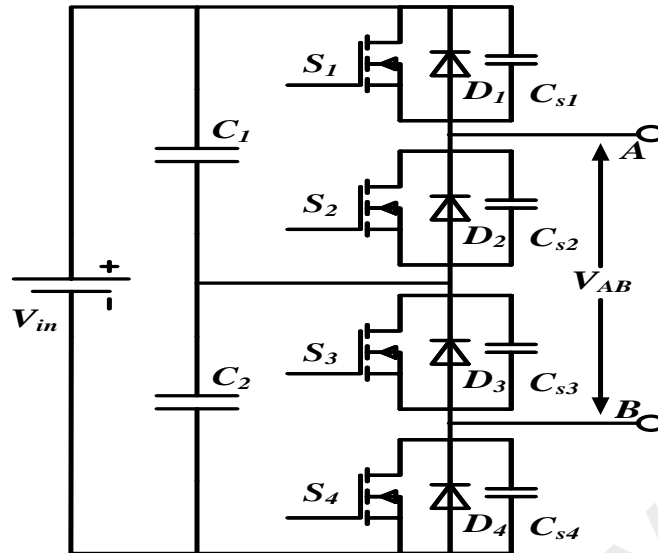


Figure 2.5: Full bridge structure

### 2.2.5 Stacked Bridge Converter

A Stacked-bridge topology has one leg in parallel with two DC-link capacitors as shown in Figure 2.6 where four switches are connected in series with each other (Wuhua et al., 2013; Zong, Luo, Li, Deng, & He, 2016; Zong et al., 2014). The series combination of four switches reduces the voltage stress across each switch equal to half of the input voltage. Due to the reduced voltage stress, it becomes best suitable for applications which requires high voltage. This type of topology also facilitates the using of low voltage ratings with lower  $R_{ds-on}$  switches for high voltage applications which actually reduced the conduction losses as compared to conventional half or full bridge structures.



**Figure 2.6: Stacked-bridge structure**

### 2.2.6 Three-Level Converter

The three-level DC/DC converter is introduced in the DC/DC converter families to minimize the voltage stresses across the semiconductor switches as well as increase the power density. It is advantageous for high voltage applications such as photovoltaic system, fuel cell system and ship electric power distribution system due to low voltage stress across semiconductor switches (Il-Oun & Gun-Woo, 2012; Wuhua et al., 2016; Yilei, Zhengyu, Lijun, Zhaoming, & Guisong, 2005). Three level topology has little influence in bi-directional DC/DC applications (F. Zhao, Wang, Dong, & Yang, 2014), mostly it is used for unidirectional DC/DC applications. However, it is associated with high switching losses due to a high input voltage, which leads to the low efficient converter. So, three-level resonant converter becomes popular for bi-directional DC/DC applications due to soft switching is granted by the integrating resonance tank. A three-level bi-directional structure with LLC resonant converter is shown in Figure 2.7 which is proposed in (Tianyang et al., 2016) where the voltage stress across switches depends on voltage gain, and ZVS appeared only in the primary switches. In this topology, an extra flying capacitor and auxiliary switches have been used, which make the converter operation complex and increased the cost of the overall system.

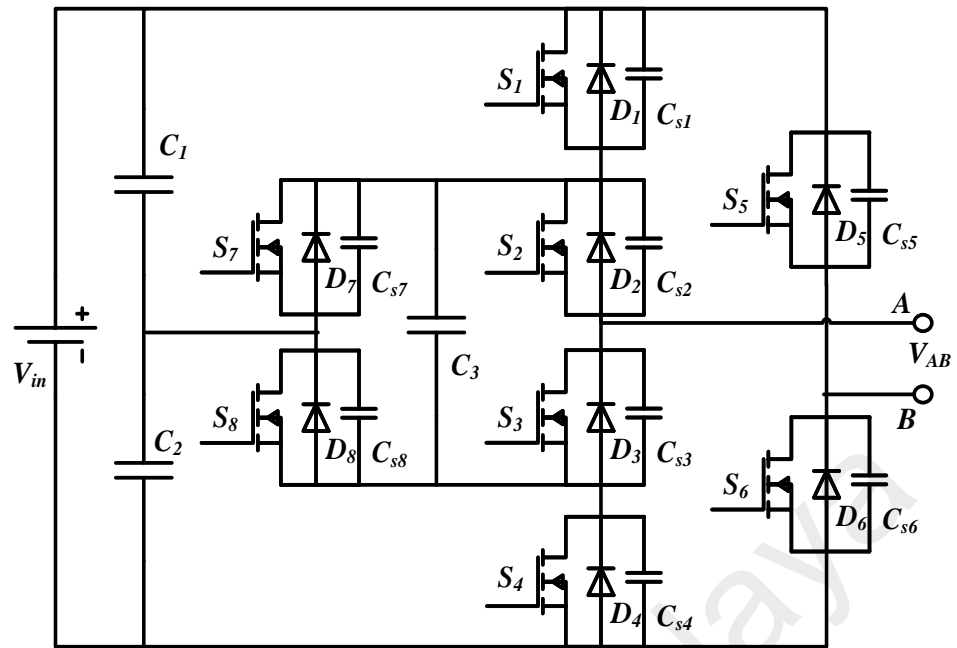


**Figure 2.7: Three-level structure**

### 2.2.7 Resonant Converter

In resonant DC/DC converters, resonant tank network plays an important role in voltage and power regulation process. The circulating energy of tank circuit can be manipulated by changing the operating frequency and phase shifted gate signals to condition the input power to the desired output voltage. The resonance frequency of the LC networks are also comparable to the operating switching frequency so that it can operate in both buck and boost mode by simply changing the switching frequency. Unlike the PWM based converters, the resonant tank can absorb the higher order harmonics and DC components from the input square wave voltage to generate AC output voltage and currents. The most prominent advantage of the resonant converter is that it can realize soft switching for the power switches. The soft-switching means that the voltage and current across the switch cross zero respectively during switching transitions. It reduces the switching losses and helps the converter to operate with higher switching frequency. Thus, higher operating frequency minimizes the size of magnetic components and increases the power density of the resonant converter as compared to

PWM based converters. The soft switching transitions also have the benefit of eliminating 'noise' generated by the converter components resulting low electromagnetic interference (EMI) can be achieved (T. S. Wu, Bellar, Tchamdjou, Mahdavi, & Ehsani, 1996). As the capability of wide voltage regulation, the resonant converter reduces the size of the DC-link capacitor in case of DC/DC converter system. Although the resonance converter has superiority in many aspects such as power efficiency and power density, it has some disadvantages. The peak values of voltage and current ripples are quite large in resonance converter which is responsible for the higher components stresses. The large variation of resonance increases the peak circulating current in the converter resulting higher conduction losses. This shortcoming especially affects the light load efficiency which arises the difficulties to optimize the converter for wide load range.

There is a wide variety of resonant tanks for constructing resonant converter. The most commonly used resonant converters are series resonant converter (SRC), Parallel resonance converter (PRC), and series-parallel resonant converter (SPRC) (R. P. Severns, 1992; Steigerwald, 1987). Besides that LLC resonant converter is gaining popularity due to the inherent quality of soft switching, wide voltage gain and load range. For the bi-directional power flow analysis, series LC network, LLC and modified version of LLC like CLLC, CLLLC are reported in the literature (Jung, Kim, Ryu, & Baek, 2013; Li & Bhat, 2010; Tianyang et al., 2015; Wei, Ping, & Zhengyu, 2010). The following subsections will describe the characteristics of resonant tanks which are used for bi-directional DC/DC power conversion systems.

#### **2.2.7.1 Series Resonant Converter (SRC)**

The combinations of two components resonant tank with load are illustrated in the Figure 2.8. It consists of a resonance capacitor  $C_r$  and a resonant inductor  $L_r$  which are

connected in series with the load resistance. For the bi-directional DC/DC converter, the series combination is preferable due to the symmetrical nature of the LC tank for both forward and backward power flow operation (Li & Bhat, 2010).

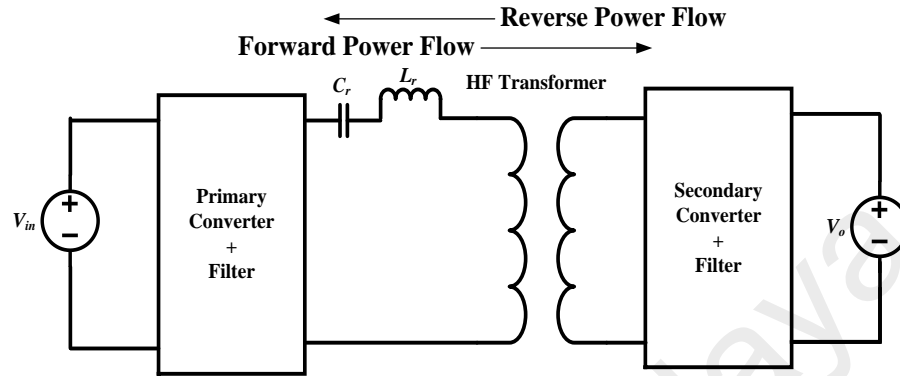


**Figure 2.8: LC series resonant DC/DC converter**

The input impedance of the resonant tank is the function of operating frequency so that the output voltage of the resonant tank can be modulated by the switching frequency. The DC characteristic of series LC resonant tank with load is shown in Figure 2.9. The input impedance at the resonance frequency (resonance frequency,  $f_r = \frac{1}{2\pi\sqrt{L_r C_r}}$ ) is zero, hence the normalized voltage gain becomes unity at this point and it is the maximum voltage gain throughout the operating region.

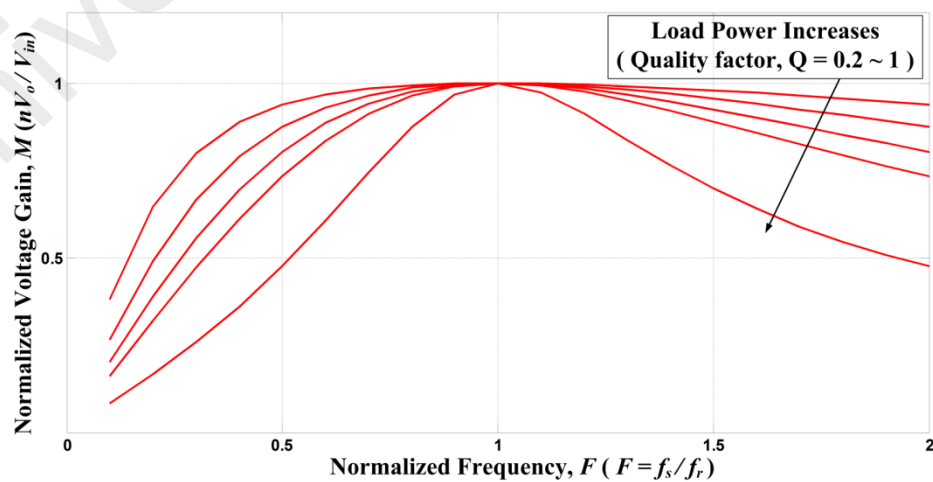


**Figure 2.9: DC characteristics of SRC over normalized frequency (Li & Bhat, 2010)**

The input impedance becomes inductive when the operating frequency higher than the resonance frequency and that makes the input current lagging from the input voltage across the resonant tank. Thus ZVS is secured in the inductive slope region. ZVS is suitable for converters that use MOSFETs and diodes, which minimizes the switching losses and EMI effect. On the other hand, the region where the switching frequency is lower than resonance is called capacitive slope region. In this region, input current leads input voltage that secured ZCS in the converter. ZCS is favorable for IGBTs rather than MOSFETs to reduce the switching losses. Also, capacitive slope region is more complicated especially for two components resonant tank due to sub-harmonic effect at lower switching frequencies. The resonant tank behaves properly to the signals with the resonant frequency rather than other frequency and it is possible that some higher order harmonics of a low switching frequency input accords with the resonance. As a result, the gain and frequency relationship is no longer monotonic for low switching frequency and therefore the region at low frequency should be generally avoided.

It can be observed from DC characteristic plot that the voltage gain curves are less steep for light load condition. Thus, wide switching frequency variation is required to regulate the output voltage even it cannot be regulated at no load (Steigerwald, 1987). It is also observed that the maximum voltage gain is limited to unity as long as operating frequency is only the control variable. The turn-off losses become significant at above resonance frequency operation, therefore series two components resonant tank based converter is not suitable for wide input voltage and load applications.

### **2.2.7.2 Parallel Resonant Converter**

The conventional form of the parallel resonant converter is shown in Figure 2.10. It has also two resonant components as like SRC where  $C_r$  is in parallel with the load. The conventional form is not suitable for bi-directional power converters due to lack of

symmetry for both forward and backward power flow conditions. To get rid of this difficulty, the resonant tank components can be set up by the four reactive components as shown in Figure 2.11 where  $L_{pr}$  and  $L_{sr}$  can be the leakage inductances of the transformer windings. The capacitors  $C_{pr}$  and  $C_{sr}$  are being parallel with the load in either direction of power flow conditions. So, it behaves like a conventional parallel resonant converter irrespective of power flow directions. The DC characteristics of PRC over normalized frequency are shown in Figure 2.12. Unlike the SRC, the peak gain of PRC is not stuck to unity rather than it is affected by the load. It can be observed from the DC gain characteristics that the normalized frequency at peak gain point is going to the lower than unity with increasing load conditions.

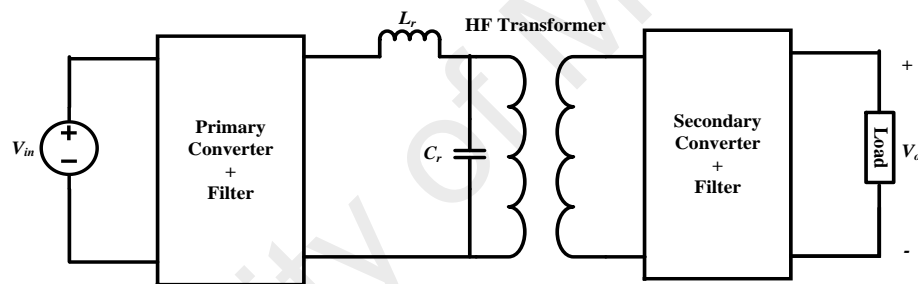


**Figure 2.10: LC parallel resonant DC/DC converter**

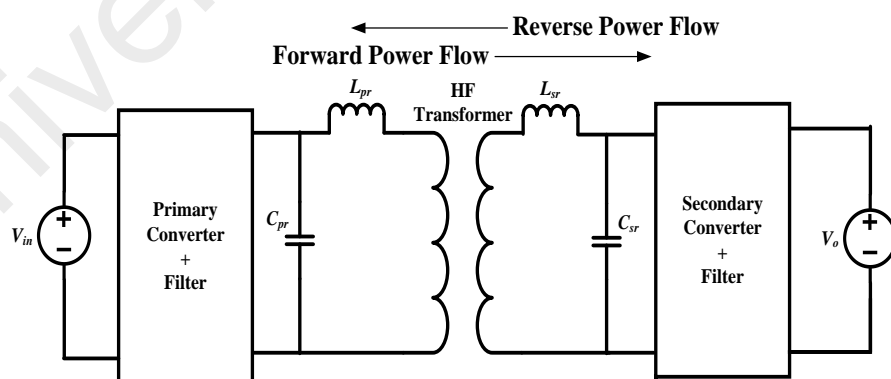


**Figure 2.11: Symmetrical bi-directional Parallel resonant DC/DC converter**

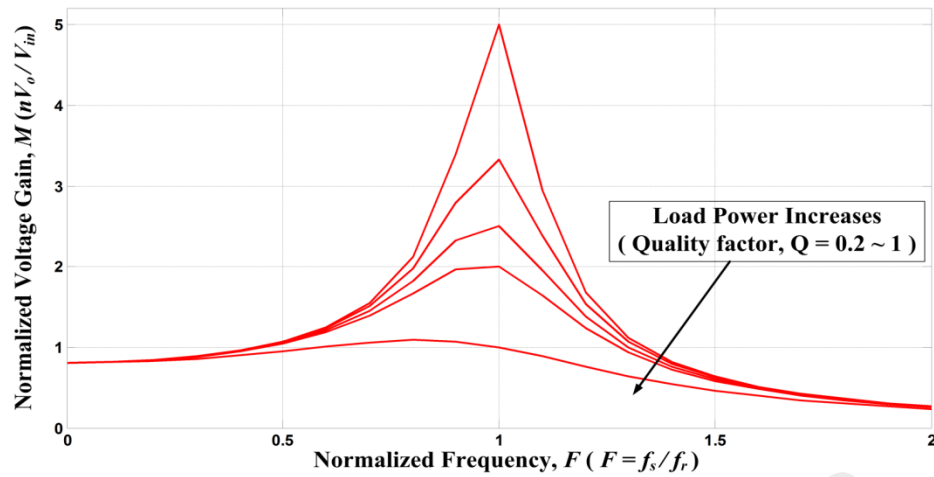


**Figure 2.12: DC characteristics of PRC over normalized frequency (Steigerwald, 1987)**

It is also seen that the gain slope at light load is steeper enough so that PRC can regulate the output voltage at light load in contrary to SRC. It also requires small switching frequency variations as compared to SRC for similar input and load range. The main drawback of PRC is that the resonant current is relatively independent of load resulting poor light load efficiency. Also, the circulating current increases as the input increases causing higher conduction losses and poor efficiency. Like SRC, ZVS can be secured in negative slope region and ZCS can be guaranteed in positive slope region where the input impedance of resonant tank and load represents inductive and capacitive respectively. In SRC, the series resonant capacitor blocks the DC component of the inverter input signal but in the case of PRC, the DC component of the inverted signal accelerates transformer saturation.

### 2.2.7.3 Series-Parallel Resonant Converter (SPRC)

LCC converter is the combination of SRC and PRC which combines the advantages of SRC and PRC while eliminating their shortcomings (R. Yang, Ding, Xu, Yao, & Xiang, 2014). It has three elements:  $C_r$ ,  $L_r$ , and  $C_p$  where  $C_p$  is in parallel with the load.

It has two resonant frequencies:  $f_r$  ( $f_r = \frac{1}{2\pi\sqrt{L_r C_r}}$ ) is the short circuit resonant frequency,

$f_o$  ( $f_o = \frac{1}{2\pi\sqrt{L_r(C_p \parallel C_r)}}$ ) is the open circuit resonant frequency. The topological structure of LCC resonant converter is shown in Figure 2.13. The characteristics of LCC depend upon the selection of component values. It behaves like SRC when power flows in reverse direction i.e secondary side to primary side of the transformer (Khalil-Abaker, Shi, & Kalam, 2016). It also resembles to the SRC more and more as  $C_p$  gets smaller and smaller. Thus, with small  $C_p$  value reduces the selectivity of the converter at light load condition like SPC. In other words, it also behaves like a PRC when  $C_p$  gets higher and higher. Thus, the circulating current in the resonant tank becomes independent of load condition which reduces the light load efficiency. So, the value of  $C_p$  should be selected in such a way that it can be regulated the output voltage at no load and the circulating current should be load dependent. However, in (Steigerwald, 1987) it is found that  $C_s = C_p$  is a good compromise design which overcomes the lacking of SRC and PRC. The voltage gain characteristics for forward power flow over normalized switching frequency are shown in Figure 2.14, where  $C_s = C_p$ . Unlike the LLC converter, open circuit resonant frequency is higher than the short circuit resonant frequency and the gains are not meet with unity point at short-circuit resonant frequency. As mentioned before, ZVS with MOSFET switches of the converter can appear only in the inductive slope region. It has higher voltage gain as compared to LLC while operating at above short circuit resonance frequency.

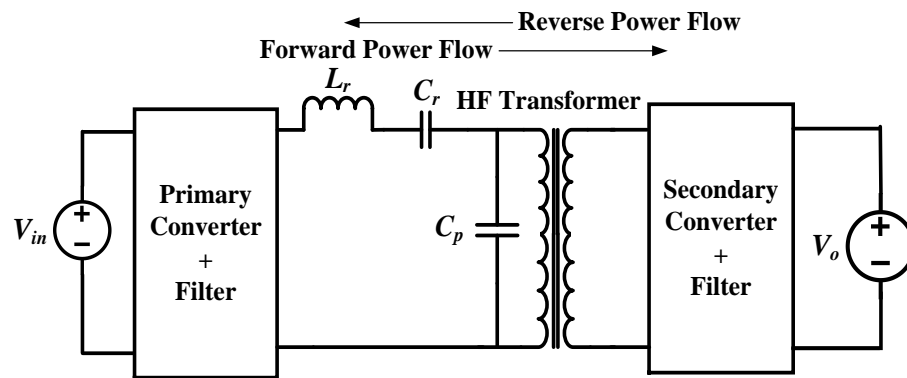


Figure 2.13: LCC resonant DC/DC converter

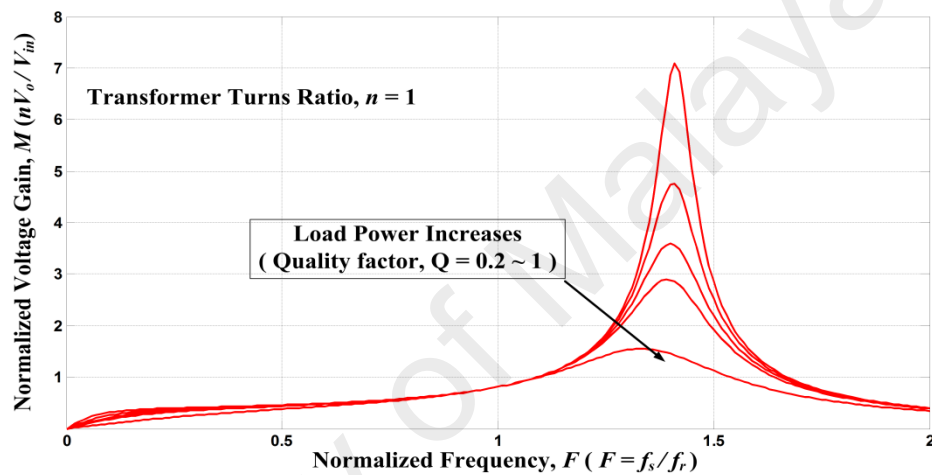
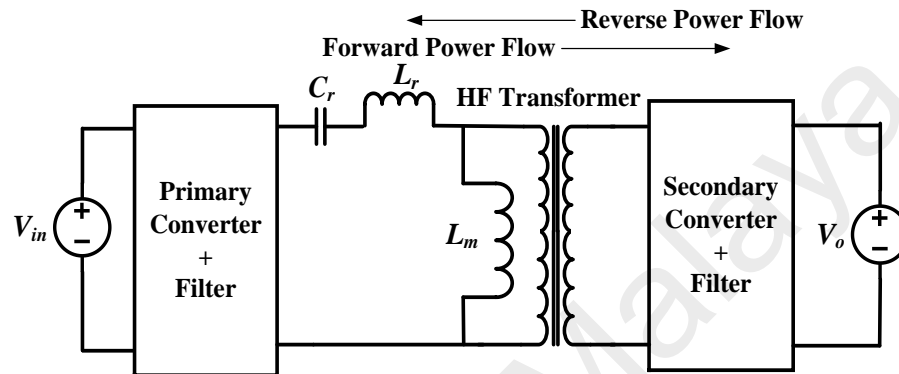


Figure 2.14: DC characteristics of LCC resonant converter over normalized frequency (Khalil-Abaker, Shi, & Kalam, 2016)

#### 2.2.7.4 LLC Resonant Converter (LLC RC)

LLC RC is advantageous in terms of wide voltage gain and ZVS range. Also, most of the parasitic components in the converter can be utilized by LLC RC. For the wide voltage gain and load range, LLC is the famous three components resonant tank is shown in Figure 2.15. Unlike the two components series resonant tank, the magnetizing inductance of the transformer participates in the resonance. Although the magnetizing inductance exists in every transformer, which makes the SRC similar like LLC resonant converter, but magnetizing inductance in SRC is very high as compared to resonance inductor and will not participate in resonance. However, LLC resonant converter doesn't have symmetrical nature for bi-directional power flow applications, it behaves

like a SRC in reverse power flow condition (Sihun et al., 2012). The magnetizing inductance can be set to desired value using gapped cores or providing air gaps in between cores, therefore, SRC can be easily changed to LLC converter without any extra costs (Bo, Rengang, & Lee, 2002; Choi, 2007; Yan, Wenduo, Bing, & Wyk, 2005).



**Figure 2.15: LLC resonant DC/DC converter**

The LLC resonant tank has two resonant frequencies:  $f_r$  ( $f_r = \frac{1}{2\pi\sqrt{L_r C_r}}$ ) is the short circuit resonant frequency,  $f_o$  ( $f_o = \frac{1}{2\pi\sqrt{(L_r + L_m) C_r}}$ ) is the open circuit resonant frequency.

The DC characteristics of LLC resonant converter over operating frequency for forward power flow are shown in Figure 2.16. It can be observed from the DC characteristics that the gain becomes unity at short circuit resonant frequency irrespective of load condition. This unity gain is the highest efficiency point of LLC which lying on the inductive slope region. Besides that LLC overcomes all the disadvantages of two components tank and provides wide voltage gain like the gain can be above and below unity. It also increases ZVS range as compared to two components resonant tank. The voltage gain is steep enough at light load condition, thus it can regulate the output voltage even at no load condition. All the parasitic components of the converter can be effectively utilized as part of the tank elements rather than other SRC or PRC. The advantages are appeared in the LLC RC over SRC when the magnetizing inductance of

the transformer comes to the resonance otherwise it behaves like SRC. The voltage gain characteristics of LLC RC for reverse power flow are same as SRC.

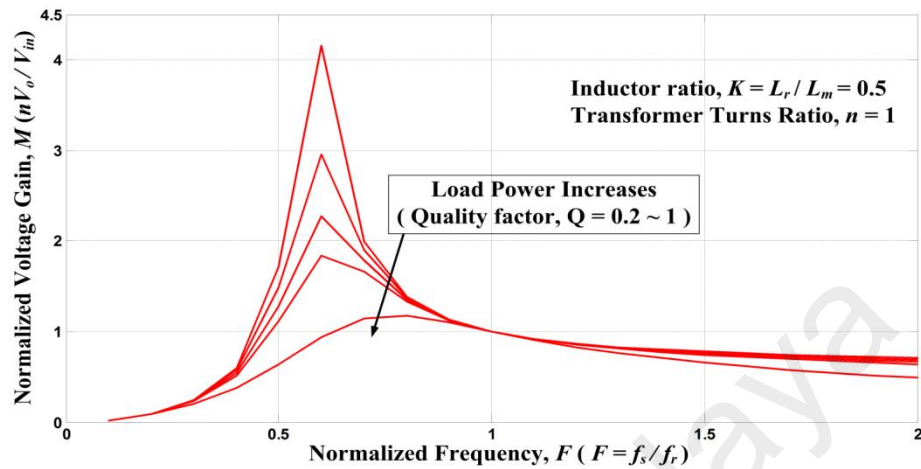


**Figure 2.16: DC characteristics of LLC resonant converter over normalized frequency (Bo, Rengang, & Lee, 2002; Choi, 2007)**

#### 2.2.7.5 CLLLC Resonant Converter (CLLLC RC)

To get the symmetrical nature for both forward and backward power flow direction, LLC resonant tank can be modified to CLLLC resonant tank with five passive elements as shown in Figure 2.17. Due to the symmetrical structure, it becomes suitable for bi-directional power flow applications (Jung et al., 2013). The leakage inductance of the transformer primary and secondary windings is merged to the resonant inductor  $L_{r1}$  and  $L_{r2}$ . The resonant capacitors  $C_{r1}$  and  $C_{r2}$  can make the automatic flux balancing in the converter. The voltage gain of the CLLLC resonant tank with respect to the switching frequency is illustrated in Figure 2.18. The voltage gain curve has a peak value at low resonant frequency where the magnetizing inductance participates in the resonance. Unlike the LLC resonant tank, it has higher peak gain at lower resonance frequency and wider inductive slope region at light load conditions. However, the gain is not unity irrespective of load condition where operating frequency is equal to the resonance frequency. In addition, the voltage gain can be decreased as decreasing operating frequency under high-load condition. The resonance in the CLLLC network becomes

more complicated than the resonance in LLC, due to the capacitor  $C_{r2}$  is added in the network.

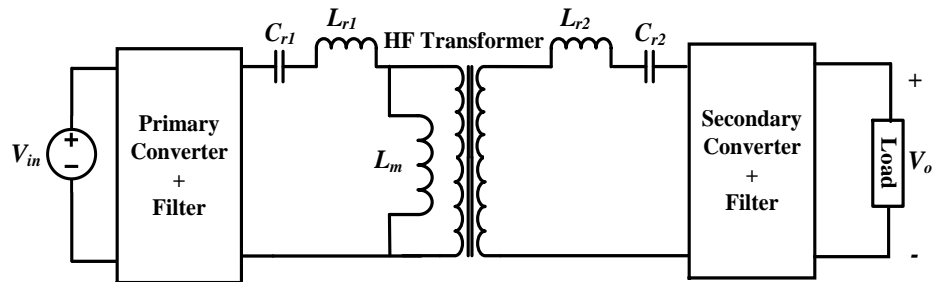


**Figure 2.17: CLLC resonant DC/DC converter**

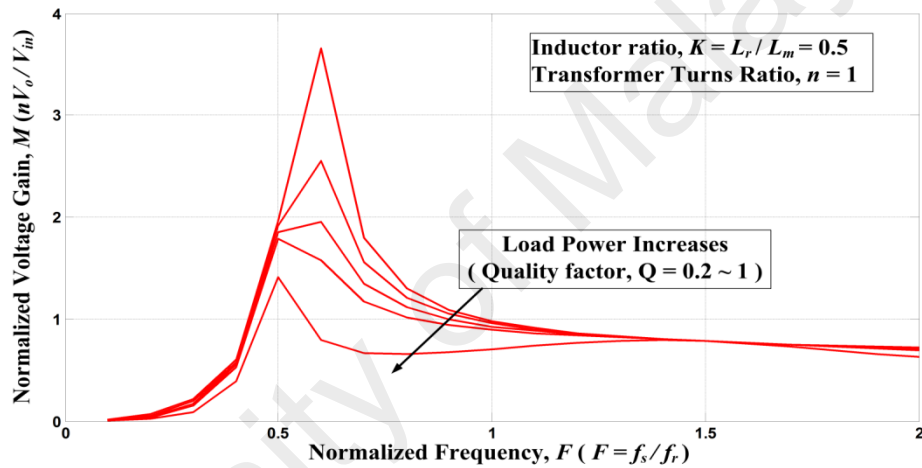


**Figure 2.18: DC characteristics of CLLC resonant converter over normalized frequency (Jung et al., 2013)**

#### 2.2.7.6 CLLC Resonant Converter (CLLC-RC)

The four components resonant tanks as shown in Figure 2.19 and Figure 2.20 are quite similar with LLC resonant tank except an extra resonant capacitor is being added in each configuration. These two types of CLLC can be combined as a bi-directional converter (Wei et al., 2010) where Figure 2.19 represents resonant tank network for forward power flow and Figure 2.20 represents the resonant tank network for reverse power flow.

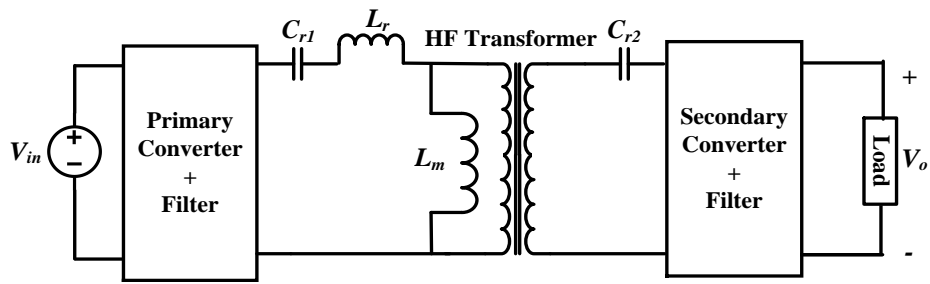


**Figure 2.19: CLLC resonant DC/DC converter (Type-1)**

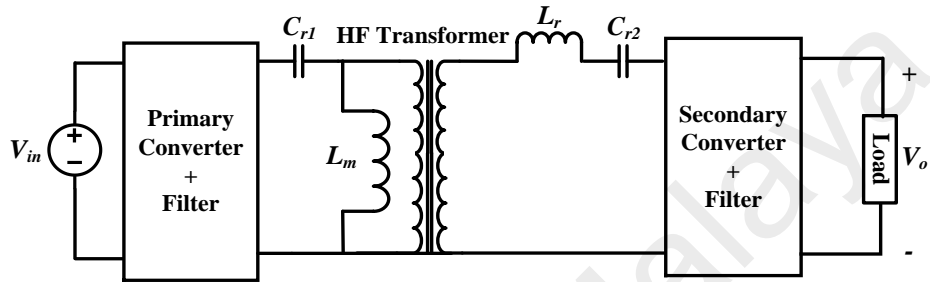


**Figure 2.20: CLLC resonant DC/DC converter (Type-2)**

Both networks have two similar inductors:  $L_r$  and  $L_m$  where the magnetizing inductance of the transformer can be acted as  $L_m$  and the leakage inductances of both windings can be merged into  $L_r$ . To make flux balancing in the transformer, the resonant capacitors  $C_{r1}$  and  $C_{r2}$  can also be functionalized as the blocking capacitors according to the direction of power flow.

From the Figure 2.21-22, it can be observed that both voltage gains have the two peaks on either side of the unity normalized frequency. Type-1 has the wide negative slope region and higher peak gain point at lower operating frequency. Although, the gain of Type-1 is quite lower than Type-2 at higher operating frequency region especially the difference shows visible in the area where the normalized switching frequency is higher than unity. However, the voltage gain for both types of resonant tanks can be decreased as decreasing the operating frequency at the heavy-load condition.

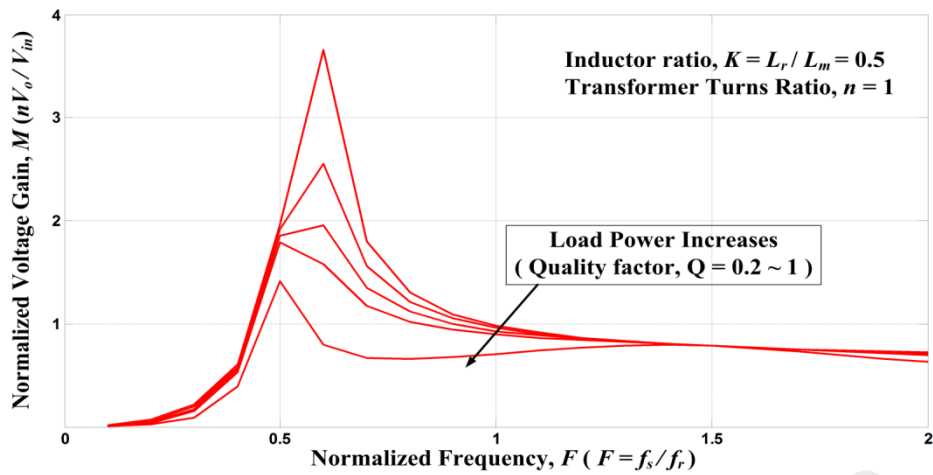


**Figure 2.21: DC characteristics of CLLC resonant converter (Type-1) over normalized frequency (Wei et al., 2010)**

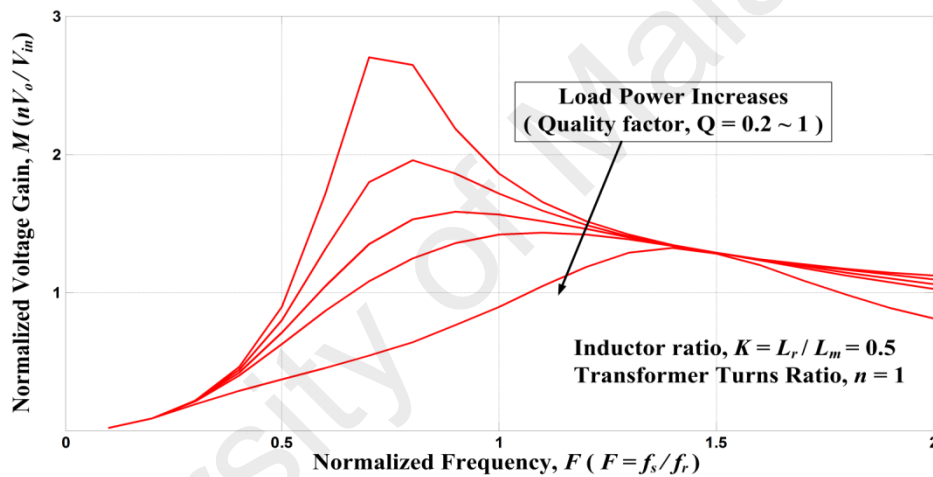


**Figure 2.22: DC characteristics of CLLC (Type-2) resonant converter over normalized frequency (Wei et al., 2010)**

### 2.3 Bi-directional Resonant Converter Hardware

The main components of the bi-directional converter are semiconductor switches and transformer. In the case of the resonant converter, the parasitic components can be added as the resonant tank elements. The variations of resonant tank elements depend on desired voltage gain and soft switching natures. Although the control laws can also be changed the characteristics of the converter besides resonant tank components. The following subsections describe the major hardware options.

### 2.3.1 Semiconductors

Switching and conduction losses of semiconductor devices in a power converter are the significant part of the overall losses. The antiparallel diodes of semiconductor switches in DC/DC converter have an important role in soft-switching and rectifying inverter voltage. But, in the case of hard switching, its reverse recovery process affects the opposing switching devices which are turned on. Its conduction losses are also significant, particularly when operating in forward biased condition. A comparison is drawn in (Elasser et al., 2003), between Silicon carbide (SiC) diodes and the other family of Silicon (Si) diodes. Although, it is found that, SiC diodes exhibit very low switching losses, but their conduction losses due to high voltage drop dominate the overall efficiency. In (Krismer, Biela, & Kolar, 2005), MOSFET intrinsic body diode is replaced by two SiC diodes which are connected in series and parallel manner with it. However, it has very poor dynamic characteristics.

In (Aggeler, Biela, Inoue, Akagi, & Kolar, 2007), a bi-directional DC/DC converter based on SiC JFET are compared to a conventional Si system for the 1MW next generation back to back system. In addition, SiC system has good material characteristics which lead to faster switching and low losses with an improved efficiency as compared to Si system. In (Inoue & Akagi, 2007c), the loss analysis is revealed that SiC based power devices can bring the significant improvement in the conduction and switching losses to the DC/DC converter. High power density and light weight can be achievable with these power devices.

In (Aggeler, Biela, & Kolar, 2008), a series combination of SiC-JFETs and one MOSFET in a cascade connection has been implemented for high power level at moderate switching frequencies. It was revealed that SiC JFETs are best suitable for

moderate frequency, high voltage, and high power density in terms of good static characteristics and switching losses.

SiC MOSFETs co-packed with JBS diodes in (Jieli, Abdallah, & Sullivan, 2001; Kadavelugu et al., 2011) is implemented in DAB converter due to its wider band gap and higher critical field strength. Especially SiC MOSFETs are favorable for high voltage and high power density applications because it offers low  $R_{ds-on}$  (On stated drain to source resistance) value at high voltage as compared to Si MOSFETS.

In (Costinett, Nguyen, Zane, & Maksimovic, 2011) GaN (Gallium Nitride) devices are compared with Si-devices for an unregulated, high step down, ZVS DAB converter. This study is drawn a conclusion that the converter with GaN devices has better performance in the inverter side at GHz frequency range and comparable on the rectifier side where conduction losses are dominated.

SiC power devices for HF DAB converter have also been used in the literature (B. Zhao, Song, Liu, & Sun, 2014). This analysis concluded that due to high thermal conductivity and efficiency, SiC devices are gaining more and more attention day by day.

In (B. Zhao, Song, & Liu, 2014; B. Zhao, Song, Liu, & Sun, 2012), a comparison between SiC and Si devices is drawn in terms of switching characteristics. It was shown that higher switching frequency and low on-state resistance reduce the volume, weight and conduction losses of the converters.

The study presented in (Wang, Haan, & Ferreira, 2009) reviewed the recent development of key components of power converters and addressed the potential of advanced components to increase the system power density with low losses. For illustrating the potential, Table 2.1 compared the power densities of air-cooled DAB

converters with three categories of components such as state-of-art components, available advanced component, and future components. The analysis is shown that the future components have ten times better loss-related properties and can be able to double the power density as compared to available advanced components.

**Table 2.1: Components Comparison of three DAB converters (Wang et al., 2009)**

Main Components	DABs with state-of-art components	DABs with available advanced components	DABs with future components
Low- Voltage switches	MOSFETs $R_{ds-on} = 2.8 \text{ m}\Omega$ $t_{on} / t_{off} = 135/150\text{ns}$	Direct-FET MOSFETs $R_{ds-on} = 1.7 \text{ m}\Omega$ $t_{on} / t_{off} = 50/10 \text{ ns}$	GaN, $R_{ds-on} = 0.17 \text{ m}\Omega$ $t_{on} / t_{off} = 5/1 \text{ ns}$
High- Voltage switches	IGBT SK80MD055	Discrete Si MOSFETs SiE806DF	GaN, 10X smaller $R_{ds-on}$ 10X smaller $t_{on} / t_{off}$
Magnetics	3C90	3F3	10X smaller loss density than Nano-crystalline
Input Output capacitors	Aluminum Electrolytic	MLCC(X7R)	10X higher energy density

The Si-substrate of GaN-on-Si wafers opens new trend of research to increase the functionality and performance of nitride-based devices. In (Chung, Ryu, Lu, & Palacios, 2010) describes the total or partial removal of Si-substrate is beneficial for advanced devices like the heterogeneous on-chip integration of GaN and Si transistors, N-face GaN devices and ultra-high-voltage GaN power switches. As a result, the devices become competitive for the Si-devices in terms of cost, breakdown voltage, and performances.

A comparison between SiC and GaN devices has been reviewed in (Kaminski & Hilt, 2014). It shows that GaN becomes ideal for high-frequency ICs applications where breakdown voltage up to 1Kv and maximum current in between 10A to 40A. On the other side, SiC devices are mostly suited for discrete devices or modules blocking 1Kv and above and virtually no current limitation. SiC devices have shown high on-state

resistances as compared to GaN devices for the breakdown voltage below 1Kv. On the contrary, at high breakdown voltages, the on-state resistance is the limiting factor for the GaN devices. However, there are some other factors to be considered. GaN devices will remain lateral for some time because of non-conductive interlayers and the high cost of the bulk GaN. At present, the concept of GaN devices on Si substrates could change the performances and cost of the wide band gap devices.

### **2.3.2 High Frequency (HF) Transformer**

An integrated magnetic transformer is proposed for a bi-directional series resonant converter in (Liu, Li, Jang, & Zhang, 2016), where the operating switching frequency varies from 300 KHz to 380 KHz over entire output voltage range. This HF transformer was symmetrical in nature for both primary and secondary windings. It is composed of two primary windings and one secondary winding. The space between one primary and secondary winding can be calculated to adjust the desired leakage inductances.

In (Atalla et al., 2016), presents a design procedure of transformer for LLC resonant bi-directional converter along with power levels up to MW range and DC link voltage up to 300 KV. This design procedure includes multiple aspects like switching frequency, power levels, AC and DC voltage insulation requirements and parasitic parameters. It is also considered the magnetic, mechanical, insulation and thermal effect with this power level.

Multi-winding transformer is designed for the integration of renewable energy sources in (Jafari et al., 2017). The reluctance network method (RNM) is used to design the transformer based on specifications like leakage and magnetizing inductances. This method requires less computational time due to iterative nature of the transformer design and has reasonable accuracy rather than other methods. According to this design,

the leakage inductances can be adjusted by varying the thickness of the insulators between the windings and the magnetic core.

An interleaving technique named maximum interleaving is used for HF transformer design with foil conductors in (Barrios, Urtasun, Ursua, Marroyo, & Sanchis, 2015). This technique successfully reduced the winding losses and constructional complexities as compared to other interleaving methods. The proposed method of HF transformer is achieved higher efficiency and higher power density.

In (Iyer, Prabhakaran, & Vijayan, 2015), described the modified magnetics design for a 2kW LLC converter which operates at 100KHz with SiC devices. A hybrid solution is proposed in this study which combines foil and litz wires for the high voltage transformation ratio and high output currents output. This combination provides better fill factor in the windings and enables lower winding losses. The design also minimized the leakage inductance which decreases the core losses.

A two-core planar matrix converter is designed for a 1MHz 1kW LLC resonant converter using GaN devices (Mu & Lee, 2016). The proposed design reduced the total transformer losses (winding and core losses) with respect to the footprint. It is also explained that more cores matrix transformer can reduce the winding loss further. Thus, for high current applications, this method becomes very effective with more cores to reduce the conduction loss and increased the efficiency.

In (Bahmani, Thiringer, & Kharezy, 2015), described a design methodology for medium-frequency transformer where loss calculation, isolation requirements, and thermal management taking into consideration. To validate this procedure, a 50kW, 1/3 kV, 5kHz prototype was designed. The isolation level was 6kV which is two times the voltage of high voltage side and the measured efficiency was 99.48%.

A planar transformer for the multiple module systems is designed in (Fan & Li, 2011) where coils are encapsulated within multilayer PCB to achieve higher power density as compared to the conventional wire-wound transformer. A triple interleaved winding is utilized to reduce the high-frequency AC resistance of the transformer winding and resulting lower winding loss as compared to no interleaved winding.

An analytical methodology for the design of an HF transformer is presented in (Barrios, Ursua, Marroyo, & Sanchis, 2015). This methodology is suitable for the calculation of transformer core and windings losses, and thermal resistance. A design example of 5kW, 50Hz has been presented for PV converter application with a higher efficiency of 99.70%. Due to this optimal design, the power density is increased to more than 46.5% as compared to commercial one.

#### **2.4 Control of the Bi-directional Resonant Converter**

In this section, the control strategies that have been reported in the literature for the bi-directional resonant DC/DC converter are presented and their key features are critically reviewed. Parameters like wide voltage gain range, reverse energy and soft-switching are all dependent on the control variables that implemented on the resonant DC/DC converter. Figure 2.23 is classified the reported control schemes which will be described in the following subsections.

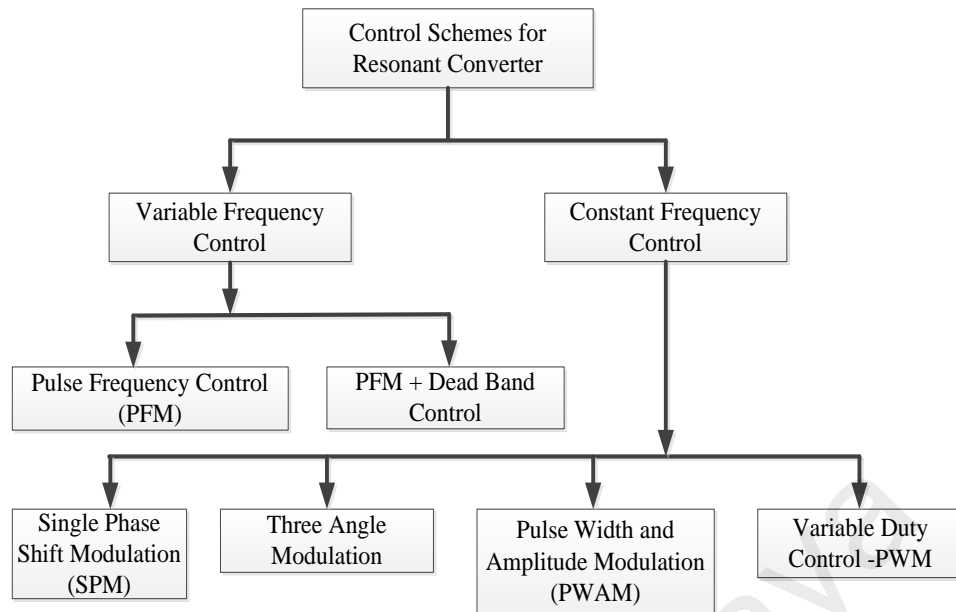


**Figure 2.23: Classification of control schemes of bi-directional resonant converter**

#### 2.4.1 Variable Frequency Control

The variable frequency control is also known as Pulse frequency modulation (PFM) control scheme which is the most widely used method for a resonant converter. This control is performed by varying the switching frequency ( $f_s$ ) with respect to the resonant frequency ( $f_r$ ). Figure 2.24 shows the simplified block diagram of a variable frequency controller. The output voltage of the converter is compared with the reference and the error voltage ( $V_{err}$ ) is feed to the PI controller. Finally, the following block generates the switching pulses using the calculated switching frequency generated by PI controller. There have been many papers that are either proposing improvements to the modulation or adding an extra control circuitry with PFM. A representative selection of these is reported in chronological order:

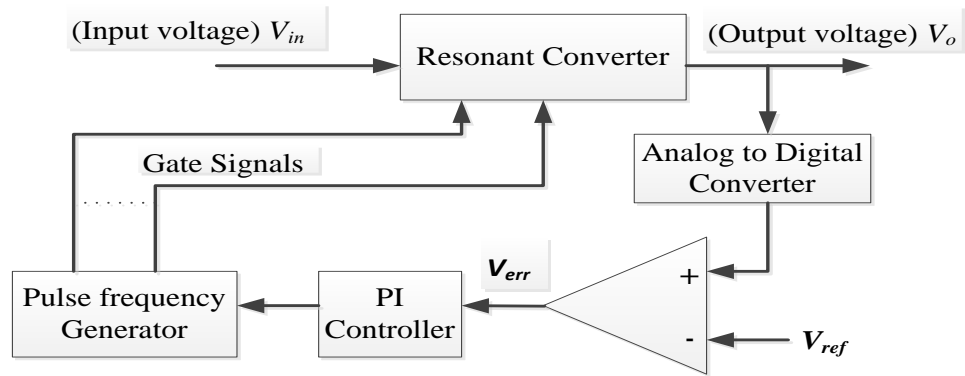


**Figure 2.24: Block diagram of a variable frequency control for resonant converter.**

In (Wei et al., 2010), a bi-directional CLLC type converter is reported for the uninterrupted power supply system. The conventional PFM with two current sensors is used to control the power flow and gate pulses. It is not stated clearly that, how the extra capacitor with LLC resonant tank has become advantageous in BDC and how the asymmetric CLLC network would work in the reverse direction. Like unidirectional LLC resonant converter, wide frequency variation is required to achieve desired voltage gain which increased the size of the magnetics in the converter. The forward efficiency is degraded at minimum input and light load condition due to the high circulating current flowing for long time in the converter.

A bi-directional CLLC type resonant converter (Jung et al., 2013) is designed for a low voltage direct current power distribution system. This converter is similar to the one presented by (Wei et al., 2010). An extra inductor is used to make the converter symmetrical for both forward and backward power flow directions. The proposed converter has combined three control techniques associated with PFM: a Dead band control for deciding power flow directions, a switch control for power flow transitions, and a soft-start control for reducing electrical stresses in the converter devices. But the converter still has high turn-off switching losses and conduction losses due to wide

frequency variation under wide input voltage. A 5kW prototype has been designed to validate the concept. The highest efficiency of 97.8% is achieved at 4kW.

In (Zahid, Dalala, Chen, Chen, & Lai, 2015), a detailed design procedure is represented for a bi-directional CLLC type resonant converter for a battery charging application. This converter is similar to LLC type resonant converter except an extra inductor and capacitor used on the secondary side. The structure becomes symmetrical with CLLC tank but the voltage gain characteristics for both BCM (battery charging mode) and RM (regeneration mode) are different for all loads and switching frequency variations. Simple PFM has been implemented in this converter to regulate the output voltage, while there was no other control associated with PFM for the automatic transition in between BCM to RM or vice versa. The circulating current still exists for the longer time period at minimum input voltage condition which hinders the efficiency of this converter. To achieved maximum voltage gain, the magnetizing inductance is designed to very low value which is responsible for the high magnetizing current resulting in huge conduction losses, increased apparent power requirements for switches and also increased peak voltage requirements for the primary side capacitor.

A bi-directional DAB LLC type resonant converter for energy storage systems is proposed in (Tianyang et al., 2015). An extra inductor is added to make the topology symmetrical in any operating modes, which increases the power loss and cost for the system. A new variable frequency control scheme has been proposed where the power flow direction and output power of the bi-directional LLCL converter can be changed automatically and continuously. According to this control, the converter is always operated below the resonance frequency and having the same frequency to all switches, but the pulse width of gate drive signals for primary and secondary switches are different based on the voltage gain. The voltage gain is still limited to maintain high

conversion efficiency otherwise reverse energy will be increased with switching frequency variation to achieve high gain range. The converter is like unidirectional LLCL converter with diode rectifier when the gain more than unity and ZVS can be maintained up to parallel resonance frequency for both forward and backward power flow. On the other hand, the converter becomes out of ZVS especially at forward mode when the gain lower than unity. This converter is validated with 1kW prototype and has a maximum efficiency approximately 96% at full load condition. The measured efficiency in forward operation is lower compare to conventional LLC converter with diode rectifier due to high switching and conduction losses at gain 0.8. Though, the efficiency is approximately 5% greater than conventional DAB converter over most of the load and designed dc link voltage conditions.

Pulse frequency modulation for resonance converter is advantageous in terms of wider soft switching range and voltage regulation while it requires extra control circuitry for the bi-directional power flow applications.

#### **2.4.2 Constant Frequency Control**

The conventional phase shift modulation provides the constant frequency operation for the resonant converter. The power flow direction and magnitude can be easily controlled by changing the switch control signals. Figure 2.25 shows the simplified block diagram of a constant frequency phase shift controller. Due to the improved topologies and variants, the conventional phase-shift modulation has been modified in several ways. In this section, the most widely used methods are presented in chronological order:

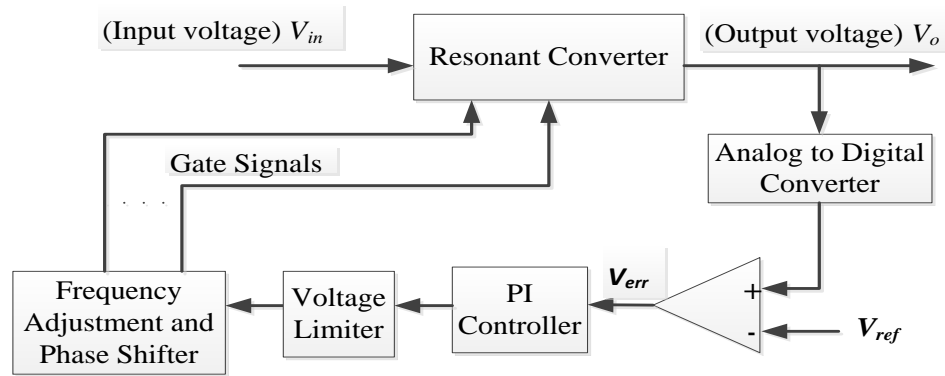


**Figure 2.25: Block diagram of a constant frequency phase shift control for resonant converter (Li & Bhat, 2010).**

In (Li & Bhat, 2010), authors are presented a DAB series resonance converter (DABSRC) for a certain range of input voltage and load conditions. Single phase-shift modulation (SPM) with a constant frequency is implemented to regulate the amount of power transfer to the load, whereas the direction of power flow was also dependent on the polarity of the controlled variable. All the switches worked either in ZVS or ZCS for a certain range of input voltage and load variations. The gain range is limited to maintain the soft-switching for all the input/output and load variations. However, the DABSRC has inherent limitation for ZVS to all switches for the wide range of input/output and load variations. This type of converter undergoes hard-switching for certain operating ranges and causes serious switching losses that degrade the converter performances in terms of efficiency. The proposed design is validated by a 200W prototype.

In (Xiaodong, 2014), a dual-bridge LLC resonant converter with fixed frequency single phase shift control is proposed and analyzed using modified fundamental harmonic approximation approach. ZVS is secured to all switches for all load variations at unity voltage gain. This converter has similar performance like (Li & Bhat, 2010), except that magnetizing inductance of the HF transformer has been added to the resonant tank components to secure ZVS. Due to the low value of magnetizing

inductance, high circulating current appeared at light load condition which degraded the efficiency. The voltage gain of this converter is limited to unity to maintain the ZVS over the wide load range and the switching losses are appeared, especially when the voltage gain deviates from the unity. Therefore, the converter becomes unsuitable for wide input voltage applications.

In (Twiname, Thrimawithana, Madawala, & Baguley, 2014), presents a new DAB converter with a tuned LCL resonant tank network. A simple control scheme with a constant frequency is employed, where each bridge is driven with equal PWM as keeping the constant phase shift between the bridges. The phase shift is fixed at  $+90^{\circ}$  or  $-90^{\circ}$ , to regulate the direction of power flow. The magnitude of the power transfer is controlled by the pulse width of three-level AC voltages from the bridges while keeping the phase shift between them constant. The tuned network with this controlled technique minimizes the bridge currents and reactive power requirement of the converter which reduces the conduction and switching losses and also the VA rating associated with the bridges. It also successfully reduced the multiple resonant modes by employing the converter with the resonant frequency. But, the ZVS operation does not maintain to all switches for all the load variations even half of the switches lost ZVS at 50% load condition. Thus, efficiency degraded linearly due to higher switching losses appeared at light load conditions. A 2.5kW prototype with 95% full load efficiency designed to validate the theoretical analysis.

The converter presented in (Twiname, Thrimawithana, Madawala, & Baguley, 2015) is similar to the LCL DAB proposed in (Twiname et al., 2014) except that employed a tuned capacitor-inductor-capacitor (CLC) network which actually used the leakage and magnetizing inductances of the HF transformer. The behavior of the CLC network to the harmonic exist in the inverting voltages from the full bridges is significantly

different as compared to LCL network. In addition, the rest of the pros and cons are similar to the converter presented in (Twiname et al., 2014).

The authors of (Corradini et al., 2012) presented a series resonant DC/DC converter, which is controlled by the three independent phase shift angles to minimize the root mean square (RMS) current from the LC resonant tank. A fundamental harmonic analysis (FHA) is used to calculate the tank voltages, currents and hence the power of the DABSRC. This three angles control strategy increases the input bridge ZVS interval for the wide gain range compared to single phase shift modulation type DABSRC reported in (Li & Bhat, 2010). However, the soft switching range is still limited to the power level. Hard switching is occurred in the input bridge for the wide gain range when the power level below 50%. Furthermore, the input hard switching on this converter is much less severe than the hard switching occurring along the single phase shift modulation type converters. A 1kW prototype is designed with constant switching frequency 100 KHz to validate the theoretical analysis. The measured efficiency is reported above 95% for most of the power range at unity gain condition. The efficiency is degraded at light load nonentity gain condition due to high switching losses. As the minimization of circulating RMS tank current, the efficiency becomes high as compared to efficiency reported in (Wei et al., 2010).

An LC-type DAB series resonant converter with switch controlled inductor is presented in (Yaqoob, Loo, & Lai, 2017) for a wide range of output voltages and currents. A simple single phase shift modulation is used with the switch controlled inductor to maintain the bidirectional flow and voltage gain variations. A common problem of SPM based DAB resonant converter is that the secondary bridge fails to provide soft switching operation especially at light load conditions for wide gain range under unity. However, switch controlled inductor has successfully overcome the

problem of resonant DAB converter and also minimized the circulating current at a nominal operating point. An inductor and switches on the secondary side added extra cost and losses as compare to converter presented in (Li & Bhat, 2010). A prototype of 480W is designed to validate the proposed method. The maximum efficiency of 94.6% is achieved using the designed topology and modulation scheme.

A constant frequency variable duty control (CFVDC) based non-isolated bi-directional current-fed LCL resonant DC/DC converter is proposed in (Rathore et al., 2016) for the DC micro grid application. This converter has superiority in terms of lower magnetic bulk, compactness and higher voltage conversion ratios. The voltage gain should be limited by the high circulating current with high duty ratio, even though there was no such explanation in this study. One of the switches becomes out of the ZVS at light load conditions resulting high switching losses degraded the efficiency at low power conditions. The maximum efficiency is achieved 95.5% at full load for boost operation and 95% for the buck operation. There was no extra control scheme associated with duty control for the automatic transition in between back mode to boost mode or vice versa.

A bi-directional three level LLC resonant converter is designed in (Tianyang et al., 2016) with a constant frequency pulse width and amplitude modulation (PWAM). It has three modes of operation and it can switch among these modes to maintain wide voltage gain. The voltage stresses across the switches and ZVS depend on the converter voltage gain, though ZVS appears only in the primary side switches. In this topology, an extra flying capacitor and auxiliary switches are used, which make the converter operation complex and increases the cost of the converter. Finally, a 1kW prototype is designed to verify the theoretical analysis. The maximum efficiency at high voltage gain is achieved 96.5% with full load condition.

## 2.5 Comparison of Bi-directional Resonant Converter Topologies and Control Techniques

The resonant converters have different soft switching ranges and characteristics due to the variation of resonant tank parameters and control strategies. Compared to the LC type resonant converter, CLLC and CLLLC have wider voltage gain and soft switching range but extra components in the resonance tank which increase the size and cost. And also CLLC and CLLLC resonant converters with PFM need an extra control scheme for the automatic transition between forward to backward power flow. In addition, asymmetric CLLC resonant converter shows the different operations between forward and backward power flow directions as compared to the symmetric resonant converter. On the other hand, phase shifted modulation control schemes have faster bi-directional transition but narrow voltage gain and ZVS range. Phase shifted LLC resonant converter can secure ZVS for the both bridges as compare to other resonant converters. The other two types: LCL and CLC have similar performance but narrow voltage gain and soft switching range. PFM has superiority than constant frequency phase shift control schemes in terms of efficiency and voltage regulation. For instance, a CLLC type asymmetric resonant converter with PFM control (Chen et al., 2010) has reported higher maximum efficiency than LLC type resonant converter (Xiaodong, 2014) at 300W which are 96% and 94.5% respectively.

**Table 2.2: Comparison of Bi-directional Resonant Converter Topologies and Control Techniques**

Topology	Power control	Soft switching Characterization	Soft switching range	Voltage gain range	Bi-directional transition speed	Maximum Efficiency
CLLC type asymmetric resonant, (Wei et al., 2010)	PFM	ZVS for inverter switches, ZCS for rectifier switches	Wide	Wide	Slow	96% (At, 300W)
CLLC type symmetric resonant, (Jung et al., 2013)	PFM + Dead band control	ZVS for inverter switches, ZCS for rectifier switches	Wide	Wide	Slow	97.8% (At, 4kW)
CLLLC type Symmetric resonant, (Zahid et al., 2015)	PFM	ZVS for inverter switches, ZCS for rectifier switches	Wide	Wide	Slow	97.7% (At, 3.15 kW)
LLC type resonant (Tianyang et al., 2015)	PFM	ZVS for inverter switches, ZCS for rectifier switches	Wide	Narrow	Slow	96% (At, 1 kw)
LLC type resonant (Xiaodong, 2014)	SPM	ZVS in both bridges	Narrow	Unity gain only	Fast	94.5% (At, 300 W)
LLC type (Tianyang et al., 2016)	PWAM	ZVS for inverter switches, ZCS for rectifier switches	Wide	Wide	Fast	96% (At, 1 kW)
LCL type Resonant (Rathore et al., 2016)	CFVDC-PWM	ZVS for all switches	Narrow	Wide	Slow	95% (At, 350 W)
LCL type resonant (Twiname et al., 2014)	Phase shift modulation	ZVS for half of the total switches	Narrow	Narrow	Fast	96% (At, 2.5 kW)
CLC type resonant (Twiname et al., 2015)	Phase shift modulation	ZVS for half of the total switches	Narrow	Narrow	Fast	95% (At, 4 kW)

Table 2.2: Continued

Topology	Power control	Soft switching Characterization	Soft switching range	Voltage gain range	Bi-directional transition speed	Maximum Efficiency
LC type series resonant, (Li & Bhat, 2010)	SPM	ZVS for inverter switches, ZCS for rectifier switches	Narrow	Narrow	Fast	95% (At, 200 W)
LC type series resonant, (Corradini et al., 2012)	Three angles phase shift modulation	ZVS secured up to 50% load only	Narrow	Narrow	Fast	98.3% (At, 530 W)
LC type series resonant, (Yaqoob et al., 2017)	SPM	ZVS for inverter switches, ZCS for rectifier switches	Narrow	Narrow	Fast	94.6% (At, 480 W)

## 2.6 Summary

The topological structures that have been designed to operate, both in terms of maximum power and their interface voltages are reviewed in this chapter. Among all the topologies, stacked type structure is the best suitable for high voltage applications due to low voltage stress across the switches. It is used only for unidirectional power flow applications. For this study, it is incorporated with the active rectifier to enable bi-directional power flow.

Both variable and constant frequency control schemes which are used in previous studies are critically reviewed and their advantages and disadvantages in terms of the converter switching losses, conduction losses and voltage gain range. Based on the reported control schemes, SPM control has the faster transition speed in bi-directional power flow applications. The next chapter explains the stacked bridge based bi-

directional LLC resonant DC/DC converter with SPM control and its steady state operation in terms of control variables.

University of Malaya

## CHAPTER 3: OPERATION ANALYSIS OF PROPOSED LLC RESONANT CONVERTER

### 3.1 Introduction

In this chapter, the topology of bi-directional LLC resonant DC/DC converter with its equivalent circuit model is described. The circuit operation of this converter is explained based on the secondary side single phase shift modulation control scheme for both forward and backward power flow conditions. Besides that, the steady state analysis is investigated on the basis of fundamental harmonic approximation (FHA). Finally, basic characteristics like the converter voltage gain and reactive power are realized with respect to the control variable.

### 3.2 LLC Resonant Converter Topology

The LLC resonant DC/DC converter is shown in Figure 3.1. It consists of two bridges where the stack structure in the primary side of the transformer and the active rectifier in the secondary side. The output can be a DC voltage source like energy storage system, for getting bi-directional power flow or a resistive load with a capacitive filter for getting unidirectional power flow only. The switches on both sides are connected in series with an LLC resonant tank and a high frequency transformer. An extra inductor is used with transformer leakage inductor to get the desired circuit operation.

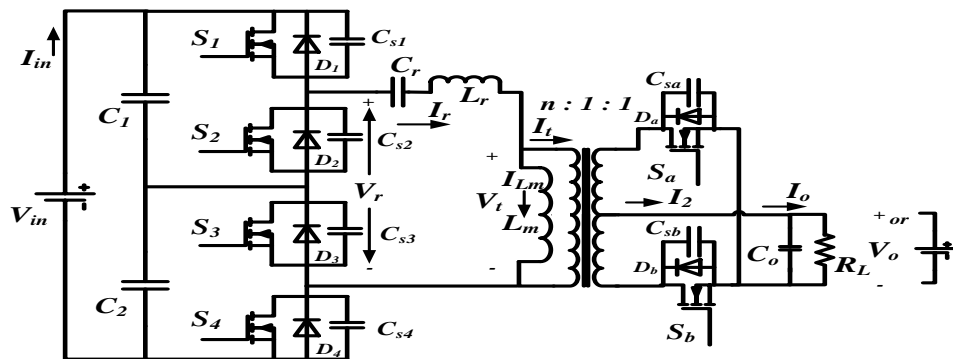


**Figure 3.1: Proposed LLC resonant converter**

The series resonance capacitor  $C_r$  absorbs the DC component from the inverted signal which hinders the transformer saturation (Steigerwald, 1987). In practical application,  $C_r$  can be split into two capacitors and placed on both side of the HF transformer which is suitable for bi-directional power flow applications (Inoue & Akagi, 2007b). The input series capacitors  $C_1$  and  $C_2$  have the same capacitance value, and they used to clamp the primary switch voltage stress to half of the  $V_{in}$  voltage. The value of output capacitor  $C_o$  should be chosen high enough to keep the output voltage free from ripple. The transformer has to be designed in such a way, which keeps the  $L_m$  as high as possible to reduce the conduction losses from the system. The converter always operates with continuous conduction mode, so that the switching frequency is chosen higher than the resonance frequency. The amount of power transfer and voltage regulation is controlled by the phase shift angle between primary and secondary switches, whereas, the power flow direction is also dependent on the polarity of the phase shift angle (Li & Bhat, 2010; Xiaodong, 2014). Based on the power flow direction, two different operating modes are explained in the following sections by means of the typical operational waveforms.

### 3.2.1 Forward Mode of Operation

In this mode, power flows from transformer primary side to the secondary side. The output resistance  $R_L$  represents the real resistive load or the equivalent resistance of the voltage type load. Figure 3.2 shows the steady state waveforms for the forward power flow operation where all the switches in both primary and secondary side have the constant duty cycle of 0.5. The outer pair of a primary switches  $S_1$  and  $S_4$  share the same gate signals, while the inner pair of switches  $S_2$  and  $S_3$  turns on and off simultaneously. The secondary active rectifier switches  $S_a$  and  $S_b$  also turn-on and off with a constant duty cycle of 0.5. The switching frequency always remains higher than the resonant frequency, thus the converter operated in the negative slope region. The phase shift

angle  $\psi$  between primary and secondary switches is used to control the power flow and output voltage regulation. If the phase shift angle is greater than zero i.e.  $\psi > 0$ , power flows from the primary side to the secondary side, otherwise (i.e.  $\psi < 0$ ) power flows in the reverse direction. The forward power flow of proposed LLC resonant DC/DC converter for each switching cycle is divided into the 16 stages. Only  $t_0$ - $t_8$  is introduced and explained due to the symmetrical nature of every half switching cycle.

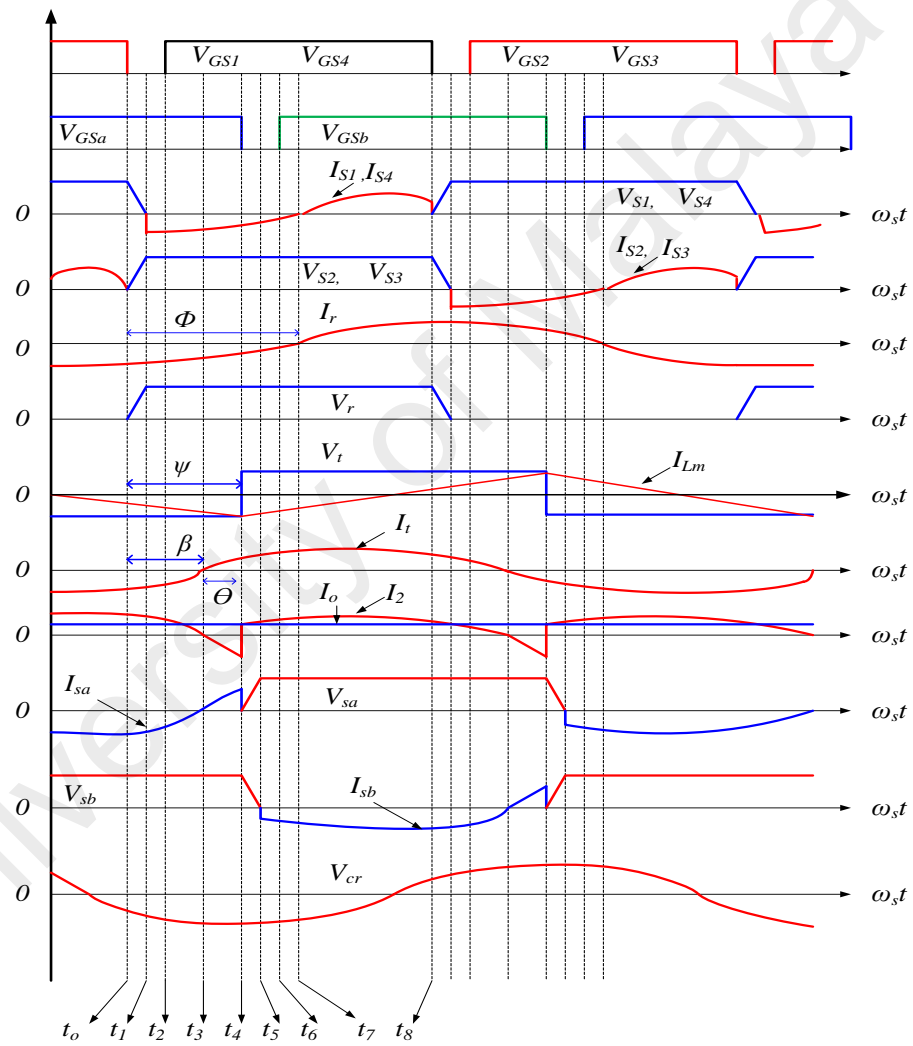


**Figure 3.2: Key operating waveforms of LLC resonant converter in forward mode of operation**

**Interval 1 ( $t_0 \sim t_1$ ):** In the beginning of this interval ( $t = t_0$ ), the gate signals across  $S_2$  and  $S_3$  are turned off. Then, drain-to-source capacitors  $C_{s2}$  and  $C_{s3}$  start charging by the resonance current  $I_r$ . Accordingly, the voltages  $V_{s2}$  and  $V_{s3}$  across  $S_2$  and  $S_3$  rise

gradually from zero to half of the input voltage. On the other hand, the voltages  $V_{s1}$  and  $V_{s4}$  across  $S_1$  and  $S_4$  decrease rapidly from  $V_{in}/2$  to zero by discharging of  $C_{s1}$  and  $C_{s4}$ . In this interval,  $S_2$  and  $S_3$  turn-off with ZVS transition and the voltage across the resonant tank rises gradually to the  $V_{in}$ . This interval lasts until the parallel capacitors in the primary side switches charged and discharged fully.

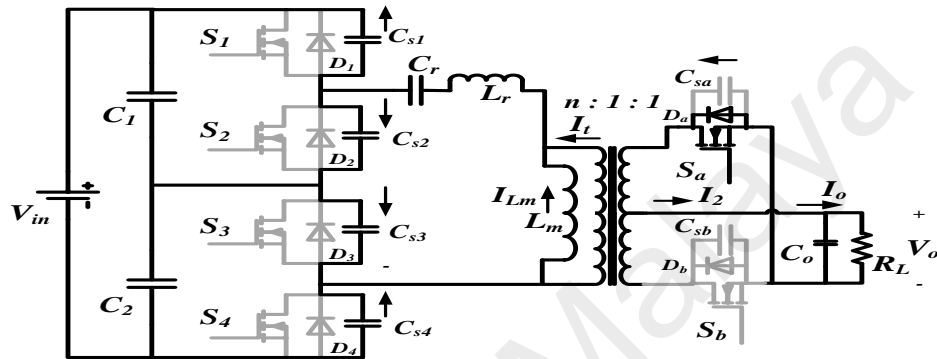


**Figure 3.3: Operation in forward mode during interval 1 ( $t_0 \sim t_1$ )**

**Interval 2 ( $t_1 \sim t_2$ ):** This interval starts when  $V_{s1}$  and  $V_{s4}$  are forced to be zero at  $t = t_1$ ; then, their antiparallel diodes  $D_1$  and  $D_4$  become in forward biased. Thus, tank power is pumped back into the primary side with a negative resonant current flowing through  $D_1$  and  $D_4$  while the secondary current still flows into the load through  $D_a$ . Interval 2 completes as the gating signals of the switch  $S_1$  and  $S_4$  are given.

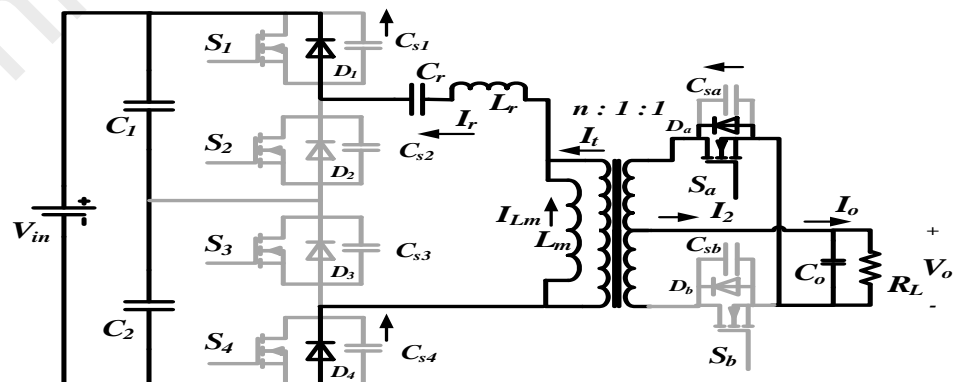


**Figure 3.4: Operation in forward mode during interval 2 ( $t_1 \sim t_2$ )**

**Interval 3 ( $t_2 \sim t_3$ ):** The signals for  $S_1$  and  $S_4$  are triggered, while  $D_1$  and  $D_4$  are still conducting. The current  $I_t$  and  $I_2$  become zero at the end of this interval. Furthermore, the resonant current flows towards zero; consequently, ZVS turn-on can be achieved in  $S_1$  and  $S_4$ .

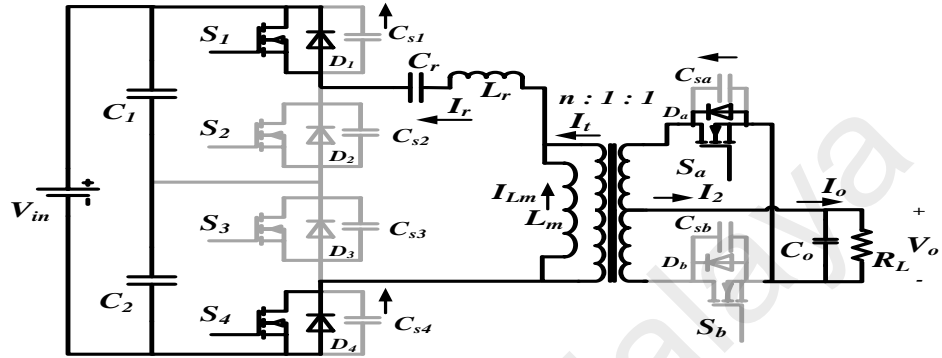


**Figure 3.5: Operation in forward mode during interval 3 ( $t_2 \sim t_3$ )**

**Interval 4 ( $t_3 \sim t_4$ ):** At  $t_3$ ,  $I_t$  reaches zero and starts increasing towards positive value while the secondary current flows in reverse direction through  $S_a$ . Reverse power persists throughout this interval, which increases the conduction losses. This stage ends when the  $S_a$  is turned off.

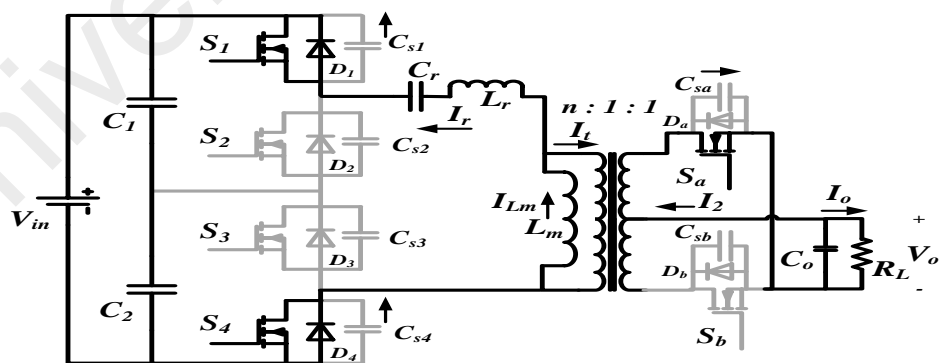


**Figure 3.6: Operation in forward mode during Interval 4 ( $t_3 \sim t_4$ )**

**Interval 5 ( $t_4 \sim t_5$ ):** In the beginning of this interval, the secondary current again flows in positive direction towards the load. The capacitors across  $S_a$  and  $S_b$  are charging and discharging gradually during this interval. Thus, the switch current

commutates to the parallel capacitor and ZVS turn-off can be achieved in the secondary switch  $S_a$ . The reflected voltage across the transformer primary side is switched to a positive value, which increases the magnetizing current ( $I_{Lm}$ ) linearly towards a positive direction.

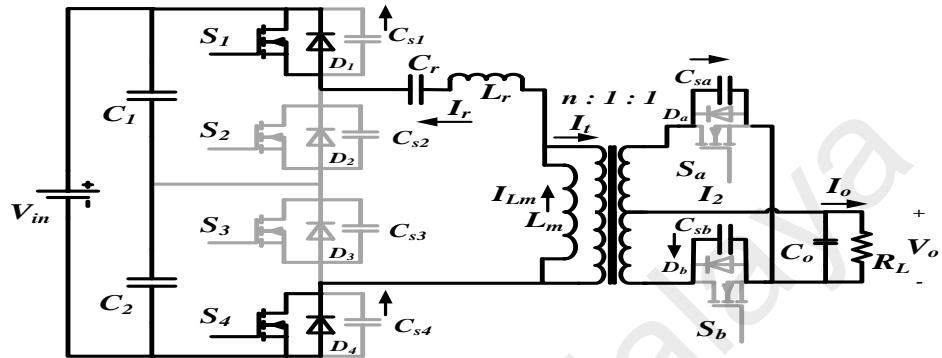


**Figure 3.7: Operation in forward mode during Interval 5 ( $t_4 \sim t_5$ )**

**Interval 6 ( $t_5 \sim t_6$ ):** This interval begins when  $V_{sb}$  is forced to be zero at  $t_5$ ; then the antiparallel diode  $D_b$  becomes in forward biased. As  $D_b$  conducted, the voltage across the transformer becomes positive and the magnetizing current  $I_{Lm}$  flows towards the positive peak. This interval ends when the gate signal is applied across the switch  $S_b$ .

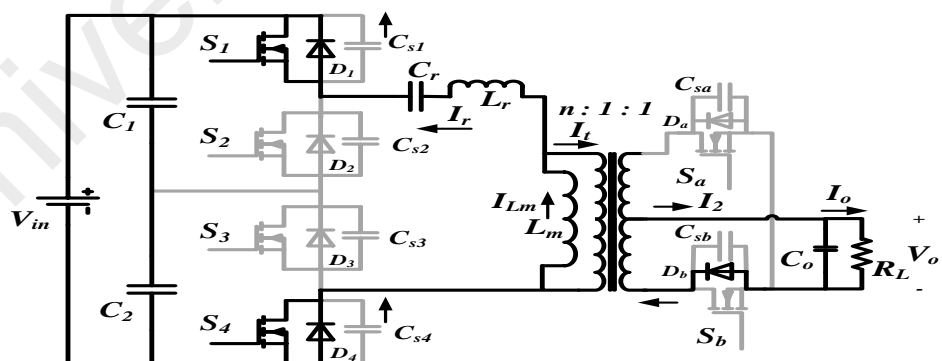


**Figure 3.8: Operation in forward mode during interval 6 ( $t_5 \sim t_6$ )**

**Interval 7 ( $t_6 \sim t_7$ ):** In this interval starts, when gate signal at the switch,  $S_b$  is applied. As the body diode conducted before applying gate signal at switch  $S_b$ , it turns

on with ZVS. The resonant current  $I_r$  remains negative throughout the interval and becomes zero at the end of the interval.

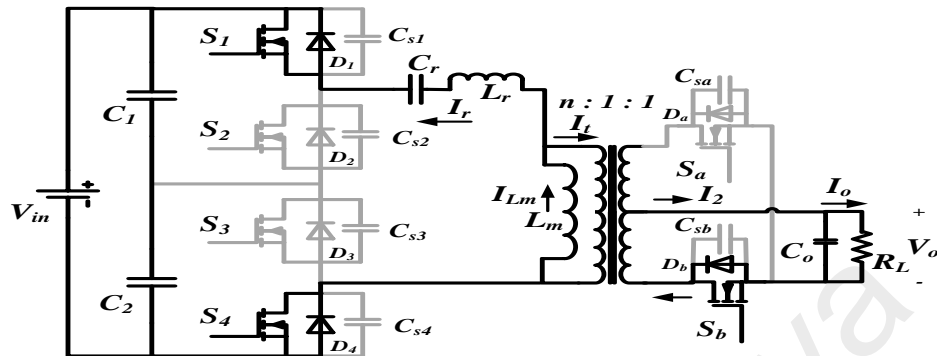


Figure 3.9: Operation in forward mode during interval 7 ( $t_6 \sim t_7$ )

**Interval 8 ( $t_7 \sim t_8$ ):** The resonance current ( $I_r$ ) changes the direction and shifts from body diodes to the corresponding switches in this interval. Thus, the power is transferred from the primary side to the secondary side through the resonant tank. During the half of the switching cycle, this is the only interval where power is transferred from source to the load. This interval completes when  $S_1$  and  $S_4$  are turned off.

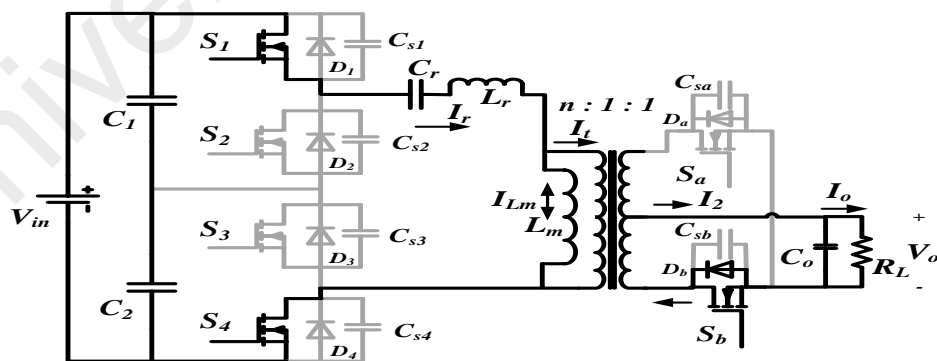


Figure 3.10: Operation in forward mode during interval 8 ( $t_7 \sim t_8$ )

**Table 3.1: Summary of forward mode of operation**

Modes	Switches				Comments
	$S_1$ & $S_4$	$S_2$ & $S_3$	$S_b$	$S_a$	
1	OFF	OFF	OFF	ON	Charging and discharging interval of parallel capacitors across primary side switches
2	OFF	OFF	OFF	ON	Body diodes $D_1$ and $D_4$ become in forward biased
3	ON	OFF	OFF	ON	$S_1$ and $S_4$ turn-on with ZVS
4	ON	OFF	OFF	ON	Reverse energy exists in this mode
5	ON	OFF	OFF	OFF	Charging and discharging interval of parallel capacitors across secondary side switches
6	ON	OFF	OFF	OFF	Body diode of $D_b$ becomes in forward biased
7	ON	OFF	ON	OFF	ZVS turn-on in switch $S_b$
8	ON	OFF	ON	OFF	Power flows from source to the load

### 3.2.2 Backward Mode of Operation

The secondary side becomes the input side when the converter is in the backward mode of operation and the power is transferred to the transformer primary side from the secondary side. The circuit for the backward power flow operation is shown in Figure 3.11, where the output resistance is the real DC load or the equivalence resistance of the voltage type load. Figure 3.12 shows the steady state waveforms for backward mode of operation where each switching cycle is divided into the 16 stages. Only  $t_0$ - $t_8$  is introduced and explained due to the symmetrical nature of every half switching cycle.

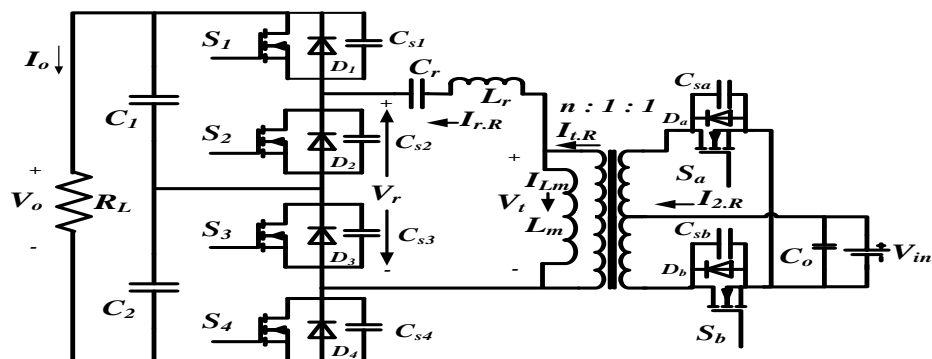


**Figure 3.11: Backward power flow operation**

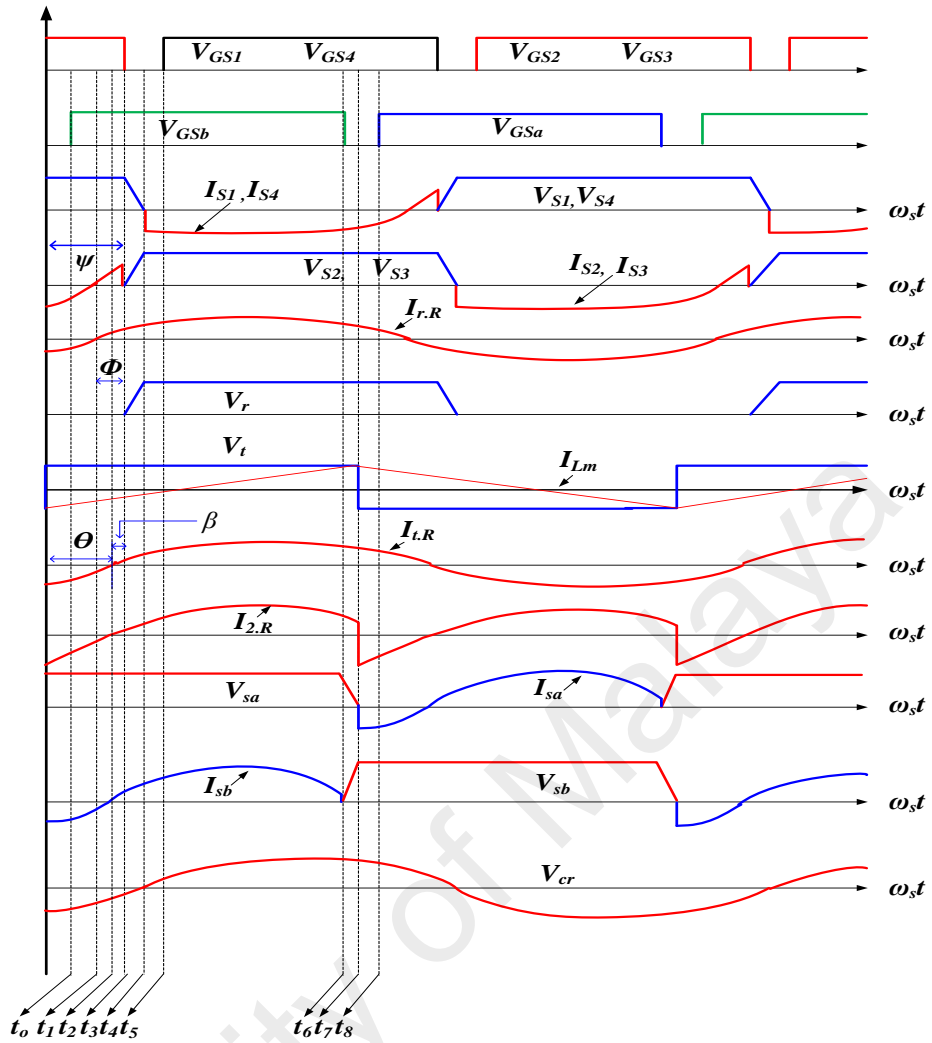


**Figure 3.12: Key operating waveforms of LLC resonant converter in backward mode of operation**

**Interval 1 ( $t_0 \sim t_1$ ):** In the beginning of this interval, the gate signal is applied to the switch  $S_b$  and it turns on with ZVS. Reverse energy persists in this interval due to the negative current on the secondary side. As the switches  $S_2$  and  $S_3$  turn-on, the voltage  $V_r$  remains zero and the resonance tank current is still flowing through the body diodes of the switches. This interval completes when the tank current becomes zero.

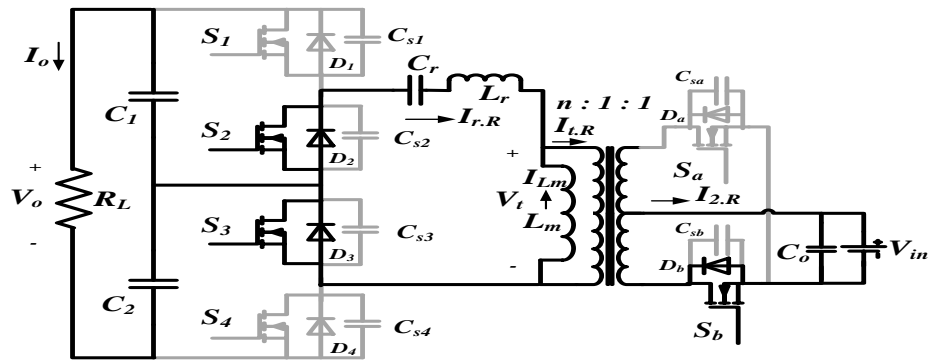


Figure 3.13: Operation in backward mode during interval ( $t_0 \sim t_1$ )

**Interval 2 ( $t_1 \sim t_2$ ):** This interval is similar to **interval 1** except the resonance current  $I_{r,R}$  changes the direction towards positive and shifts from body diodes to corresponding switches. Reverse energy still exists throughout the interval. The interval completes when  $I_{2,R}$  and  $I_{t,R}$  become zero.

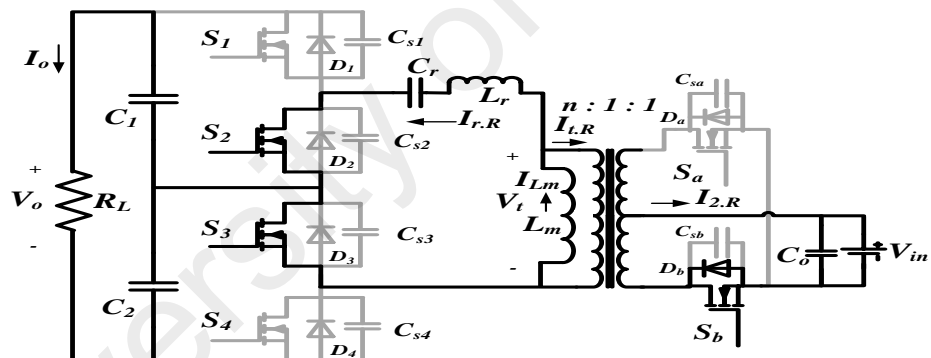


Figure 3.14: Operation in backward mode during interval ( $t_1 \sim t_2$ )

**Interval 3 ( $t_2 \sim t_3$ ):** The secondary current  $I_{2,R}$  flows toward positive direction and shifts from body diodes to the corresponding switch in this interval. So, in this interval, power is transferred from secondary side to primary side. This interval ends when the gate signal of  $S_2$  and  $S_3$  are completely reduced to zero.

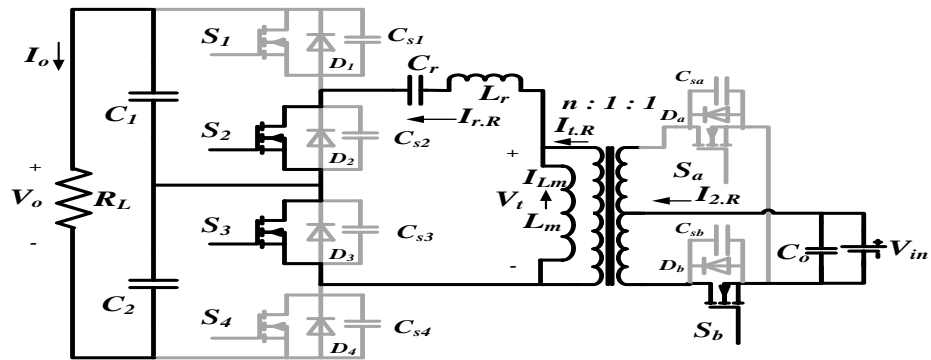


Figure 3.15: Operation in backward mode during interval ( $t_2 \sim t_3$ )

**Interval 4 ( $t_3 \sim t_4$ ):** In this stage, the gate signals across  $S_2$  and  $S_3$  are turned off. Then, drain-to-source capacitors  $C_{s2}$  and  $C_{s3}$  start charging by the resonance current  $I_{r,R}$ . Accordingly, the voltages  $V_{s2}$  and  $V_{s3}$  across  $S_2$  and  $S_3$  rise gradually from zero to half of the input voltage. At the same time, the voltages  $V_{s1}$  and  $V_{s4}$  across  $S_1$  and  $S_4$  decrease rapidly from  $V_o/2$  to zero by discharging of  $C_{s1}$  and  $C_{s4}$ . The current in the switches  $S_2$  and  $S_3$  commutates to the corresponding parallel capacitors to turn-off with ZVS. Meanwhile, the voltage across the resonant tank rises gradually to the  $V_o$ . This interval lasts until the parallel capacitors in the primary side switches charged and discharged fully.

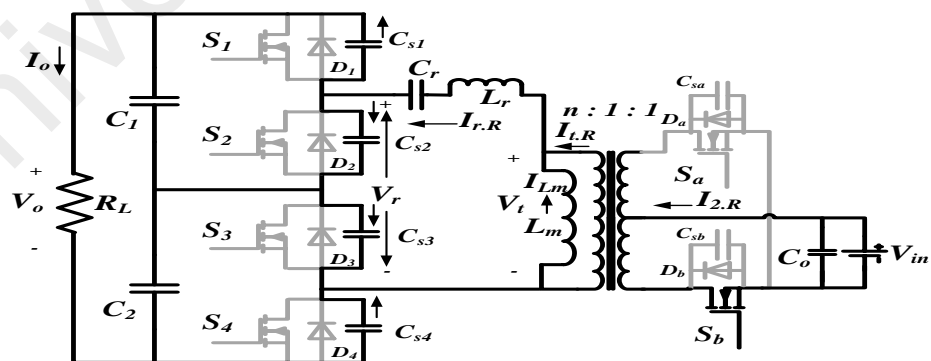
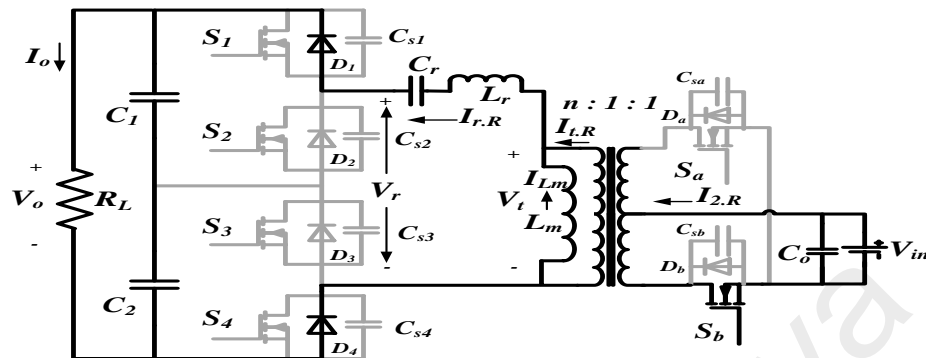


Figure 3.16: Operation in backward mode during interval ( $t_3 \sim t_4$ )

**Interval 5 ( $t_4 \sim t_5$ ):** This interval starts when  $V_{s1}$  and  $V_{s4}$  are forced to be zero and then, their antiparallel diodes  $D_1$  and  $D_4$  become in forward biased. Thus, the power is

transferred from source to the load and resonance tank voltage becomes equal to the  $V_o$ .

This interval completes as the gating signals of the switch  $S_1$  and  $S_4$  are given.



**Figure 3.17 : Operation in backward mode during interval ( $t_4 \sim t_5$ )**

**Interval 6 ( $t_5 \sim t_6$ ):** The signals for  $S_1$  and  $S_4$  are triggered, while  $D_1$  and  $D_4$  are still conducting. Thus, ZVS turn-on can be achieved in  $S_1$  and  $S_4$ . The power is also transferred from source to load via resonance tank throughout this interval. This interval ends when the gate signal across  $S_b$  is turned off.

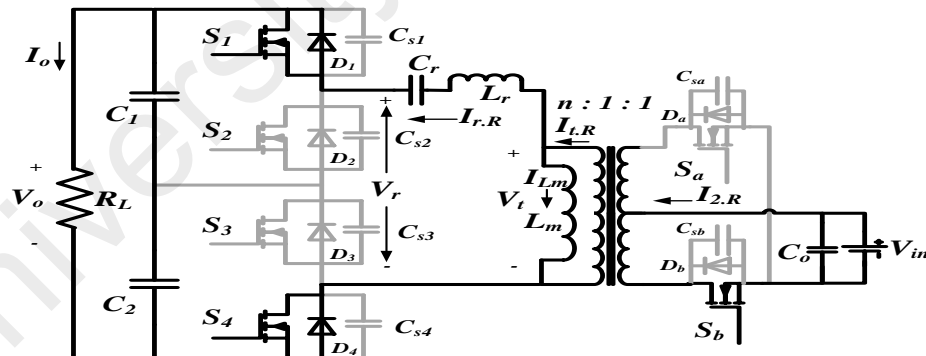


**Figure 3.18: Operation in backward mode during interval ( $t_5 \sim t_6$ )**

**Interval 7 ( $t_6 \sim t_7$ ):** The capacitors across  $S_b$  and  $S_a$  are charging and discharging gradually during this interval. Thus, ZVS turn-off can be achieved in the secondary switch  $S_b$ . The reflected voltage across the transformer primary side and secondary current are switched to the negative at the end of this interval, which increases the

magnetizing current ( $I_{Lm}$ ) linearly towards a negative direction. This interval lasts until the voltage across  $S_b$  is reached to the  $2V_o$ .

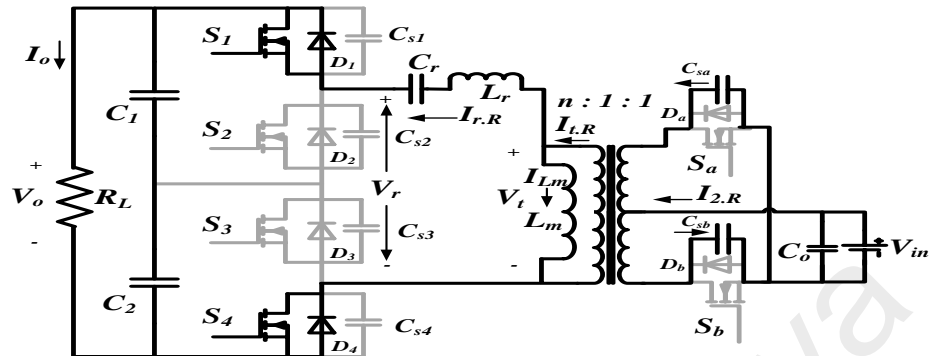


Figure 3.19: Operation in backward mode during interval ( $t_6 \sim t_7$ )

**Interval 8 ( $t_7 \sim t_8$ ):** This interval begins when  $V_{sb}$  is forced to be zero and then the antiparallel diode  $D_a$  becomes in forward biased. Thus, the reflected voltage across the primary side becomes negative in this interval. Reverse energy exists in this stage which helps to secondary switch  $S_a$  to turn-on with ZVS. This interval ends when the gate signal is applied across the switch  $S_a$ .

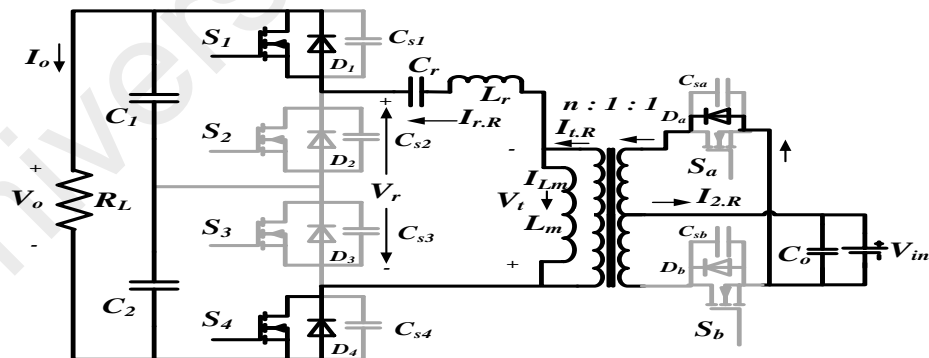


Figure 3.20: Operation in backward mode during interval ( $t_7 \sim t_8$ )

**Table 3.2: Summary of backward mode of operation**

Modes	Switches				Comments
	$S_1$ & $S_4$	$S_2$ & $S_3$	$S_b$	$S_a$	
1	OFF	ON	ON	OFF	$S_b$ turn-on with ZVS
2	OFF	ON	ON	OFF	Reverse energy exists in this mode
3	OFF	ON	ON	OFF	Power flows from source to the load
4	OFF	OFF	ON	OFF	Lossless snubbing capacitors in the primary side switches start charging and discharging
5	OFF	OFF	ON	OFF	Body diodes $D_1$ & $D_4$ become in forward biased
6	ON	OFF	ON	OFF	Power flows from source to the load
7	ON	OFF	OFF	OFF	Lossless snubbing capacitors in the secondary side switches start charging and discharging
8	ON	OFF	OFF	OFF	Body diode $D_a$ becomes in forward biased

### 3.3 Steady State Analysis

The operation of the converter has the similar operation for both forward and backward power flow. So steady state analysis is performed based on forward power flow in this study. The power is transferred from input to the load with the aid of resonant tank components,  $C_r$ ,  $L_r$ , and  $L_m$ . Hence, the current in the resonant tank nearly sinusoidal as shown in Figure 3.2. This allows the use of FHA to analyze the DC characteristic of the converter, which considers that only the fundamental component of the square wave is responsible for transferring the power to the load. Based on the FHA, the AC equivalent two port model is derived as shown in Figure 3.21. All the inductors, capacitors, diodes, switches and the high frequency transformer are assumed to be ideal in this model.

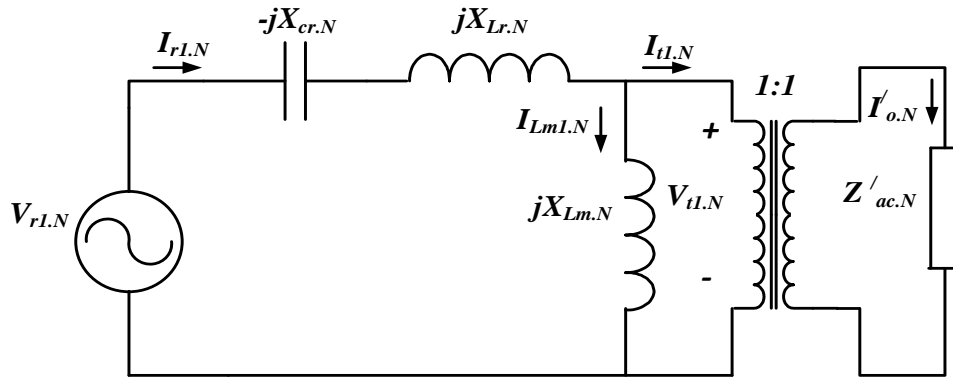


**Figure 3.21: AC equivalent circuit of LLC resonant converter**

The parameters which are transferred to the primary side are denoted by superscript ('/'). The following parameters are normalized for the resonance converter,

$$V_{base} = \frac{V_{in}}{2}, Z_{base} = \sqrt{\frac{L_r}{C_r}} = \omega_r L_r = \frac{1}{\omega_r C_r}$$

$$\omega_{base} = \omega_r = \frac{1}{\sqrt{L_r C_r}}; I_{base} = \frac{V_{base}}{Z_{base}} \quad (3-1)$$

Where,  $\omega_r$  is the angular series resonance frequency.

The normalized switching frequency can be defined as

$$F = \frac{\omega_s}{\omega_r} \quad (3-2)$$

Where,  $\omega_s = 2\pi f_s$  and  $f_s$  is the switching frequency.

The normalized reactances of the resonant tank can be expressed as

$$X_{Lr.N} = F; X_{Cr.N} = \frac{1}{F}; X_{Lm.N} = \frac{F}{K} \quad (3-3)$$

Where,  $K = \frac{L_r}{L_m}$  is defined as inductance ratio.

In Figure 3.21, the input of the resonant tank is a square wave voltage which is generated by the switch network prestage. It is assumed that the higher order harmonics of the inverter output voltage are absorbed by the resonance tank components except the fundamental one,  $V_{rL.N}(t)$ . It can be defined by the equation (3-4) based on the Fourier decomposition. Following that the voltage across the transformer or the equivalent output voltage of the transformer referred to the primary is also a square wave voltage

whose fundamental component can be expressed in equation (3-5), where  $\psi$  is the controlled phase shift between primary and secondary switches.

$$V_{r1.N}(t) = \sqrt{2} V_{r1.N.R} \sin \omega_s t = \frac{4}{\pi} \sin \omega_s t \quad (3-4)$$

$$V_{i1.N}(t) = \sqrt{2} V_{i1.N.R} \sin(\omega_s t - \psi) = \frac{4V_o'}{\pi V_{base}} \sin(\omega_s t - \psi) \quad (3-5)$$

Where,  $V_{r1.N.R} = \frac{\sqrt{8}}{\pi}$  and  $V_{i1.N.R} = \frac{\sqrt{8}V_o'}{\pi V_{base}}$  are the normalized fundamental RMS voltage of  $V_r$  and  $V_i$ .

Due to the approximation of fundamental component of the input voltage, the current in the resonant tank would also be a sinusoidal function. Thus, the normalized fundamental components of resonant current ( $I_{r1.N}(t)$ ) can be defined in equation (3-6), where  $\Phi$  is the phase difference between  $V_{r1.N}(t)$  and  $I_{r1.N}(t)$ . In a similar manner, the normalized fundamental transformer current ( $I_{i1.N}(t)$ ) can be expressed in (3-7) where  $\beta$  is the phase angle with respect to  $V_{i1.N}(t)$ .

$$I_{r1.N}(t) = \sqrt{2} I_{r1.N.R} \sin(\omega_s t - \Phi) \quad (3-6)$$

where,  $I_{r1.N.R}$  is the normalized fundamental RMS resonant current.

$$I_{i1.N}(t) = \sqrt{2} I_{i1.N.R} \sin(\omega_s t - \beta) \quad (3-7)$$

where,  $I_{i1.N.R}$  is the normalized fundamental RMS transformer current.

It can be seen from Figure 3.21 that the output DC current  $I'_{o.N}$  would be equal to the average value of  $I_{i1.N}(t)$  after being actively rectified at angle  $\psi$

$$I'_{o.N} = \frac{1}{\pi} \int_{\psi}^{\pi+\psi} I_{i1.N}(t) d \omega_s t = \frac{2\sqrt{2}}{\pi} I_{i1.N.R} \cos(\psi - \beta) \quad (3-8)$$

Solving equation (3-8) yields to

$$I_{i1.N.R} = \frac{I'_{o.N} \pi}{\sqrt{8} \cos(\psi - \beta)} \quad (3-9)$$

There is a phase difference in between transformer voltage and current due to the active control of the secondary switches. So, AC equivalent resistance ( $R_{ac} = 8R_L'/\pi^2$  or  $\pi^2 R_L'/8$  depending on the type of filter) to represent the secondary side circuit including

HF transformer, the rectifier circuit, output filter and load is no longer valid to analyze the converter equivalent circuit. The current on the secondary side always remains in continuous conduction mode and maintain a phase difference  $\Theta$ , with respect to transformer secondary voltage. However, the circuit, including HF transformer, active rectifier, output filter and load can be represented by equivalent impedance ' $Z'_{ac.N}$ ' instead of  $R_{ac}$ . From the equation (3-5) and (3-9), it can be expressed as the ratio of transformer voltage and current in phasor form.

$$Z'_{ac.N} = \frac{\sqrt{2}V_{t1.N,R} < (-90^\circ - \psi)}{\sqrt{2} I_{t1.N,R} < (-90^\circ - \beta)} = \frac{\cos \Theta}{Q} < (-\Theta) \quad (3-10)$$

Where  $\Theta = (\psi - \beta)$  is the phase angle of the  $Z'_{ac.N}$  and  $Q$  is the quality factor which can be expressed as follows

$$Q = \frac{Z_{base}}{8n^2 R_L / \pi^2} = \frac{\pi^2 Z_{Base} P_o}{8n^2 V_o^2} \quad (3-11)$$

where  $P_o$  is the output power delivered to the load.

From the AC equivalent circuit, the phase angle  $\Theta$  and  $\beta$  can be calculated in terms of controllable phase shift,  $\psi$  and normalized switching frequency as follows

$$\Theta = \tan^{-1} \left( \frac{FK + F - K/F}{Q(F^2 - 1)} - \cot \psi \right) \quad (3-12)$$

$$\beta = \tan^{-1} \left( \frac{Q(F^2 - 1) \csc^2 \psi}{k(F + F/K - 1/F)} - \cot \psi \right) \quad (3-13)$$

The equivalent input impedance of the two port network shown in Figure 3.21 can be calculated as follows

$$\begin{aligned} Z_{in.N} &= \frac{V_{r1.N}}{I_{r1.N}} = j \left( F - \frac{1}{F} \right) + Z'_{ac.N} \parallel j \frac{F}{K} \\ &= |Z_{in.N}| < \Phi = \frac{A + jB}{C} \end{aligned} \quad (3-14)$$

Where,

$$A = Q \left( \frac{F}{K} \right)^2$$

$$B = - \left( \frac{F}{K} \right)^2 Q \cot \psi + \left( \frac{QF}{K \sin \psi} \right)^2 \left( F - \frac{1}{F} \right)$$

$$C = \left(\frac{QF}{K \sin \psi}\right)^2 + \left(\frac{F^2}{K(F^2-1)}\right)^2 - \frac{2QF^3 \cot \psi}{K^2(F^2-1)}$$

$$\Phi = \tan^{-1}\left[\left(F - \frac{1}{F}\right)\left(\frac{K^2}{QF^2} - \frac{2K \tan \Theta}{F} + \frac{Q}{\cos^2 \Theta}\right) + \frac{K}{FQ} - \tan \Theta\right] \quad (3-15)$$

From the  $Z_{in.N}$ , the fundamental normalized resonance RMS current  $I_{r1.N.R}$  can be defined by following equation.

$$I_{r1.N.R} = \frac{V_{r1.N.R}}{\|Z_{in.N}\|} \quad (3-16)$$

Based on the  $I_{r1.N.R}$  value, the maximum voltage stress across resonance capacitor can be determined. Besides that, the DC component of the input voltage also increases the voltage stress of the resonance capacitor. Considering the  $V_{base}$  bias on  $C_r$ , the maximum voltage stress on resonance capacitor is given by

$$V_{cr.max} = \frac{\sqrt{2} I_{r1.N.R}}{F} * V_{base} + V_{base} \quad (3-17)$$

The normalized input DC current is discontinuous and can be the average value of  $I_{r1.N}(t)$ . It can be defined from  $I_{r1.N}(t)$  as

$$I_{in.N} = \frac{1}{T_s} \int_0^{T_s} I_{r1.N}(t) dt = \frac{\sqrt{2}}{\pi} I_{r1.N.R} \cos \Phi \quad (3-18)$$

The normalized DC input power can be expressed as follows

$$P_{in.N} = \frac{4}{\pi^2} I_{r1.N.R} \cos \Phi \quad (3-19)$$

The normalized RMS value of ripple current ( $I_{P.N.R}$ ) flowing in the capacitive filter  $C_o$  can be calculated as follows,

$$I_{P.N.R} = n \sqrt{I_{t1.N.R}^2 - I_{o.N}^2} = \frac{\sqrt{\pi^2 - 8 \cos^2 \Theta}}{\sqrt{8} \cos \Theta} I_{o.N} \quad (3-20)$$

### 3.4 Converter Voltage Gain

From the equivalent circuit in Figure 3.21, the voltage gain can be written as follows:

$$\text{Voltage gain, } \mathbf{G} = \left| \frac{V_{t1.N}}{V_{r1.N}} \right| \quad (3-21)$$

The voltage gain is simplified as follows

$$G = \frac{1}{\sqrt{\left\{ \left( 1 + K - \frac{K}{F^2} \right) - \left[ \frac{Q(F^2 - 1)}{F} * \left( \frac{FK + F - K/F}{Q(F^2 - 1)} - \cot \psi \right) \right]^2 + \left\{ \frac{Q(F^2 - 1)}{F} \right\}^2 \right.}} \quad (3-22)$$

It is seen that, when  $\Theta = 0^\circ$ , the operation of the proposed LLC resonant converter is the same as a conventional LLC resonant converter with diode rectifier and equivalent load can be seen as a resistor (Bo, Lee, Zhang, & Guisong, 2002), (Ivensky, Bronshtein, & Abramovitz, 2011). These two voltage gains are drawn in Figure 3.22. It is observed that the voltage gain of conventional LLC converter always remains under unity in the negative slope region at high  $Q$  values like 2.5. On the other hand, the gain of the proposed converter can be varied widely in the negative slope region even at high quality factor. Thus, the proposed converter can be operated at wide input voltages from no load to full load.

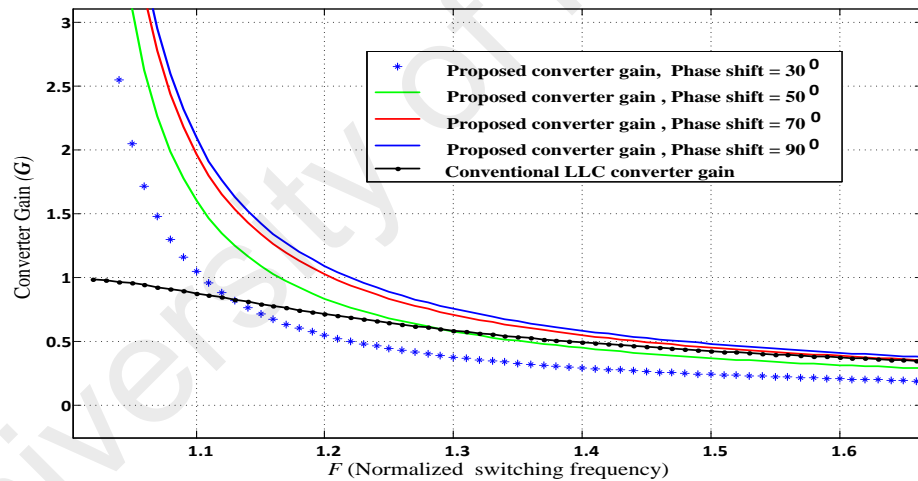


**Figure 3.22: Plots of voltage gain with regards to  $F$  at  $K=0.2$ ,  $Q=2.5$**

### 3.5 Reverse Power

The reverse energy persists in the converter when the phase difference between transformer voltage and current occurs. It increases the conduction losses due to the part of the energy is transferred back and forth between output and input side. It will be high at minimum input voltage condition. The minimum input voltage is limited due to a large amount of reactive power in the system. To simplify the calculation, the reverse

energy per unit time can be represented by the reactive power. The ratio of reverse power to the output power is given in (3-23), which is also shown in Figure 3.23, (Hua & Mi, 2008; Jiang, Chen, Zhang, & Wang, 2013; Tianyang et al., 2015).

$$\left[ \begin{aligned} \frac{P_r}{P_o} &= \frac{1}{2\pi} \tan \theta - \frac{\theta}{2\pi} \\ &= \frac{\left( \frac{FK + F - K/F}{Q(F^2 - 1)} - \cot \psi \right) \tan^{-1} \left( \frac{FK + F - K/F}{Q(F^2 - 1)} - \cot \psi \right)}{2\pi} \end{aligned} \right. \quad (3 - 23)$$

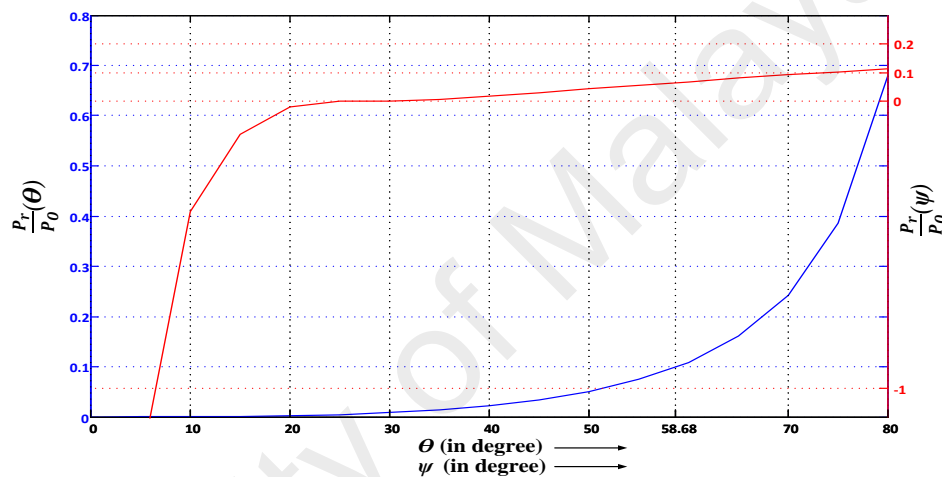


**Figure 3.23: Plots of power ratio with regards to  $\theta$  and  $\psi$  ( $K=0.1, F=1.11, Q=2.5$ )**

From the Figure 3.23, it is seen that reverse power becomes large at the high value of phase shifted angle (i.e. minimum input voltage condition). In order to minimize the conduction losses, reactive power should be as low as possible.

### 3.6 Summary

The modes of operation of proposed converter have been explained in details. Three different analyses: frequency domain method, state plane method, time domain method, can be applied for the steady state analysis of the resonant converter. Due to the complicated calculation in the other two methods, frequency domain approach using Fourier series analysis has been implemented. The so called complex AC circuit

analysis or FHA is considered in the analysis because of nearly sinusoidal AC voltages and currents in the resonant converters. Based on this analysis, the details design procedure and the modified phase shift control scheme with added new control variable besides phase shift will explain in the next chapter.

University of Malaya

## CHAPTER 4: DESIGN OF THE PROPOSED LLC RESONANT CONVERTER

### 4.1 Introduction

This chapter explains the design procedure of resonant tank components and describes the ZVS constraints. To maintain the ZVS to all possible input voltage and load range, an adaptive control scheme is proposed in this chapter. The design is focused on ensuring constant output voltage with high and wide input voltage variations for all load conditions. The prime issues of the design objectives are to increase the gain range and maintain ZVS operation from no load to full load. The power loss models of power components are explained in details. Besides, load characteristic is also evaluated in terms of adaptive control scheme. The specifications of the designed example are as follows: Input voltage,  $V_{in} = 200-400$  V, Output voltage,  $V_o = 48$  V, Output power,  $P_o = 1$  kW.

### 4.2 ZVS in the Primary Side Switches

For the ZVS, the instantaneous value of resonance current at the switching transition should be large enough to charge and discharge the parallel capacitors across the switches fully. Each parallel capacitor across the switch is the combination of MOSFET drain-to-source capacitance and stray capacitance. When,  $S_2$  and  $S_3$  turn-off, the instantaneous value of resonance current charges and discharges the parallel capacitors  $C_{s2}$ ,  $C_{s3}$  and  $C_{s1}$ ,  $C_{s4}$  respectively. Thus, ZVS turn-on for the switches  $S_1$  and  $S_4$  can be achieved once  $C_{s1}$  and  $C_{s4}$  are discharged completely. In similar fashion, the realization of ZVS for another pair of switches is same. Assuming, all the parallel capacitances across the switches have the same value i.e  $C_{s1} = C_{s2} = C_{s3} = C_{s4} = C_{op}$ . The condition of ZVS turn-on in the primary bridge can be derived as

$$\sqrt{2} I_{r1.N.R} \sin(\Phi) \geq \frac{2 C_{op} V_{base}}{t_d} \quad (4-1)$$

$$\tan(\Phi) \geq \frac{C_{op}V_{in}^2}{\pi P_{in}t_d} \quad (4-2)$$

$$f(\Phi) \geq \frac{C_{op}V_{in}^2}{\pi P_{in}t_d} \quad (4-3)$$

where  $t_d$  is the dead time of gate signals.

It should be noted that the ZVS turn-on for the primary side switches can also be secured if the resonance converter will operate with inductive slope region. In this region, the resonance current becomes inductive with respect to inverted square voltage. It can be assumed that the ZVS turn-on will be occurred in the primary side switches if the input impedance of the converter represents inductive. In order to secure the ZVS, the phase angle ( $\Phi$ ) of the input impedance should be positive ( i.e  $\Phi > 0$  ). It can be expressed by equation (3-15) as,

$$\tan^{-1}\left[\left(F - \frac{1}{F}\right)\left(\frac{K^2}{QF^2} - \frac{2K \tan \Theta}{F} + \frac{Q}{\cos^2 \Theta}\right) + \frac{K}{FQ} - \tan \Theta\right] > 0 \quad (4-4)$$

In Figure 4.1, describes the variations of  $\Phi$  and  $G$  with respect to  $\psi$  for different  $Q$  values. The value of normalized frequency ( $F$ ) and inductor ratio ( $K$ ) has been chosen arbitrarily in the Figure 4.1 to find out the ZVS range with regards to wide load variations (i.e  $Q$ ) and control variable  $\psi$ . It is seen that  $\Phi$  goes to the negative value when the voltage gain more than unity at light load conditions (Xiaodong, 2014). Thus, it can be assumed that ZVS will be lost in the primary side switches if  $G$  is larger than one especially at light load conditions. Thus, for the fixed frequency SPM control based converter, voltage gain is limited to unity to maintain ZVS turn-on in the primary side switches at light load conditions.

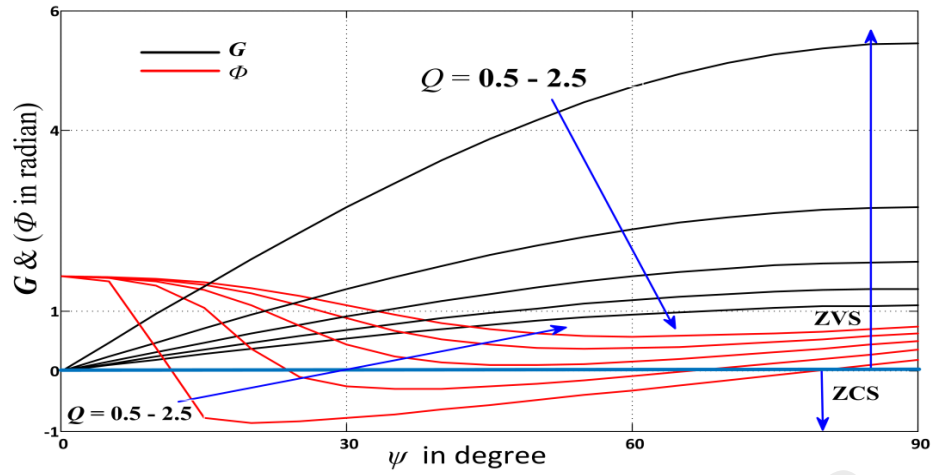


**Figure 4.1: Plots of  $\Phi$  and  $G$  with respect to  $\psi$  for the fixed switching frequency ( $F = 1.2$ ), and  $K$  ( $K=0.6$ )**

A new control variable can be added with SPM control scheme to overcome the aforementioned drawback. The equation (4-4) is the function of  $Q$ ,  $F$  and  $\psi$  respectively. As a function of both  $F$  and  $\psi$ , the ZVS range can be increased by manipulating those control variables with respect to loaded conditions. This could be helpful to mitigate the problem of unity gain with ZVS for the fixed frequency SPM control based converter. To do so, the equation (4-4) can be expressed as follows after some manipulation.

$$\frac{\pi^2 Z_B P_o}{8n^2 V_o^2} \left( F - \frac{1}{F} \right) > \frac{\sin(2\psi)}{2} \quad (4-5)$$

To satisfy the requirements of ZVS in the primary side, solving equation (4-5) at the extreme condition (i.e  $\psi = 45^\circ$ ) yields to

$$\left( F - \frac{1}{F} \right) > \frac{4n^2 V_o^2}{(\pi^2 Z_B P_o)} \quad (4-6)$$

The above equation defines the relationship between normalized frequency and the loaded quality factor. So, the switching frequency can be calculated in each load condition to secure ZVS in the primary bridge within allowable phase shift angle.

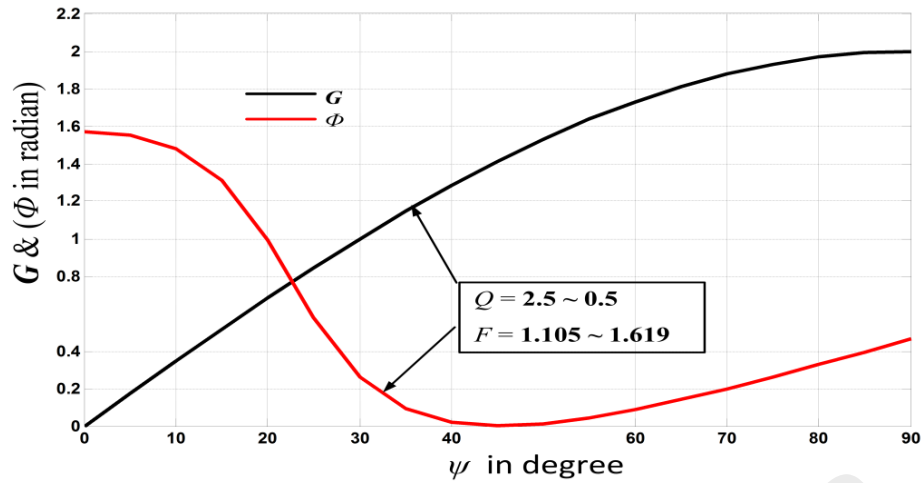


**Figure 4.2: Plots of  $\Phi$  and  $G$  with respect to  $\psi$  at different  $Q$  and  $F$  values respectively**

According to equation (4-6), the frequency is selected sequentially with the load changes. Figure 4.2, describes the variations of  $\Phi$  and  $G$ , as compared to both phase shift angle and switching frequency for different  $Q$  values. In this technique  $f_s$  increases with decreasing load i.e.  $f_s$  changes until the  $\Phi$  becomes positive for all  $\psi$  variations. It is also confirmed from the Figure 4.2, that the frequency selection minimized the effect of  $Q$  values on converter voltage gain ( $G$ ) i.e. the converter gain becomes independent on load conditions.

The ZVS turn-off of the switches depends on the parallel capacitors which are limiting the rate of rise of (dv/dt) voltage during the turn-off. The larger the parallel capacitors are lesser the turn-off losses would be caused. However, the current commutates to the parallel capacitors after removing the gate signals and that help to the switches to turn-off completely before raising the drain-to-source voltages significantly.

### 4.3 Selection of Quality Factor at Full Load

In order to minimize the reactive components, RMS currents and total operating switching frequency variations, full load quality factor ( $Q$ ) should be chosen wisely.  $Q$  is proportional to the size of inductive components and inversely proportional to the size

of the capacitive components. Although,  $Q$  is expected to be small to get the small inductive components including magnetic cores, but, the operating frequency range will be higher under all loads due to the selection of small full load  $Q$  value. So, based on the discussion above,  $Q = 2.5$  at full load is selected.

#### 4.4 Gain Selection

It is seen from Figure 4.2, that, the maximum gain is limited to numerical value 2. The maximum gain also depends on the allowable reactive power in the converter circuit. Figure 4.3, describes the relationship between  $\theta$  and  $G$  for different  $Q$  and  $F$  values. It is seen that  $\theta$  increases with  $G$  and in a particular  $G$  value,  $\theta$  becomes maximum at light load conditions (i.e at low  $Q$  values). As mentioned in equation (3-23),  $\theta$  is related to the ratio of reactive power to output power and it should be limited by  $58.68^\circ$  to allow maximum 10% reactive power in the converter circuit.  $G_{max}$  is chosen as 1.8 for this converter to minimize the reactive power from the converter circuit.

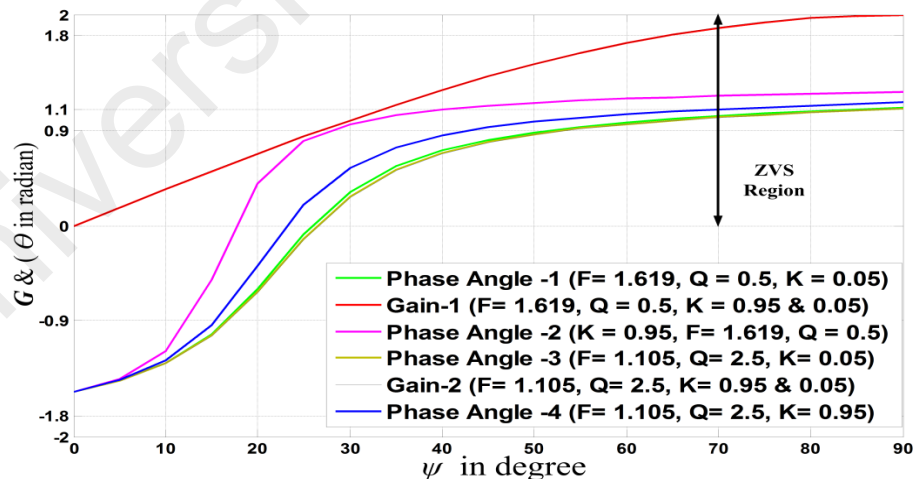


**Figure 4.3: Plots of  $\theta$  and  $G$  with respect to Phase-shift  $\psi$  at different  $Q$ ,  $F$ , and  $K$  values respectively**

So, the transformer turns ratio is calculated as follows

$$n = \frac{N_p}{N_s} = \frac{G_{max} \cdot V_{in-min}/2}{V_o} = 15 : 4 \quad (4-7)$$

The minimum voltage gain is obtained as,

$$G_{min} = \frac{n \cdot V_o}{V_{in-max}/2} = 0.9 \quad (4-8)$$

#### 4.5 ZVS in the Secondary Side Switches

Like the primary side switches, the instantaneous value of the transformer current should be large enough in the switching transition to charge and discharge the secondary side parallel capacitors across the secondary switches. Assuming, the parallel capacitors have the same value, i.e  $C_{sa} = C_{sb} = C_{os}$ .

$$\sqrt{2} I_{t1.N.R} \sin(\Theta) \geq \frac{2 C_{os} V_o}{t_d} \quad (4-9)$$

$$\tan(\Theta) \geq \frac{4 C_{os} V_o^2}{\pi P_o t_d} \quad (4-10)$$

$$f(\Theta) \geq \frac{C_{op} V_{in}^2}{\pi P_{in} t_d} \quad (4-11)$$

The ZVS can also be realized by evaluating the phase angle between transformer voltage and current. It would be secured, if the transformer current is capacitive with respect to the transformer square voltage. Thus, to maintain the ZVS in the secondary side,  $\Theta$  should be positive. From the equation (3-22), it can be written as,

$$\left[ \begin{array}{l} \Theta = \tan^{-1} \left( \frac{B}{A} - \sqrt{\frac{1}{A^2 G^2} - 1} \right) > 0 \\ \text{where, } A = \frac{Q(F^2 - 1)}{F}; B = 1 + K - K/F^2 \end{array} \right. \quad (4-12)$$

#### 4.6 Selection of Inductor Ratio $K$

In the proposed converter, the inductor ratio  $K$  has no effects on the voltage gain. Although,  $K$  increases the range of ZVS on the secondary switches.

If  $\theta$  is positive, equation (4-12) can be further simplified as follows

$$K > \left| \frac{[A \cdot (\sqrt{\frac{1}{A^2 G^2} - 1}) - 1]}{1 - \frac{1}{F^2}} \right| \quad (4-13)$$

According to the modified SPM control scheme, the switching frequency increases with decreasing load, and it will be high at no load. Thus, based on this fact, the inductor ratio  $K$  is calculated. The inductor ratio  $K$  at extreme condition like  $Q=2.5$  (i.e: full load) with,  $G_{min}=0.9$  and  $F = 1.105$  (from equation 4-6), calculated as,

$$K > \left| \frac{[A \cdot (\sqrt{\frac{1}{A^2 G^2} - 1}) - 1]}{1 - \frac{1}{F^2}} \right| > 0.0429 \quad (4-14)$$

It can be confirmed from Figure 4.3, the gain of the converter is unaffected by the inductor ratio  $K$ . It is observed that a small  $L_m$  (i.e large  $K$ ) is useful to extend the ZVS range on the secondary side. But with large  $K$  value, the reverse energy will be more due to the high value of  $\theta$  especially at light load condition. This reverse energy will increase the conduction losses which are responsible for reducing the system efficiency. Thus, if the choice of high  $K$  value is not reasonable, efficiency will be degraded. So,  $K=0.043$  is to be selected in this system to reduce excessive reverse energy as well as to get suitable gain with ZVS.

#### 4.7 Design of Resonance Tank Components

The relationship among  $\Phi$ ,  $\theta$ , and  $G$  with regards to  $\psi$  for different  $Q$  and  $F$  values are plotted in Figure 4.4, where  $K = 0.043$ . It can be confirmed that  $\Phi$  and  $\theta$  are always

positive for the whole operating voltage gain range i.e ZVS transition on the both primary and secondary side switches is maintained when  $G$  in between 0.9 to 1.8. It is also confirmed that the value of  $\theta$  at the maximum gain point is equal to  $57.29^\circ$  (1 in radian) which indicates that the ratio between the reactive power to output power remains within 10% for all phase shift angles according to the desired gain range.

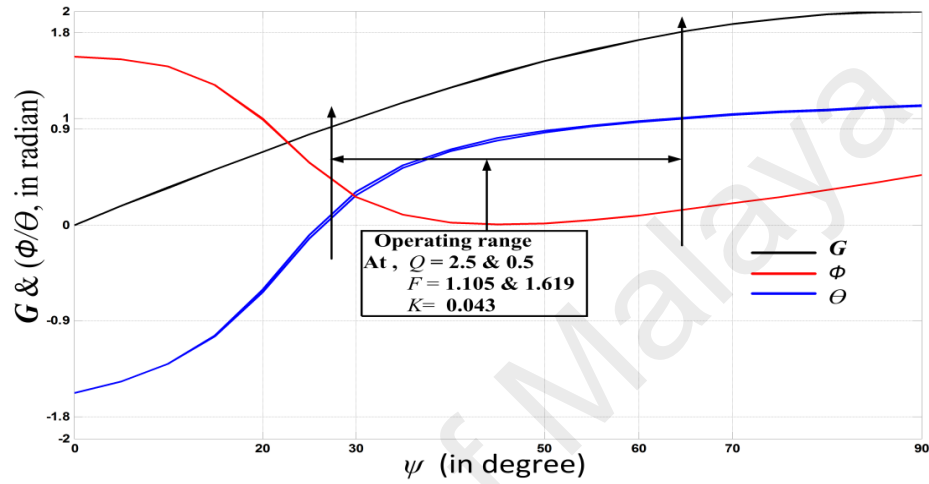


**Figure 4.4: Plots of  $\Phi$ ,  $\theta$  and  $G$  with respect to  $\psi$**

Finally with the help of equations ((3-1), (3-2), (3-3) and (3-11)) resonant tank elements are calculated as follows:

$$L_r = \frac{8QR_L n^2}{\pi^2 \omega_r} \quad (4-15)$$

$$C_r = \frac{\pi^2}{8QR_L \omega_r n^2} \quad (4-16)$$

$$L_m = \frac{L_r}{K} \quad (4-17)$$

The design specifications of the proposed converter are summarized in Table 4.1.

**Table 4.1: Specifications of the Designed Converter**

Parameter - Symbol	Value - unit
Input voltage, $V_{in}$	200 - 400 V
Output voltage, $V_o$	48 V
Resonant Inductor, $L_r$	241.58 $\mu$ H
Resonant Capacitor, $C_r$	55.93 nF
Parallel Inductor, $L_m$	5.61 mH
Rated load Resistance (full load)	2.304 $\Omega$
Rated output power, $P_o$	1 kW

#### 4.8 Modified SPM Control Scheme

To overcome the unity gain problem with ZVS, an adaptive control is added with SPM control scheme. This combination is called frequency adaptive phase shift modulation (FAPSM) control whose has two control variables such as  $\psi$  and  $F$ . These two control variables are independent of each others. According to the control scheme, switching frequency is selected in every load condition to ensure the ZVS in the primary side switches. This frequency selection minimized the effect of loaded  $Q$  values and kept the converter voltage gain characteristics identical for every phase shifted angle. Later, the phase shift angle ( $\psi$ ) can be regulated the output voltage to the desired one with regards to input voltages. The method used to obtain such a signal is shown in Figure 4.5.

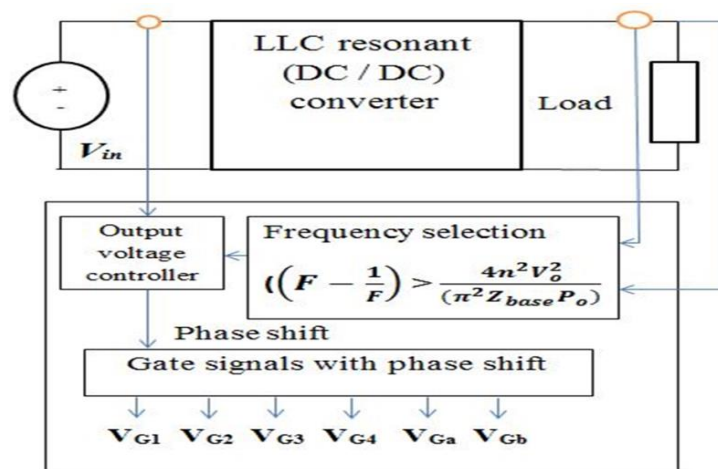


**Figure 4.5: Simplified block diagram of the proposed FAPSM control**

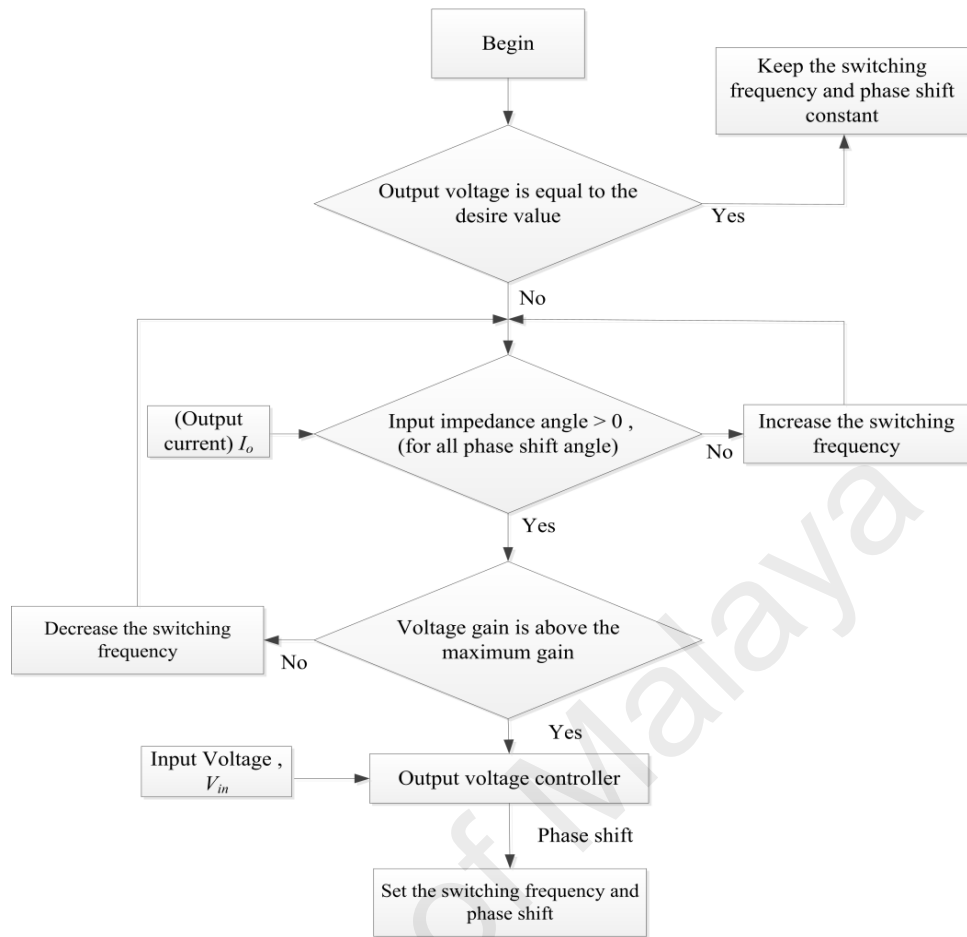


**Figure 4.6: Flow chart of Output regulation method using the proposed control scheme**

The control law is implemented on DSP TMS320F28335 from TI. The DSP samples the inputs by its A/D input and controls the switching frequency ( $f_s$ ) and phase shift by simply changing the register values. Thus, the output can be regulated to the desired value based on the flow chart shown in Figure 4.6.

#### 4.9 Converter Power Losses

The waveforms and magnitudes of currents and voltages are defined by equations in the previous chapter that were based on a lossless circuit model. The lossless model is reasonable if the voltage drops in the switching networks and other circuit components are small relative to the source value. However, to obtain an accurate power model, all possible losses have to take into consideration. Normally the major power loss

contributors are the switching and conduction losses of the switching networks, magnetizing and resistive losses of the magnetic components in the power converters.

The circuit model shown in Figure 3.1 is the ideal model, where all the devices are in ideal conditions. Conduction losses in the switches depend on the switch drain-to-source on state resistances and the currents flowing through them. Resistive losses in the form of  $I^2R$  also form in the winding resistance of the magnetic components and equivalent series resistance (ESR) in capacitors. On the other hand, switching losses depend on the switching nature of the devices.

#### **4.9.1 Conduction Power Losses**

The conduction losses in the primary side switches are dependent on RMS currents following through the switches and on state drain-to-source resistance of the switches. Also, conduction losses in the resonance inductor and transformer are defined by the respective RMS currents and equivalent series resistances. For the secondary side, it is shown in Figure 3.2, that current flows through the switch in reverse direction for the longer time duration in a half switching period. So, switching currents could be divided to flow in between body diode and switch or only through switch itself. However, for the high voltage MOSFET switch, the reverse voltage is large enough to forward bias its body diode, then the current will be partitioned between MOSFET and its diode to achieve the reverse voltage drop. For the low voltage MOSFET, it can be assumed that the body diode will not conduct as the MOSFET drain-to-source on state resistance is insufficiently small that the body diode will not reach the threshold. The body diodes conduct only for short interval of time before turning on the MOSFETs in the primary side and the magnitudes of the currents at that time are very small. Hence, the conduction losses due to body diode can be negligible in this case. Thus, the total conduction losses can be defined as follows,

$$P_{con.losses} = 2 \cdot (I_{r1.N.R})^2 \cdot R_{on-ds-p} + (I_{r1.N.R})^2 \cdot R_{ESR-L} + (I_{l1.N.R})^2 \cdot R_{ESR-T} + (n \cdot I_{l1.N.R})^2 \cdot R_{on-ds-s} \quad (4-18)$$

#### 4.9.2 Switching Power Losses

Switching power losses can be divided into two parts: turn-on losses and turn-off losses. As ZVS maintains in both sides of the switches in the designed system, turn-on energy losses can be assumed to zero completely. Besides, turn-off losses are considered when stored energy in the parallel capacitors is transferred from one MOSFET to another. From (Sukesh, Pahlevaninezhad, & Jain, 2014), the expression for turn-off losses is given by

$$P_{Turn-off-loss} = V_{ds} I_d \left( \frac{t_{ru} + t_{fall}}{2} \right) f_s \quad (4-19)$$

$$t_{ru} = \frac{1}{2} \left[ \frac{(V_{ds} - I_d R_{ds-on}) R_G}{V_{plateau}} (C_{gd1} + C_{gd2}) \right] \quad (4-20)$$

where,  $V_{ds}$  - Drain-to-source voltage at turn-off;

$I_d$  - Drain current at turn-off instant;

$t_{fall}$  - fall time of MOSFET;

$t_{ru}$  - Voltage rise time;

$R_G$  - MOSFET gate resistance;

$V_{plateau}$  - Gate plateau voltage;

$C_{gd1-2}$  - Gate-drain capacitances;

#### 4.9.3 Gate Driver Losses

Gate driver losses for one switching device depend on the energy that supplied by the driver itself during the charging process of the gate and the energy which is stored in the gate of the device at the end of the turn-on. The total energy loss can be defined by the following equation.

The energy loss per switching period is given by

$$E_g = 2 \cdot \left( \int V_g I_g(t) dt - \frac{1}{2} Q_g V_g \right) = Q_g V_g \quad (4-21)$$

with the total gate charge depending on the gate current  $I_g(t)$ ,

$$Q_g = \int I_g(t)dt \quad (4-22)$$

where  $Q_g$  is the total gate charge,  $V_g$  and  $I_g$  are the gate driver voltage and current respectively.

The gate driver power loss can also be calculated from the total energy loss in the driver by following equation,

$$P_g = f_s E_g = f_s Q_g V_g \quad (4-23)$$

#### 4.9.4 Core Losses of Magnetic Components

The losses in the magnetic cores are caused by the magnetic flux induced either by the winding current  $I_w(t)$  as in the case of an inductor or a current fed transformer or by the applied voltage  $V_w(t)$  across the winding in the case of a voltage fed transformer.

For an inductor, the flux density of an inductance value  $L$  is given by

$$B(t) = \frac{L}{NA_e} I_w(t) \quad (4-24)$$

where it is directly proportional to the winding current  $I_w(t)$  assuming a sinusoidal flux waveform for the inductor.

For the voltage fed transformer the derivation of flux density  $B(t)$  depends on the impressed voltage  $V_w(t)$  and according to Faraday's law, it can be defined by

$$\frac{dB(t)}{dt} = \frac{V_w(t)}{NA_e} \quad (4-25)$$

where  $A_e$  is the core cross-sectional area and  $N$  is the number of turns of the winding. As the transformer is driven by the square wave voltage, its flux will be approximately triangular. The voltage is applied during the half of the square wave is  $V_m$  which causes the flux density to increase with slope

$$\frac{dB(t)}{dt} = \frac{V_m}{NA_e} \quad (4-26)$$

The peak magnitude of AC flux density can be determined by the slope of flux density and the length of first sub-interval ( $D T_s$ ).

$$\Delta B = \frac{V_m}{NA_e} (D T_s) \quad (4-27)$$

Based on the flux density, the core loss density can be determined from the manufacturer data for the given core material. For instance, plots of core loss density versus flux density and frequency for N95 material are illustrated in figure 4.7 and 4.8 respectively. It could also be calculated by the improved generalized Steinmetz equation (iGSE) (Venkatachalam, Sullivan, Abdallah, & Tacca, 2002).

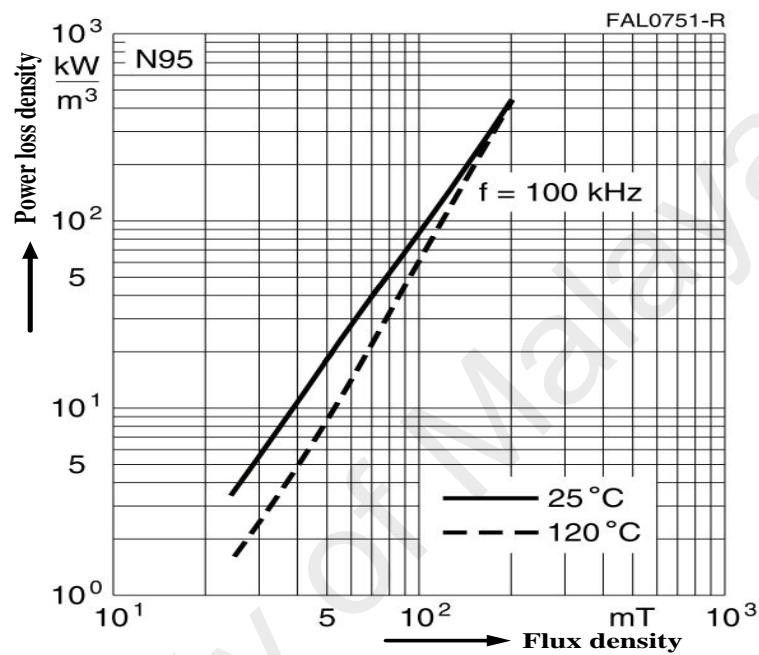


Figure 4.7: Plot of core loss density versus AC field flux density ([www.epcos.com/material](http://www.epcos.com/material))

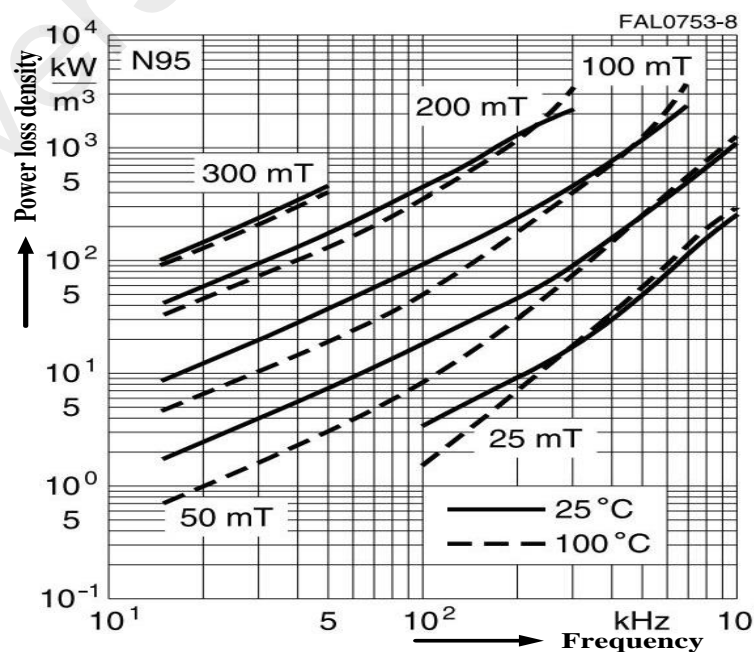
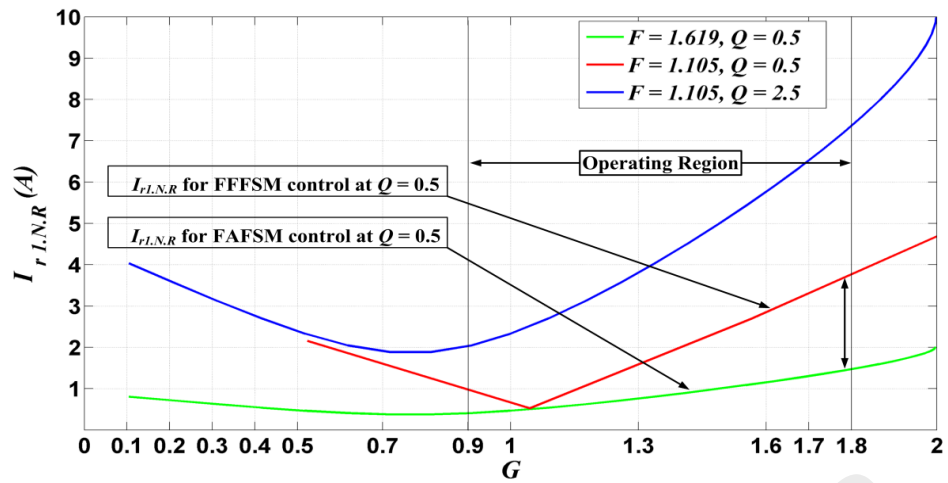


Figure 4.8: Plot of core loss density versus frequency ([www.epcos.com/material](http://www.epcos.com/material))

However, the total magnetic losses depend on the flux density which will change with switching frequency. As the two variable control proposed in this study, the magnetic losses will vary with loading conditions.

#### **4.10 Light Load Efficiency Evaluation**

In fixed frequency SPM control based converter, switching frequency has effects on converter voltage gain as well as resonance RMS current and it should be optimized to get the better efficiency characteristics in terms of loads. Frequency selection according to equation (4-6), minimizes the resonance RMS current to the values that can maintain the ZVS on the primary side and higher voltage gain. Proper selection of switching frequency improves the performance of fixed frequency SPM control based converter (Li & Bhat, 2010; Xiaodong, 2014). Figure 4.9, describes the variations of resonance RMS current in terms of converter voltage gain. Fixed frequency SPM control has larger resonance RMS current as compared to FAPSM control scheme at light load condition even at both buck and boost mode of operation. FAPSM control minimizes the resonance RMS current at light load condition (i.e low value of  $Q$ ) for the whole operating region with respect to fixed frequency SPM control scheme. At the maximum gain point, the magnitude of resonance RMS current with 20% load condition is lower than 50% as compared to fixed frequency SPM control based converter. It has tremendous effects on conduction losses as well as efficiency due to the majority portion of losses is conduction losses in the bi-directional converter. Thus, it can be assured that FAPSM control improves the light load efficiency throughout the operating region of the designed converter.



**Figure 4.9: Plots of RMS resonance current with respect to the voltage gain.**

#### 4.11 Summary

This chapter defined the ZVS range for fixed frequency SPM control based converter. In contrast, an adaptive control has been integrated with SPM control to increase the ZVS operation range for wide load and voltage gain. Based on this control, the parameters like full load quality factor, inductor ratio, and resonant tank components have been designed for the specified power range. The modified control has changed the characteristics of conventional bi-directional DC/DC converter in terms of voltage gain and ZVS range. The RMS resonant current and circulating energy have a huge impact on conduction losses, so their reduction would lead to a significant improvement in power efficiency. The next chapter will describe the simulation and experimental results for the designed converter.

## CHAPTER 5: SIMULATION AND EXPERIMENT RESULTS

### 5.1 Introduction

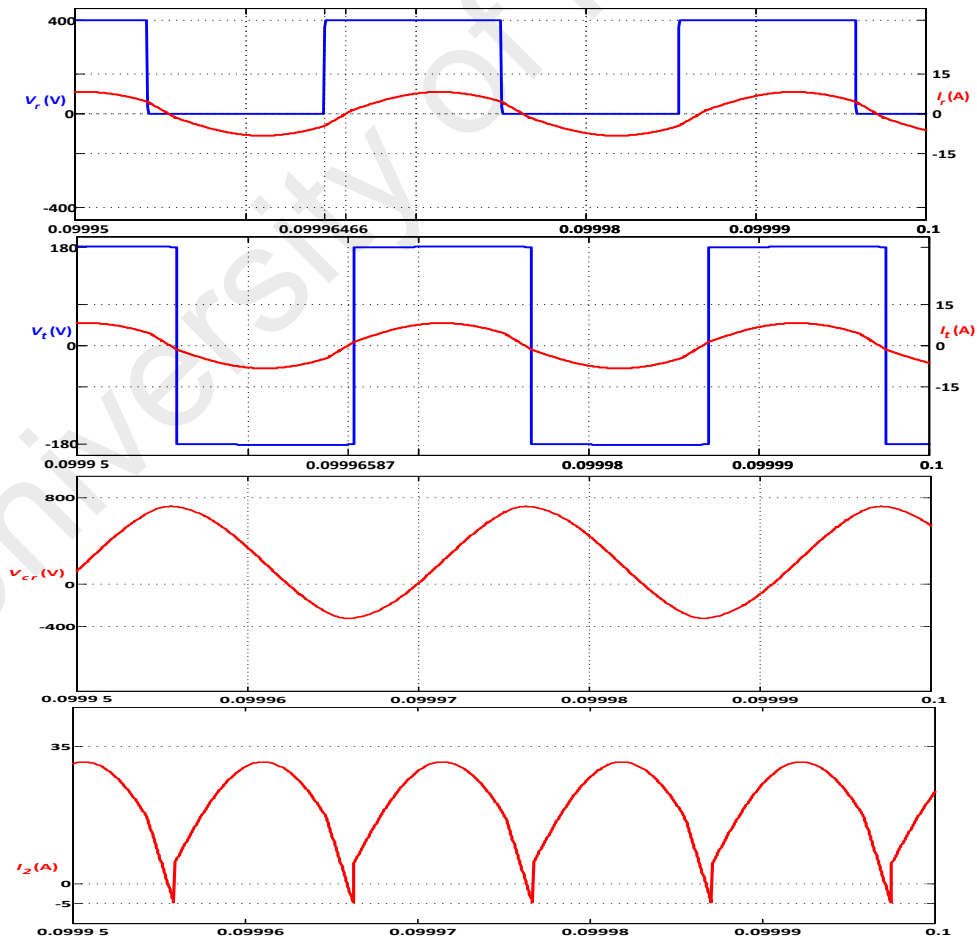
In this chapter, the simulation and experimental results for different input voltage and load conditions are presented. Firstly, all the simulation results are presented to verify the operating range of the designed converter. Secondly, all the experiment results according to simulation are presented to verify the converter experimentally. Then, the estimated power loss breakdown and measured efficiency are drawn for different input and load conditions. Finally, a comparison of designed LLC resonant DC/DC converter is performed with state of the art works.

### 5.2 Simulation Results

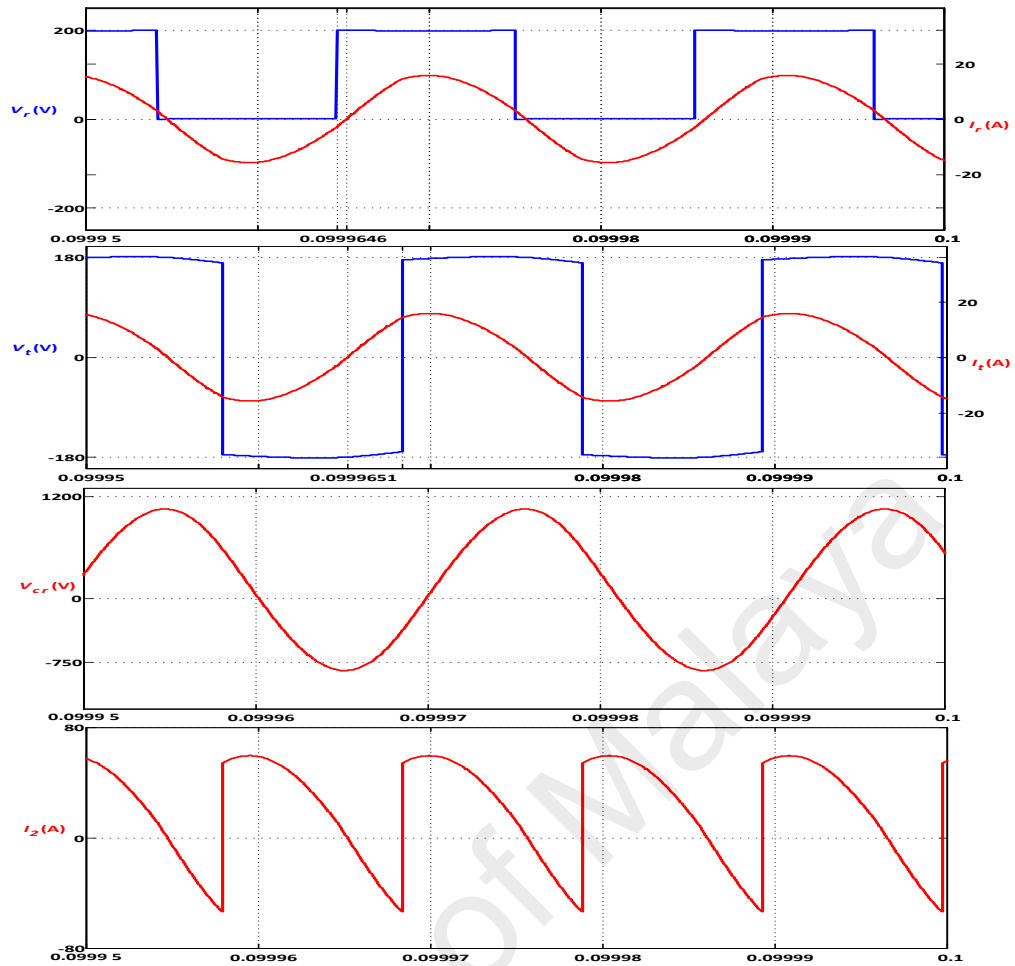
To verify the analytical result, the designed converter is simulated in MATLAB. The simulation is carried out under maximum and minimum input voltages with the full load and 20% load conditions. Figure 5.1-5.4 show the  $V_r$ ,  $I_r$ ,  $V_t$ ,  $I_b$ ,  $V_{cr}$  and  $I_2$  over different inputs and load conditions. Operating frequency changes as the load only and remains constant for the fixed load regardless of input voltages. To remain the output voltage constant,  $\psi$  changes with input variations irrespective of load conditions. It is seen that  $\theta$  becomes higher at low input voltage, which increases the reverse power as well as decreases the efficiency. Therefore, for the same output power,  $I_2$  shows the more negative percentage at 200 V than 400 V input. It is also observed that all the stresses across the resonant tank become higher at low input voltage condition. ZVS turn-on can be verified by evaluating the phase angles of  $I_r$  and  $I_t$  with respect to  $V_r$  and  $V_t$  respectively.

Figure 5.1 represents the voltage and current waveforms of 1kW output power where the input is 400V. It is observed that the output voltage ( $V_r$ ) of the primary bridge is unipolar, stepping from zero to 400V. Thus, the output voltage of the stacked bridge

fails to provide magnetic field reset functionality for the magnetic components. The resonant capacitor  $C_r$  absorbs the DC value of  $V_r$  and provides AC waves for the resonant tank. The currents  $I_r$  and  $I_t$  both are identical due to having the high value of magnetizing inductance. The currents are lagging and leading with their respected voltages. Thus, ZVS turn-on in both bridges is well achieved at the full load. The measured resonant currents in both cases are sinusoidal because of the converter operated with a frequency which is close to the resonance frequency. The angle ( $\theta$ ) between  $I_t$  and  $V_t$  is very small so that small amount of reverse energy flows in the converter circuit which is required for ZVS turn-on in the secondary switches. The secondary current  $I_2$  flows in the negative direction for a small time duration which is also defined by the phase angle  $\theta$ .

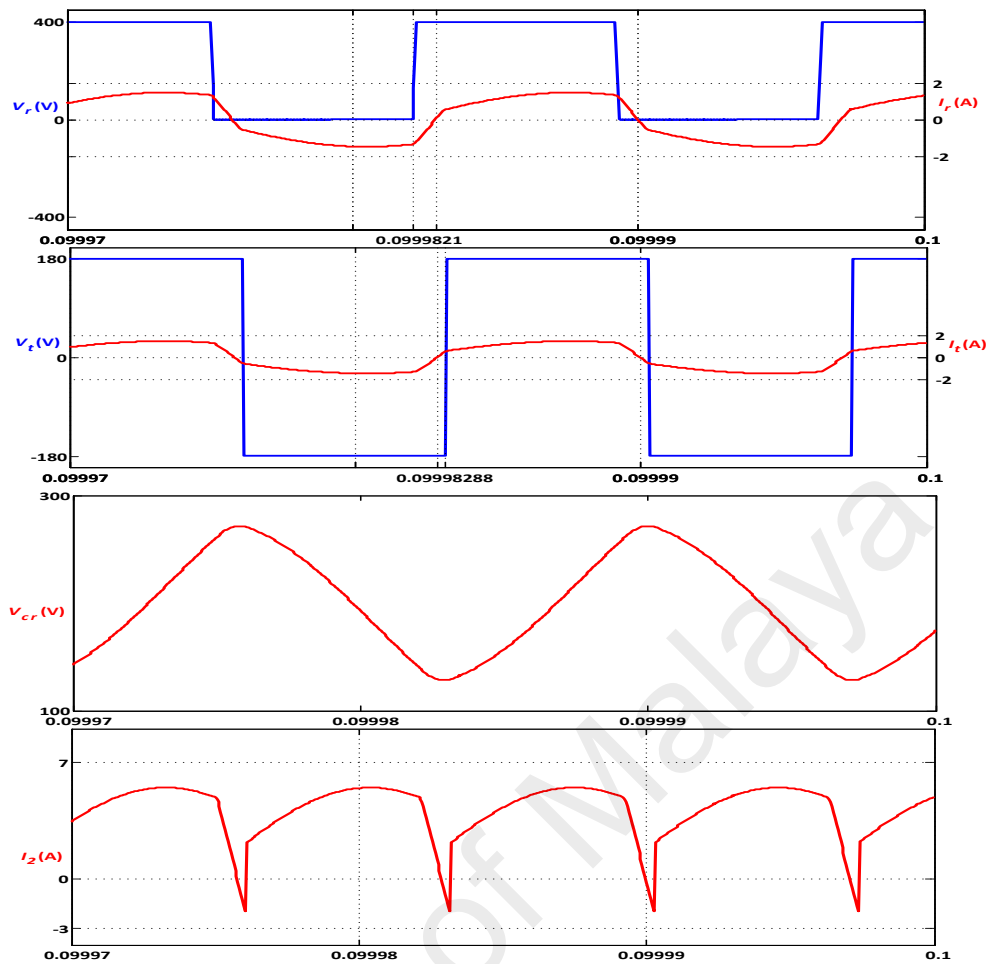


**Figure 5.1: Voltage and current waveforms of proposed converter under 400V input, 48V output and full load condition**



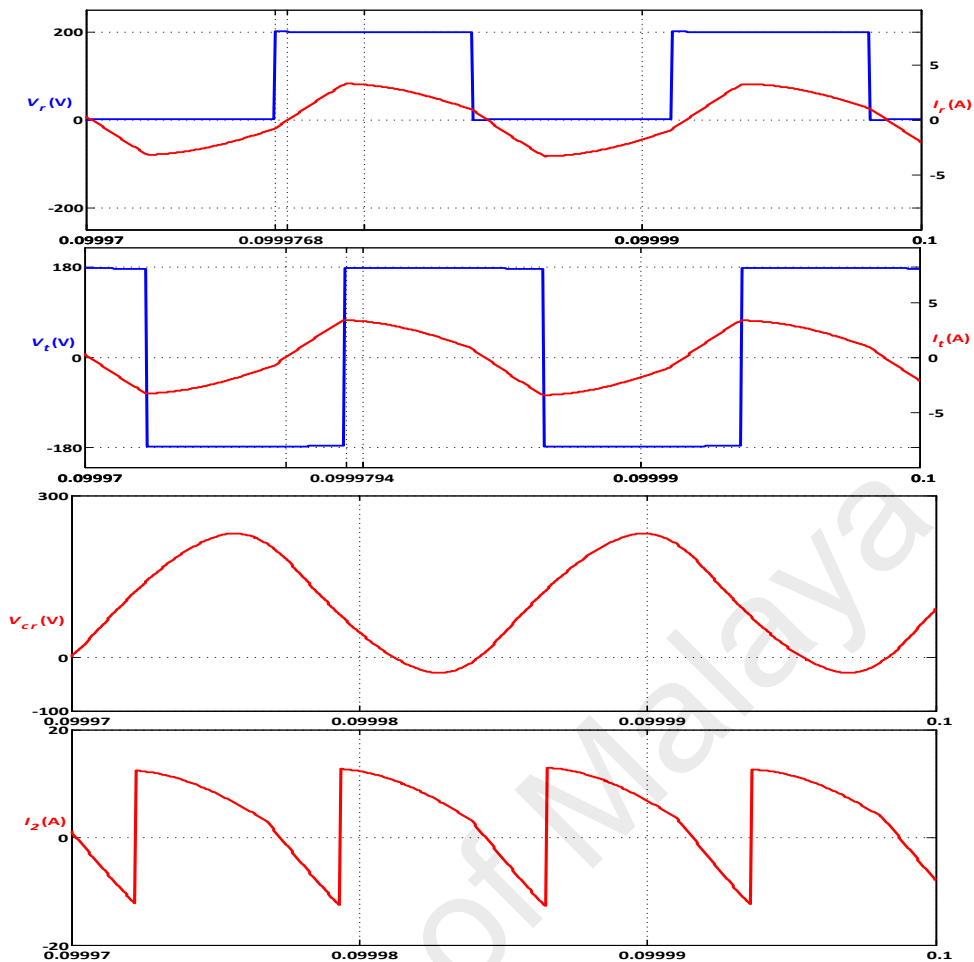
**Figure 5.2: Voltage and current waveforms of proposed converter under 200V input, 48V output and full load condition**

Figure 5.2, represents the full load voltage and current waveforms for maximum voltage gain operation. In this operation, the switching frequency is close to resonant frequency while the phase shift angle ( $\psi$ ) is quite larger to keep the output voltage constant (i.e 48V).  $I_r$  and  $I_t$  are sinusoidal and their RMS values are quite larger than minimum gain operation. As a result, the voltage and current stresses in the resonant tank are higher than the minimum gain operation. For same output power,  $I_2$  goes to the negative for the longer duration at 200V input than 400V input operation. The angle between  $I_t$  and  $V_t$  becomes maximum in this condition, thus a large amount of reverse power persists throughout the operation.



**Figure 5.3: Voltage and current waveforms of proposed converter under 400V input, 48V output and 20% load condition**

Figure 5.3, represents the voltage and current waveforms for 200W where the input voltage is 400V. The switching frequency is no longer close to resonant frequency rather it is significantly higher than the resonant frequency. This is the reason that the currents and  $V_{cr}$  waveforms have deviated from the sinusoidal shape. Like full-load condition, ZVS turn-on is well achieved in this condition also.



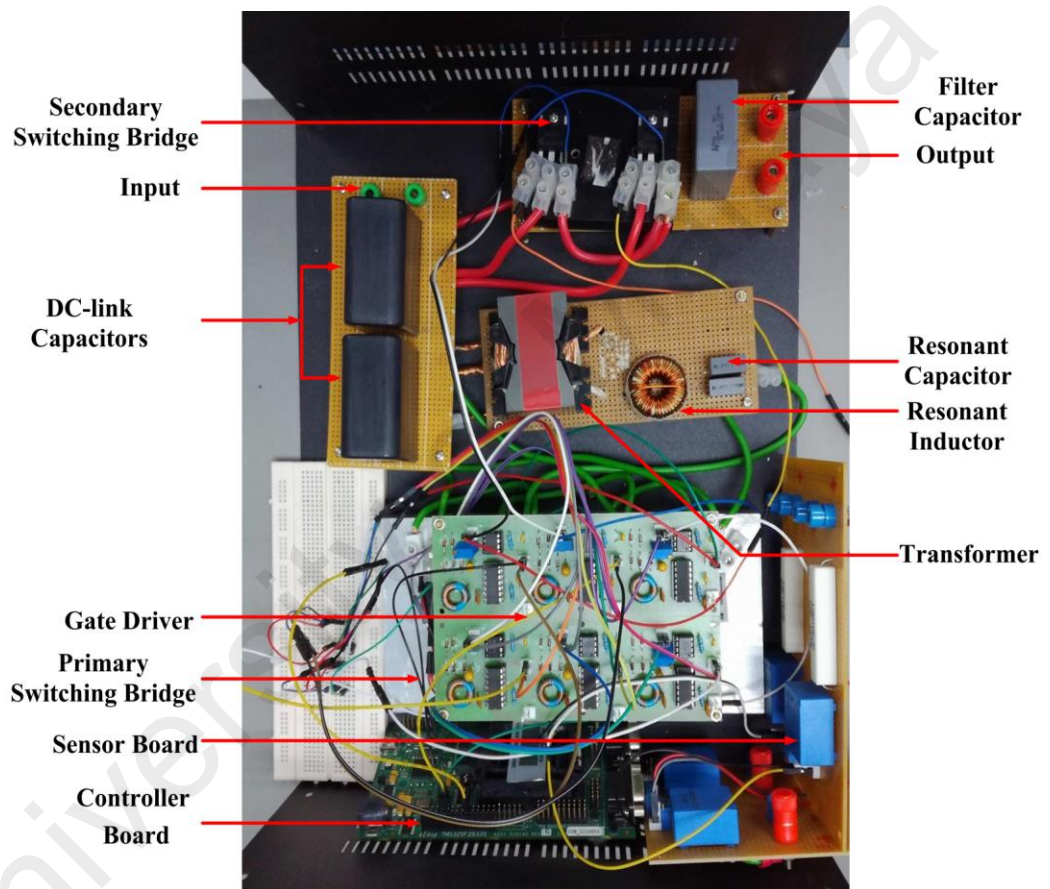
**Figure 5.4: Voltage and current waveforms of proposed converter under 200V input, 48V output and 20% load condition**

Figure 5.4, represents the voltage and current waveforms for 200W where the input voltage is 200V. The voltage and currents of the resonant tank are quite predictable like the full-load minimum gain operation except the higher switching frequency is required according to FAPSM control. It is seen that  $I_2$  has large negative percentage than 400V input operation at 20% load condition.

### 5.3 Experimental Results

A prototype converter is built and tested in the laboratory to verify the designed converter. The prototype image is shown in Figure 5.5. It is designed for maximum 1kW power throughput with MOSFET bridges, running from 200-400 V DC supplies. The resonant frequency can be chosen high to reduce the parasitic effects in the circuit.

N95 material based ferrite core (PQ 50/50) is used to build the HF transformer. An auxiliary inductor is added with HF transformer leakage inductors to get the desired resonant inductor. With the proper design, the resulted magnetizing inductance is set to 5.61 mH. This high value of magnetizing inductance reduces the conduction loss of the transformer. HEXFET MOSFET IRFR 4620PbF and MOSFET IPP200N15N3G are adopted as the primary and secondary switches respectively.



**Figure 5.5: LLC resonant converter hardware**

Figure 5.6 and 5.7 show the experimental waveforms of the designed converter at full load of 1kW for 400V and 200V input respectively. The measured resonant currents in both cases are sinusoidal because of the converter operated with a frequency which is close to resonance frequency. The current waveforms show that the ZVS in both bridges are well achieved at the full load. The voltage and current stresses across the resonant tank components are higher at 200V than 400V operation.

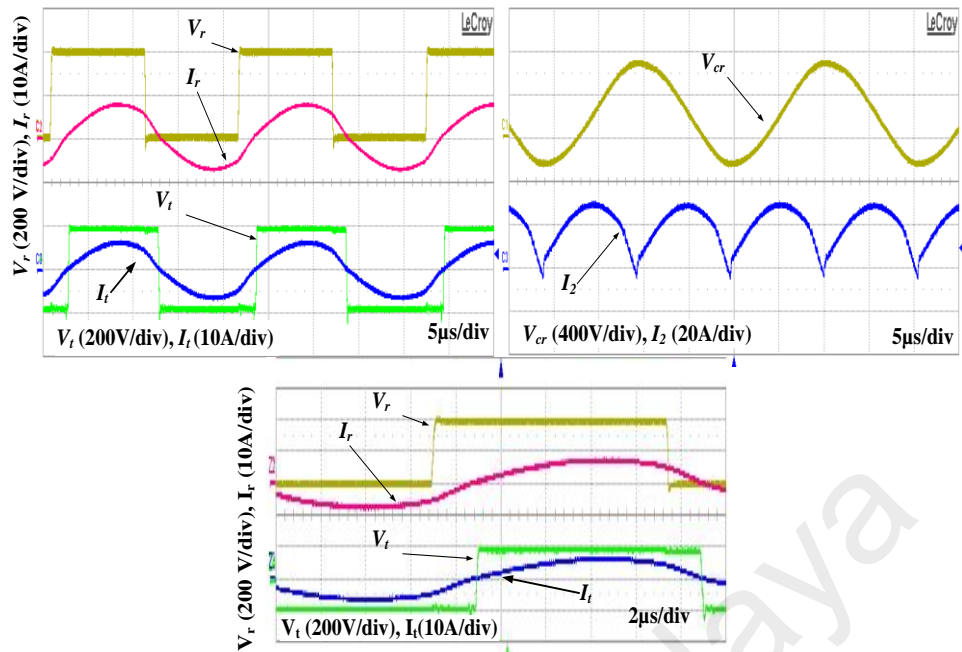


**Figure 5.6: Measured voltage and current waveforms under 400V input , 48V output and full load condition**

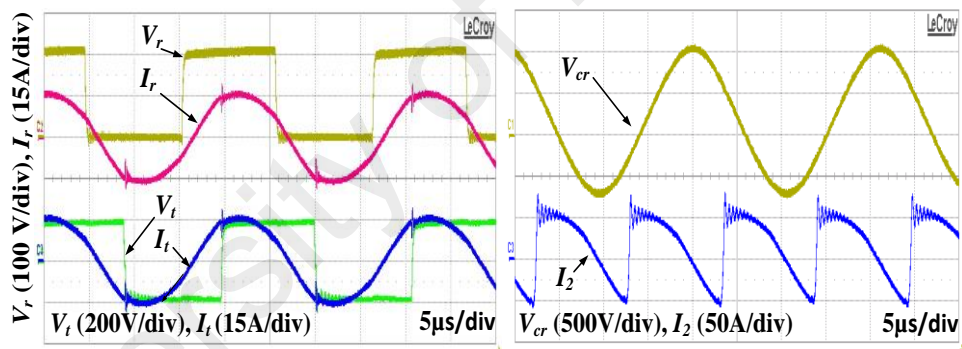


**Figure 5.7: Measured voltage and current waveforms under 200V input, 48V output and full load condition**

Figure 5.8 and 5.9 show the voltage and current waveforms of the proposed converter at the minimum load of 200W for 400V and 200V input respectively. It is seen that the resonance currents are little bit deviated from the sinusoidal shape because the converter is operated at a frequency which is far away from the resonant frequency. Like the full load operation, the component stresses become high at minimum input voltage operation. The current waveforms show that the ZVS of all switches is achieved at minimum load conditions.

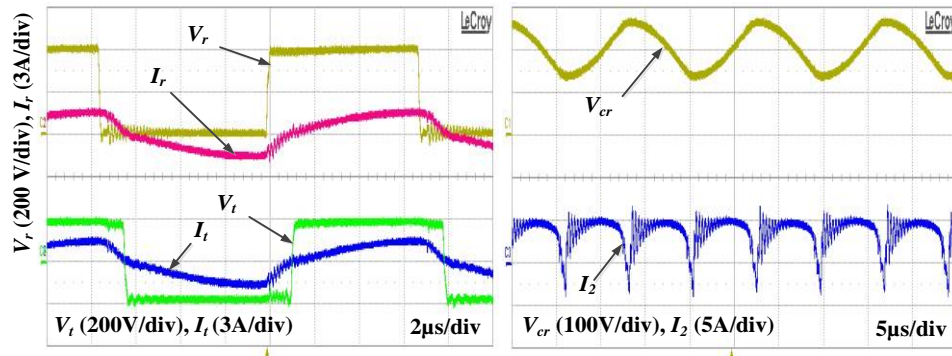


**Figure 5.8: Measured voltage and current waveforms under 400V input , 48V output and 20% load condition**

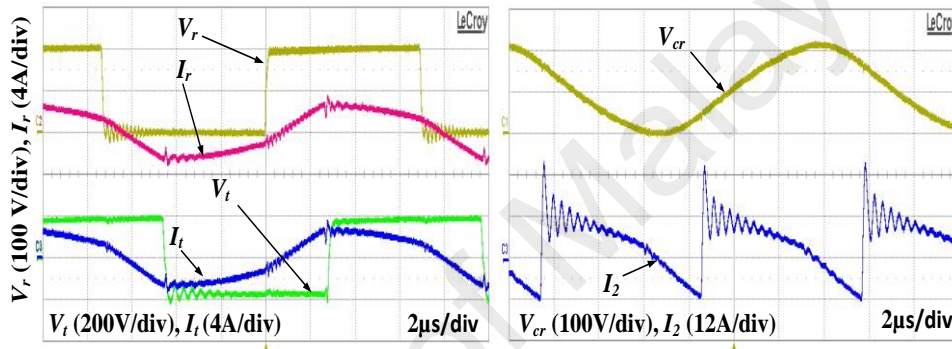


**Figure 5.9: Measured voltage and current waveforms under 200V input , 48V output and 20% load condition**

As shown in Figure 5.10, soft switching can be achieved in primary and secondary side switches. Since ZVZCS is observed on both sides during turn-on, thus the high-frequency turn-on switching losses become negligible. There are no considerable voltage spikes across the switch voltage ( $V_{ds}$ ) which signifies the small turn-off losses. The switch current commutates to the parallel capacitor instead of the switch itself and the MOSFET becomes switched off fully before the drain to source voltage rises significantly above zero. Thus, turn-off transition switching losses are reduced to the very small value. It is also seen that the voltage stress of the primary switches is about 200 V, which is half of the input voltage. As a result, the low voltage rated MOSFET with low  $R_{ds-on}$  is employed to reduce the conduction losses.

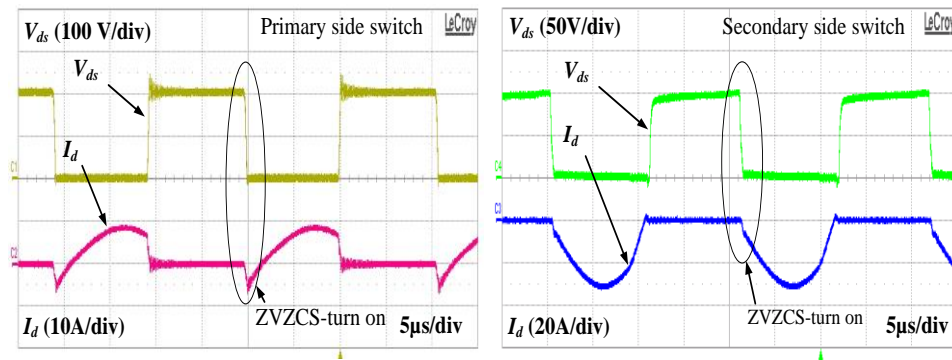


**Figure 5.10: Measured Switching waveforms of 400V and full load condition**

For the reverse power flow, the control variable  $\psi$  should be negative. Figure 5.11 shows the waveforms of  $V_r$ ,  $I_r^*$  ( $I_r = -I_r^*$ ),  $V_t$ ,  $I_t^*$  ( $I_t = -I_t^*$ ),  $V_{cr}$  and  $I_2^*$  ( $I_2 = -I_2^*$ ) for full power condition. All the voltages and currents have the similar values like full load forward power flow. ZVS operation can be confirmed by checking the phase angle of  $I_r^*$  and  $I_t^*$  with respect to  $V_r$  and  $V_t$ .

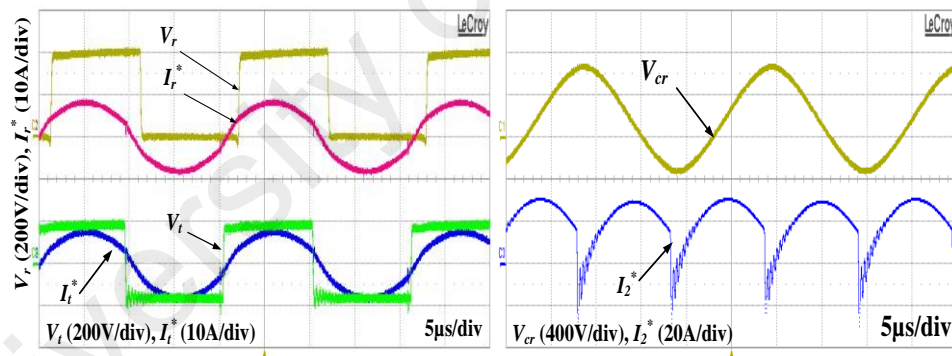
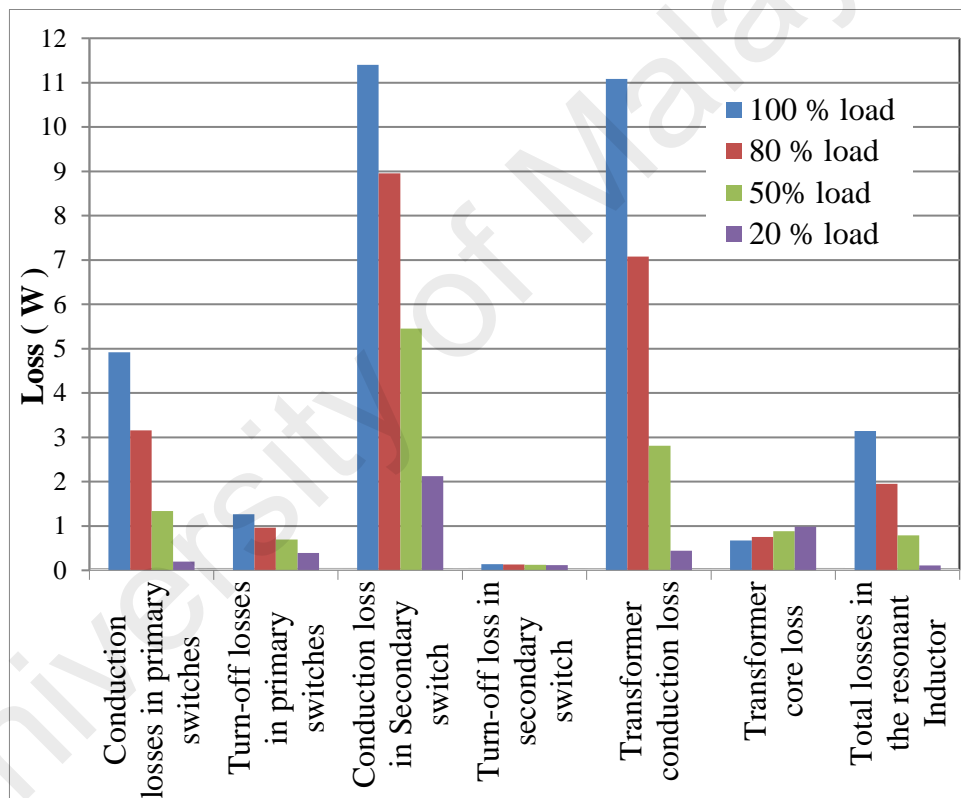


**Figure 5.11: Measured voltage and current waveforms of reverse power flow at 48 V input, 400 V output, full load condition**

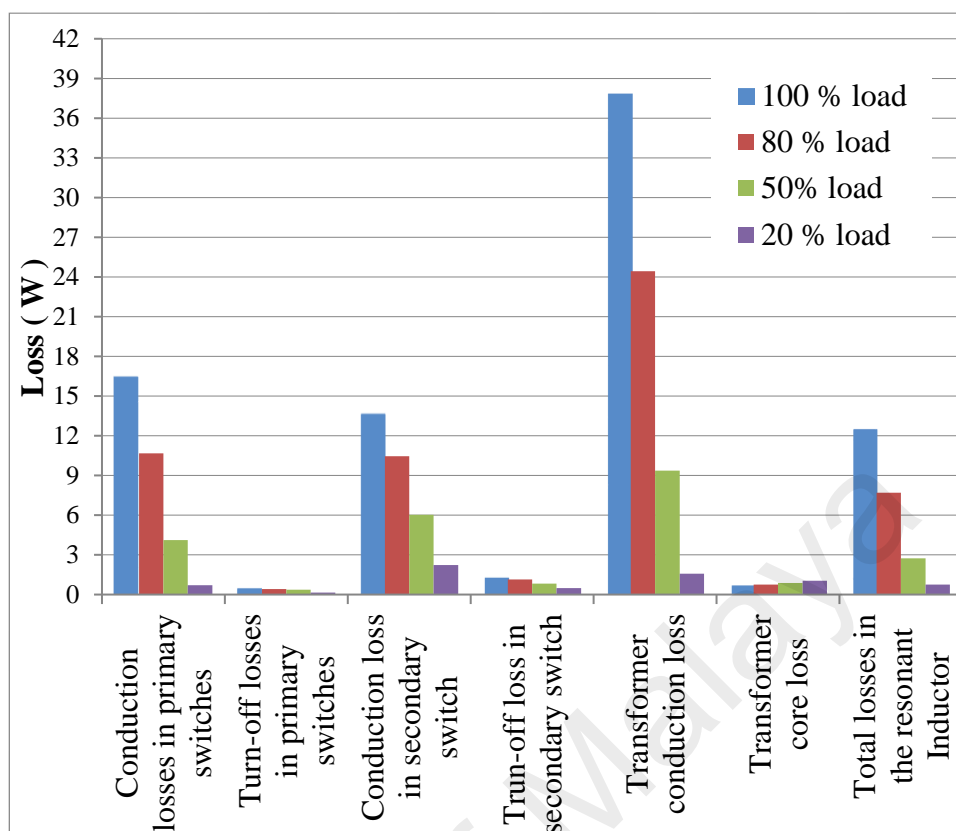
#### 5.4 Loss breakdown

According to the loss models in **chapter 4**, the calculated loss breakdown for maximum and minimum input voltages are drawn in Figure 5.12. There are a variety of losses which are ignored due to the smaller values with respect to the delivered power. These include control and gate driver circuitry losses and the ESR losses in capacitors. Figure 5.12 represents the estimated power loss breakdown for different inputs and load

conditions. Not surprisingly, conduction losses are the largest proportion of the total power losses. In Figure 5.12(b), the major power loss contributors are the conduction losses of the secondary switches and the transformer. The losses at 20% load are very small as compared to delivered power, thus the efficiency at this stage can be comparable with the state-of-the-art-work. Likewise, Figure 5.12(a) represents the losses for minimum input voltage condition. It is also seen that conduction losses are increased significantly at the low input voltage condition. In that case, the major power loss contributors are the conduction losses of primary side switches and transformer.



(a)



(b)

**Figure 5.12: Loss breakdown for (a) 400V input (b) 200V input**

### 5.5 Measured Efficiency

The efficiency of the converter under 400V and 200V on different load conditions is shown in Figure 5.13. The efficiency becomes higher all over the load range at 400V due to the minimization of reverse energy and turn-on losses in both bridges. In contrast, efficiency is degraded at 200V due to the high value of RMS resonance current and reverse energy. Thus the efficiency is decreasing gradually in boost operation with increasing conduction losses. Calculated efficiency is slightly more than the measured value due to the series resistance and other parasitic components of practical circuitry. FAPSM control scheme minimizes the RMS resonance current further with decreasing load which leads the higher efficiency at light load condition even higher than the full

load efficiency. Thus, the variation of efficiency from no load to full load for constant input voltage is narrow.

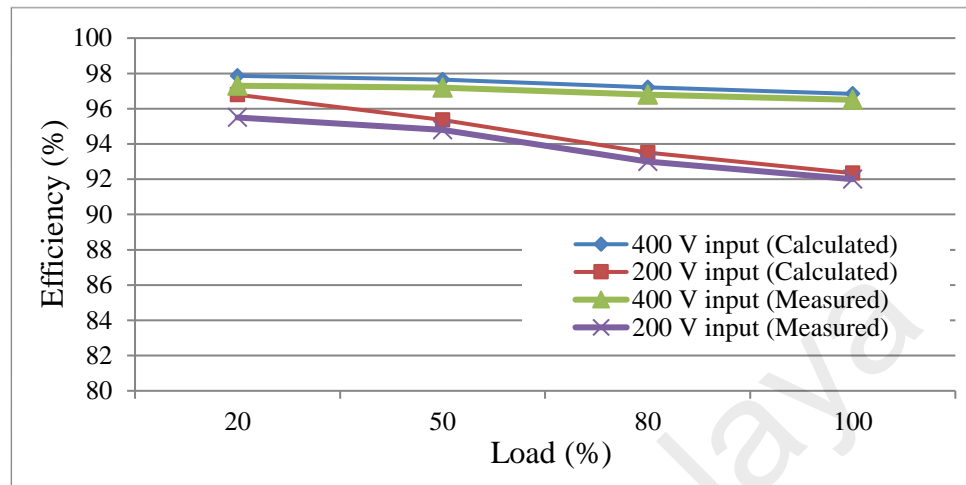


**Figure 5.13: Measured efficiency of the proposed LLC resonant converter**

## 5.6 Comparison Studies

To validate the steady-state analysis, a comparison of all important angles obtained from theoretical calculations, simulations, and experiments are given in Table 5.1. All the results are almost close to each other and also all angles follow the increasing and decreasing trend according to phase shift angle.

**Table 5.1: Comparison of Different Angles**

		$\psi^\circ$	$\Phi^\circ$	$\theta^\circ$
400V, full load condition	Theoretical	27.5	22.99	5.39
	Simulation	27.5	21.12	5.71
	Experimental	29.5	24.2	6.1
400V, 20% load condition	Theoretical	27.5	23.13	7.38
	Simulation	27.5	20.79	7.1
	Experimental	29.5	23.68	7.5
200V, full load condition	Theoretical	65	8.12	57.16
	Simulation	65	8.61	55.12
	Experimental	68	12.2	58.3
200V, 20% load condition	Theoretical	65	8.03	57.74
	Simulation	65	11.31	54.53
	Experimental	68	12.1	58.4

A comparison of five converter topologies is illustrated in Table 5.2. Unlike the other DC/DC converters, FAPSM control based LLC resonant converter increases the voltage gain range with ZVS to all switches under all operating voltage and power range. Turn-on energy losses are completely zero due to the ZVS in all semiconductor switches throughout the operating range. At 1kW output power, the measured efficiency of the proposed converter is 96.5% for maximum input voltage which is superior to other two topologies (with similar output power) reported in Table 5.2. Another promising advantage of FAPSM control is that it helps to maintain the light load efficiency high which is comparable to state-of-the-art work. In addition, the series combination of four switches is provided the opportunity of using low voltage switches which are essential to reduce the conduction losses due to having low on-state resistances. Thus, the efficiency of the proposed converter is higher than the other LLC resonant converters. On the other hand, DAB LC series resonant converter can be easily controlled by phase shift angle, but the low voltage gain range and severe circulating current at light load make it unsuitable for wide voltage and power range applications. Compare to the LC type DB LLC with SPM control scheme can maintain the ZVS in both bridges and has higher efficiency. But the voltage gain is limited to unity to maintain ZVS in both bridges and high reverse energy at light load degrades the efficiency which is still significant. Besides PFM control with LLC has wider voltage gain but slow bi-directional transitional speed. In contrast to SPM based LLC converter, three level LLC with PWAM has wide gain range, but the switches in the rectifier side lost ZVS operation. It is not also favorable in terms of the number of converter components, cost and operation complexity.

**Table 5.2: Comparison of LLC Resonant converter topologies**

Topologies	DAB LC series resonant converter (Li & Bhat, 2010)	DAB LLC converter resonant with new control Scheme (Tianyang et al., 2015)	Three level LLC resonant converter with PWAM control (Tianyang et al., 2016)	DB LLC resonant converter with phase shift Control (Xiaodong , 2014)	Proposed LLC resonant converter with FAPSM
Number of switches	8	8	12	4	6
Voltage stress across the switches is equal to half of the input voltage (for all load and voltage gain)	No (Equal to input voltage)	No (Equal to input voltage)	No (Depends on voltage gain )	No (Equal to input voltage)	Yes
Number of transformer's secondary windings	1	1	1	2	2
ZVS	Primary bridge: ZVS Secondary bridge: ZCS	Primary bridge: ZVS Secondary bridge: ZCS	Primary bridge: ZVS Secondary bridge: ZCS	Primary bridge: ZVS Secondary bridge: ZVS	Primary bridge: ZVS Secondary bridge: ZVS
Reactive power control	No	Yes	No	No	Yes
Flying capacitor	No	No	Yes	No	No
Modulation	SPM	PFM	PWAM	SPM	FAPSM
Gain range	Narrow	Narrow	Wide	Unity gain	Wide
Input /output	110-130V /75-100 V	400V/ 75-130 V	240-480 V /60 V	200 V /48V	200-400 V /48V
Full-load measured efficiency	95% At, 200W	96% At, 1 kW	96% At,1kW (480V-input)	94.5% At, 300 W	96.5% At,1kW (400V-Input)
Measured light load efficiency	77% At,10% Load(130 V-input)	92% At, 20% load	94.3% At, 20% load(480V-input)	84% At, 20% load	97.3% At, 20% load(400V-Input)
Output Power	100V/ 2 A	400V/2.5 A	60V/ 20 A	48V/6.25 A	48V/20.83 A

## 5.7 Summary

In this chapter, the validation of theoretical calculation through the simulation and experimental results has been presented. The designed resonant converter with FAPSM control scheme has provided the worthwhile improvement in the power efficiency as a result of switching and conduction losses. All the power losses are calculated and analyzed with different power and operating voltages, which help to indicate the lossiest part of the converter circuit. The measured efficiency of laboratory prototype has little differences with estimated efficiency; however, it can be possible to reach the estimated efficiency by compact design.

University of Malaya

## CHAPTER 6: CONCLUSION AND FUTURE WORK

### 6.1 Conclusion

In this study, a frequency adaptive phase shift modulation control for a dual bridge LLC resonant DC/DC converter is proposed. This control strategy makes the converter operating at a wide voltage gain range with ZVS over all load conditions. It overcomes the narrow voltage gain limitation of dual bridge LLC resonant converter. Due to the two independent control variables, the voltage gain becomes independent of  $Q$  and  $K$  values. Thus, the process of parameter design is simplified and resulting high value of magnetizing inductance is achieved which reduces the conduction losses as compared to another state-of-the-art-work. The proposed control also reduces the reverse energy at light load condition that improves the light load efficiency as well. The measured efficiency during maximum input voltage operation is about 97.86% even at 20% of full load condition.

The combination of four switches in series on the primary side of transformer reduces the voltage stress across each switch, which makes the converter capable of operating at high voltage applications. The voltage stress remains half of the input voltage over all load variations which provides the opportunity to employ low voltage (low  $R_{ds-on}$ ) rated power switches that actually improves the conduction losses. The performance of the proposed LLC resonant converter is experimentally verified with 200-400V input and 48V output converter prototype. Zero voltage switching is verified through experiment results for wide input and load range. All the switches maintain ZVS which reduces the switching losses and improves the efficiency of the converter. For the maximum and minimum input voltage condition, the measured efficiency is 96.5% and 92% respectively for the full load condition. Therefore, the designed converter becomes a good candidate for variable input and constant output voltage applications.

The overall conclusion which is drawn is that the designed LLC resonant converter presently has significant advantages for DC/DC conversion.

## 6.2 Future Work

Although the proposed DC/DC converter fulfills the research objectives, several issues require further investigation. Some suggestions for future work are summarized below:

- The proposed control scheme could be implemented for the high power converters like single-phase DAB and three phase DAB LLC resonant converter which appear to be more attractive and effective because of their low current stress in power semiconductor switches resulting low power losses. It could also be incorporated for multiport DB LLC bi-directional converters.
- Resonant DC/DC power converters with new material based ultra high frequency switching devices like GaN-HEMT and SiC could be effectively introduced to increase the power density and efficiency further.
- The voltage/current stresses on the converter components and their relationships with control variables and resonant tank parameters could be further explored. Thus the reverse energy and components stresses will be minimized at high gain mode to improve the efficiency.
- All the parasitic LC components of the converter circuit elements such as HF transformer could be modeled to mitigate the very high frequency ripple appeared in the resonance current especially under the light load condition. The modeled with all parasitic LC components could be used throughout the analysis to achieve smoother operations which will bring higher accuracy and better performance.

- The proposed control changes the resonant behavior of LLC resonant tank.  
So, the characteristics of other resonant tank networks should be investigated with the proposed control scheme.

University of Malaya

## REFERENCES

- Aggeler, D., Biela, J., Inoue, S., Akagi, H., & Kolar, J. W. (2-5 April 2007). *Bi-Directional Isolated DC-DC Converter for Next-Generation Power Distribution - Comparison of Converters using Si and SiC Devices*. Paper presented at the Power Conversion Conference - Nagoya.
- Aggeler, D., Biela, J., & Kolar, J. W. (24-28 Feb. 2008). *A compact, high voltage 25 kW, 50 kHz DC-DC converter based on SiC JFETs*. Paper presented at the Twenty-Third Annual IEEE Applied Power Electronics Conference and Exposition (APEC).
- Atalla, A., Agamy, M., Dame, M., Hao, L., Mandrisiak, G., Weeber, K., & Pan, Y. (18-22 Sept. 2016). *Advancements in high power high frequency transformer design for resonant converter circuits*. Paper presented at the IEEE Energy Conversion Congress and Exposition (ECCE).
- Bahmani, M. A., Thiringer, T., & Kharezy, M. (15-19 March 2015). *Design methodology and optimization of a medium frequency transformer for high power DC-DC applications*. Paper presented at the IEEE Applied Power Electronics Conference and Exposition (APEC).
- Barrios, E. L., Ursua, A., Marroyo, L., & Sanchis, P. (2015). Analytical Design Methodology for Litz-Wired High-Frequency Power Transformers. *IEEE Transactions on Industrial Electronics*, 62(4), 2103-2113.
- Barrios, E. L., Urtasun, A., Ursua, A., Marroyo, L., & Sanchis, P. (2015). High-Frequency Power Transformers With Foil Windings: Maximum Interleaving and Optimal Design. *IEEE Transactions on Power Electronics*, 30(10), 5712-5723.
- Beiranvand, R., Rashidian, B., Zolghadri, M. R., & Alavi, S. M. H. (2012). A Design Procedure for Optimizing the LLC Resonant Converter as a Wide Output Range Voltage Source. *IEEE Transactions on Power Electronics*, 27(8), 3749-3763.
- Bo, Y., Lee, F. C., Zhang, A. J., & Guisong, H. (10-14 March 2002). *LLC resonant converter for front end DC/DC conversion*. Paper presented at the Seventeenth Annual IEEE Applied Power Electronics Conference and Exposition (APEC).
- Bo, Y., Rengang, C., & Lee, F. C. (10-14 March 2002). *Integrated magnetic for LLC resonant converter*. Paper presented at the Seventeenth Annual IEEE Applied Power Electronics Conference and Exposition (APEC).
- Choi, H. (Feb. 25 -March 1 2007). *Analysis and Design of LLC Resonant Converter with Integrated Transformer*. Paper presented at the Twenty-Second Annual IEEE Applied Power Electronics Conference and Exposition (APEC).
- Chung, J. W., Ryu, K., Lu, B., & Palacios, T. (14-16 Sept. 2010). *GaN-on-Si technology, a new approach for advanced devices in energy and communications*. Paper presented at the Proceedings of the European Solid State Device Research Conference.

- Corradini, L., Seltzer, D., Bloomquist, D., Zane, R., Maksimovic, D., & Jacobson, B. (2012). Minimum Current Operation of Bidirectional Dual-Bridge Series Resonant DC/DC Converters. *IEEE Transactions on Power Electronics*, 27(7), 3266-3276.
- Costinett, D., Maksimovic, D., & Zane, R. (2013). Design and Control for High Efficiency in High Step-Down Dual Active Bridge Converters Operating at High Switching Frequency. *IEEE Transactions on Power Electronics*, 28(8), 3931-3940.
- Costinett, D., Nguyen, H., Zane, R., & Maksimovic, D. (6-11 March 2011). *GaN-FET based dual active bridge DC-DC converter*. Paper presented at the Twenty-Sixth Annual IEEE Applied Power Electronics Conference and Exposition (APEC).
- Das, P., Mousavi, S. A., & Moschopoulos, G. (2010). Analysis and Design of a Nonisolated Bidirectional ZVS-PWM DC/DC Converter With Coupled Inductors. *IEEE Transactions on Power Electronics*, 25(10), 2630-2641.
- Elasser, A., Kheraluwala, M. H., Ghezzi, M., Steigerwald, R. L., Evers, N. A., Kretchmer, J., & Chow, T. P. (2003). A comparative evaluation of new silicon carbide diodes and state-of-the-art silicon diodes for power electronic applications. *IEEE Transactions on Industry Applications*, 39(4), 915-921.
- Engel, S. P., Soltau, N., Stagge, H., & De Doncker, R. W. (2013). Dynamic and Balanced Control of Three-Phase High-Power Dual-Active Bridge DC/DC Converters in DC-Grid Applications. *IEEE Transactions on Power Electronics*, 28(4), 1880-1889.
- Fan, H., & Li, H. (2011). High-Frequency Transformer Isolated Bidirectional DC/DC Converter Modules With High Efficiency Over Wide Load Range for 20 kVA Solid-State Transformer. *IEEE Transactions on Power Electronics*, 26(12), 3599-3608.
- Fang, X., Hu, H. B., Shen, Z. J., & Batarseh, I. (2012). Operation Mode Analysis and Peak Gain Approximation of the LLC Resonant Converter. *IEEE Transactions on Power Electronics*, 27(4), 1985-1995.
- Hu, K. W., & Liaw, C. M. (2016). Incorporated Operation Control of DC Microgrid and Electric Vehicle. *IEEE Transactions on Industrial Electronics*, 63(1), 202-215.
- Hua, B., & Mi, C. (2008). Eliminate Reactive Power and Increase System Efficiency of Isolated Bidirectional Dual-Active-Bridge DC/DC Converters Using Novel Dual-Phase-Shift Control. *IEEE Transactions on Power Electronics*, 23(6), 2905-2914.
- Huang, A. Q., Crow, M. L., Heydt, G. T., Zheng, J. P., & Dale, S. J. (2011). The Future Renewable Electric Energy Delivery and Management (FREEDM) System: The Energy Internet. *Proceedings of the IEEE*, 99(1), 133-148.
- Il-Oun, L., & Gun-Woo, M. (2012). Analysis and Design of a Three-Level LLC Series Resonant Converter for High- and Wide-Input-Voltage Applications. *IEEE Transactions on Power Electronics*, 27(6), 2966-2979.

- Inoue, S., & Akagi, H. (2007). A Bidirectional DC/DC Converter for an Energy Storage System With Galvanic Isolation. *IEEE Transactions on Power Electronics*, 22(6), 2299-2306.
- Inoue, S., & Akagi, H. (2007). A Bidirectional Isolated DC/DC Converter as a Core Circuit of the Next-Generation Medium-Voltage Power Conversion System. *IEEE Transactions on Power Electronics*, 22(2), 535-542.
- Inoue, S., & Akagi, H. (2007). A Bidirectional Isolated DC/DC Converter as a Core Circuit of the Next-Generation Medium-Voltage Power Conversion System. *IEEE Transactions on Power Electronics*, 22(2), 535-542.
- Ivensky, G., Bronshtein, S., & Abramovitz, A. (2011). Approximate Analysis of Resonant LLC DC-DC Converter. *IEEE Transactions on Power Electronics*, 26(11), 3274-3284.
- Iyer, V. M., Prabhakaran, S., & Vijayan, P. (20-24 Sept. 2015). *High-frequency, high-current transformer designs for Silicon Carbide based LLC converters*. Paper presented at the IEEE Energy Conversion Congress and Exposition (ECCE).
- Jafari, M., Malekjamshidi, Z., Lei, G., Wang, T. S., Platt, G., & Zhu, J. G. (2017). Design and Implementation of an Amorphous High-Frequency Transformer Coupling Multiple Converters in a Smart Microgrid. *IEEE Transactions on Industrial Electronics*, 64(2), 1028-1037.
- Jain, A. K., & Ayyanar, R. (10-13 Nov. 2008). *PWM control of dual active bridge: comprehensive analysis and experimental verification*. Paper presented at the 34th Annual IEEE Industrial Electronics Conference (IECON).
- Jiang, T., Chen, X., Zhang, J., & Wang, Y. (17-21 March 2013). *Bidirectional LLC resonant converter for energy storage applications*. Paper presented at the Twenty-Eighth Annual IEEE Applied Power Electronics Conference and Exposition (APEC).
- Jieli, L., Abdallah, T., & Sullivan, C. R. (Sept. 30 -Oct. 4 2001). *Improved calculation of core loss with nonsinusoidal waveforms*. Paper presented at the 36th Annual IEEE Industry Applications Conference.
- Jung, J. H., Kim, H. S., Ryu, M. H., & Baek, J. W. (2013). Design Methodology of Bidirectional CLLC Resonant Converter for High-Frequency Isolation of DC Distribution Systems. *IEEE Transactions on Power Electronics*, 28(4), 1741-1755.
- Kadavelugu, A., Baek, S., Dutta, S., Bhattacharya, S., Das, M., Agarwal, A., & Scofield, J. (6-11 March 2011). *High-frequency design considerations of dual active bridge 1200 V SiC MOSFET DC-DC converter*. Paper presented at the Twenty-Sixth Annual IEEE Applied Power Electronics Conference and Exposition (APEC).
- Kakigano, H., Miura, Y., Ise, T., & Uchida, R. (2-5 April 2007). *DC Voltage Control of the DC Micro-grid for Super High Quality Distribution*. Paper presented at the Power Conversion Conference - Nagoya.

- Kaminski, N., & Hilt, O. (2014). SiC and GaN devices - wide bandgap is not all the same. *IET Circuits, Devices & Systems*, 8(3), 227-236.
- Khalil-Abaker, M., Shi, J., & Kalam, A. (25-28 Sept. 2016). *Design of a 100W bi-directional LCC series-parallel resonant DC-DC converter*. Paper presented at the Australasian Universities Power Engineering Conference (AUPEC).
- Krismer, F., Biela, J., & Kolar, J. W. (2-6 Oct. 2005). *A comparative evaluation of isolated bi-directional DC/DC converters with wide input and output voltage range*. Paper presented at the Fourtieth IAS Annual IEEE Industry Applications Conference.
- Krismer, F., & Kolar, J. W. (2012). Efficiency-Optimized High-Current Dual Active Bridge Converter for Automotive Applications. *IEEE Transactions on Industrial Electronics*, 59(7), 2745-2760.
- Li, X., & Bhat, A. K. S. (2010). Analysis and Design of High-Frequency Isolated Dual-Bridge Series Resonant DC/DC Converter. *IEEE Transactions on Power Electronics*, 25(4), 850-862.
- Lin, C. c., Yang, L. s., & Wu, G. W. (2013). Study of a non-isolated bidirectional DC-DC converter. *IET Power Electronics*, 6(1), 30-37.
- Lisserre, M., Sauter, T., & Hung, J. Y. (2010). Future Energy Systems: Integrating Renewable Energy Sources into the Smart Power Grid Through Industrial Electronics. *IEEE Industrial Electronics Magazine*, 4(1), 18-37.
- Liu, G., Li, D., Jang, Y., & Zhang, J. (20-24 March 2016). *Over 300kHz GaN device based resonant bidirectional DC/DC converter with integrated magnetics*. Paper presented at the IEEE Applied Power Electronics Conference and Exposition (APEC).
- Monteiro, V., Pinto, J. G., & Afonso, J. L. (2016). Operation Modes for the Electric Vehicle in Smart Grids and Smart Homes: Present and Proposed Modes. *IEEE Transactions on Vehicular Technology*, 65(3), 1007-1020.
- Mu, M., & Lee, F. C. (2016). Design and Optimization of a 380-12 V High-Frequency, High-Current LLC Converter With GaN Devices and Planar Matrix Transformers. *IEEE Journal of Emerging and Selected Topics in Power Electronics*, 4(3), 854-862.
- Oggier, G., Garc, G. O., & Oliva, A. R. (2011). Modulation strategy to operate the dual active bridge DC-DC converter under soft switching in the whole operating range. *IEEE Transactions on Power Electronics*, 26(4), 1228-1236.
- Peng, F. Z., Hui, L., Gui-Jia, S., & Lawler, J. S. (2004). A new ZVS bidirectional DC-DC converter for fuel cell and battery application. *IEEE Transactions on Power Electronics*, 19(1), 54-65.
- Qin, H., & Kimball, J. W. (2012). Generalized Average Modeling of Dual Active Bridge DC/DC Converter. *IEEE Transactions on Power Electronics*, 27(4), 2078-2084.

- Rani, B. I. (5-7 March 2015). *Design and control of isolated bi-directional DC-DC converter for photovoltaic applications*. Paper presented at the IEEE International Conference on Electrical, Computer and Communication Technologies (ICECCT).
- Rathore, A. K., Patil, D. R., & Srinivasan, D. (2016). Non-isolated Bidirectional Soft-Switching Current-Fed LCL Resonant DC/DC Converter to Interface Energy Storage in DC Microgrid. *IEEE Transactions on Industry Applications*, 52(2), 1711-1722.
- Renewables, Global status report, 2016, REN21 (Renewable energy policy network for the 21st century). from <http://www.ren21.net>
- Severns, R. (11-16 March 1990). *Topologies for three element resonant converters*. Paper presented at the Fifth Annual IEEE Applied Power Electronics Conference and Exposition (APEC).
- Severns, R. P. (1992). Topologies for three-element resonant converters. *IEEE Transactions on Power Electronics*, 7(1), 89-98.
- Sihun, Y., Shoyama, M., Zaitzu, T., Yamamoto, J., Abe, S., & Ninomiya, T. (11-14 Nov. 2012). *Detail operating characteristics of Bi-directional LLC resonant converter*. Paper presented at the International Conference on Renewable Energy Research and Applications (ICRERA).
- Steigerwald, R. L. (2-6 March 1987). *A comparison of half-bridge resonant converter topologies*. Paper presented at the 2<sup>nd</sup> Annual IEEE Applied Power Electronics Conference and Exposition (APEC).
- Sukesh, N., Pahlevaninezhad, M., & Jain, P. K. (2014). Analysis and Implementation of a Single-Stage Flyback PV Microinverter With Soft Switching. *IEEE Transactions on Industrial Electronics*, 61(4), 1819-1833.
- Tianyang, J., Junming, Z., Xinke, W., Kuang, S., & Yousheng, W. (2015). A Bidirectional LLC Resonant Converter With Automatic Forward and Backward Mode Transition. *IEEE Transactions on Power Electronics*, 30(2), 757-770.
- Tianyang, J., Junming, Z., Xinke, W., Kuang, S., & Yousheng, W. (2016). A Bidirectional Three-Level LLC Resonant Converter With PWAM Control. *IEEE Transactions on Power Electronics*, 31(3), 2213-2225.
- Twinaime, R. P., Thrimawithana, D. J., Madawala, U. K., & Baguley, C. A. (2014). A New Resonant Bidirectional DC/DC Converter Topology. *IEEE Transactions on Power Electronics*, 29(9), 4733-4740.
- Twinaime, R. P., Thrimawithana, D. J., Madawala, U. K., & Baguley, C. A. (2015). A Dual-Active Bridge Topology With a Tuned CLC Network. *IEEE Transactions on Power Electronics*, 30(12), 6543-6550.
- Venkatachalam, K., Sullivan, C. R., Abdallah, T., & Tacca, H. (3-4 June 2002). *Accurate prediction of ferrite core loss with nonsinusoidal waveforms using only*

- Steinmetz parameters*. Paper presented at the IEEE Workshop on Computers in Power Electronics, 2002.
- Wang, Y., Haan, S. W. H. d., & Ferreira, J. A. (8-10 Sept. 2009). *Potential of improving PWM converter power density with advanced components*. Paper presented at the 13th European Conference on Power Electronics and Applications.
- Weearsinghe, S., Thrimawithana, D. J., & Madawala, U. K. (2015). Modeling Bidirectional Contactless Grid Interfaces With a Soft DC-Link. *IEEE Transactions on Power Electronics*, 30(7), 3528-3541.
- Wei, C., Ping, R., & Zhengyu, L. (2010). Snubberless Bidirectional DC/DC Converter With New CLLC Resonant Tank Featuring Minimized Switching Loss. *IEEE Transactions on Industrial Electronics*, 57(9), 3075-3086.
- Wu, H., Mu, T., Gao, X., & Xing, Y. (2015). A Secondary-Side Phase-Shift-Controlled LLC Resonant Converter With Reduced Conduction Loss at Normal Operation for Hold-Up Time Compensation Application. *IEEE Transactions on Power Electronics*, 30(10), 5352-5357.
- Wu, T. S., Bellar, M. D., Tchamdjou, A., Mahdavi, J., & Ehsani, M. (6-10 Oct 1996). *A review of soft-switched DC-AC converters*. Paper presented at the Thirty-First Annual IEEE Industry Applications Conference (IAS).
- Wuhua, L., Qingjing, L., Ye, M., Sheng, Z., Xiangning, H., & Changliang, X. (2016). Flying-Capacitor-Based Hybrid LLC Converters With Input Voltage Autobalance Ability for High Voltage Applications. *IEEE Transactions on Power Electronics*, 31(3), 1908-1920.
- Wuhua, L., Sheng, Z., Fangrui, L., Huan, Y., Xiangning, H., & Bin, W. (2013). Secondary-Side Phase-Shift-Controlled ZVS DC/DC Converter With Wide Voltage Gain for High Input Voltage Applications. *IEEE Transactions on Power Electronics*, 28(11), 5128-5139.
- Xiaodong, L. (2014). A LLC-Type Dual-Bridge Resonant Converter: Analysis, Design, Simulation, and Experimental Results. *IEEE Transactions on Power Electronics*, 29(8), 4313-4321.
- Yan, L., Wenduo, L., Bing, L., & Wyk, J. D. v. (2-6 Oct. 2005). *Design of integrated passive component for a 1 MHz 1 kW half-bridge LLC resonant converter*. Paper presented at the Fourtieth Annual IEEE Industry Applications Conference (IAS).
- Yang, G., Dubus, P., & Sadarnac, D. (2015). Double-Phase High-Efficiency, Wide Load Range High- Voltage/Low-Voltage LLC DC/DC Converter for Electric/Hybrid Vehicles. *IEEE Transactions on Power Electronics*, 30(4), 1876-1886.
- Yang, R., Ding, H., Xu, Y., Yao, L., & Xiang, Y. (2014). An Analytical Steady-State Model of LCC type Series-Parallel Resonant Converter With Capacitive Output Filter. *IEEE Transactions on Power Electronics*, 29(1), 328-338.

- Yaqoob, M., Loo, K. H., & Lai, Y. M. (2017). Extension of Soft-Switching Region of Dual-Active-Bridge Converter by Tunable Resonant Tank. *IEEE Transactions on Power Electronics*, *PP(99)*, 1-1.
- Yilei, G., Zhengyu, L., Lijun, H., Zhaoming, Q., & Guisong, H. (2005). Three-level LLC series resonant DC/DC converter. *IEEE Transactions on Power Electronics*, *20(4)*, 781-789.
- Zahid, Z. U., Dalala, Z. M., Chen, R., Chen, B., & Lai, J. S. (2015). Design of Bidirectional DC/DC Resonant Converter for Vehicle-to-Grid (V2G) Applications. *IEEE Transactions on Transportation Electrification*, *1(3)*, 232-244.
- Zhao, B., Song, Q., & Liu, W. (2012). Power Characterization of Isolated Bidirectional Dual-Active-Bridge DC/DC Converter With Dual-Phase-Shift Control. *IEEE Transactions on Power Electronics*, *27(9)*, 4172-4176.
- Zhao, B., Song, Q., & Liu, W. (2013). Efficiency Characterization and Optimization of Isolated Bidirectional DC/DC Converter Based on Dual-Phase-Shift Control for DC Distribution Application. *IEEE Transactions on Power Electronics*, *28(4)*, 1711-1727.
- Zhao, B., Song, Q., & Liu, W. (2014). Experimental Comparison of Isolated Bidirectional DC/DC Converters Based on All-Si and All-SiC Power Devices for Next-Generation Power Conversion Application. *IEEE Transactions on Industrial Electronics*, *61(3)*, 1389-1393.
- Zhao, B., Song, Q., Liu, W., Liu, G., & Zhao, Y. (2015). Universal High-Frequency-Link Characterization and Practical Fundamental-Optimal Strategy for Dual-Active-Bridge DC-DC Converter Under PWM Plus Phase-Shift Control. *IEEE Transactions on Power Electronics*, *30(12)*, 6488-6494.
- Zhao, B., Song, Q., Liu, W., & Sun, Y. (25-28 Oct. 2012). *Characterization and application of next-generation SiC power devices for high-frequency isolated bidirectional DC-DC converter*. Paper presented at the 38th Annual IEEE Industrial Electronics Conference (IECON).
- Zhao, B., Song, Q., Liu, W., & Sun, Y. (2014). A Synthetic Discrete Design Methodology of High-Frequency Isolated Bidirectional DC/DC Converter for Grid-Connected Battery Energy Storage System Using Advanced Components. *IEEE Transactions on Industrial Electronics*, *61(10)*, 5402-5410.
- Zhao, F., Wang, C., Dong, R., & Yang, X. (5-8 Nov. 2014). *Performance analysis of half bridge three-level full bridge bi-directional DC-DC converters*. Paper presented at the International Power Electronics and Application Conference and Exposition (APEC).
- Zhou, H., & Khambadkone, A. M. (2009). Hybrid Modulation for Dual-Active-Bridge Bidirectional Converter With Extended Power Range for Ultracapacitor Application. *IEEE Transactions on Industry Applications*, *45(4)*, 1434-1442.

Zong, S., Luo, H., Li, W., Deng, Y., & He, X. (2016). Asymmetrical Duty Cycle-Controlled LLC Resonant Converter With Equivalent Switching Frequency Doubler. *IEEE Transactions on Power Electronics*, 31(7), 4963-4973.

Zong, S., Luo, Q., Li, C., Li, W., He, X., & Su, S. (16-20 March 2014). *Three-level frequency-doubling LLC resonant converter with high step-down ratio for high input voltage applications*. Paper presented at the Twenty-Ninth annual IEEE Applied Power Electronics Conference and Exposition (APEC).

University of Malaya

## LIST OF PUBLICATIONS AND PAPERS PRESENTED

### Journal Article

1. S M Showybul Islam Shakib; Saad Mekhilef, “A Frequency Adaptive Phase Shift Modulation Control Based LLC Series Resonant Converter for Wide Input Voltage Applications” *IEEE Transaction on Power Electronics* , Volume-32, Issue-11, 2017.

### Conference Proceeding

1. S M Showybul Islam Shakib; Saad Mekhilef, “*Dual Active Bridge (DAB) LLC Resonant Converter with Frequency Adaptive Phase Shift Modulation Control for Wide Gain Range*” IEEE ENERGY CONVERSION CONGRESS & EXPO, ECCE 2017, Cincinnati, OH, USA. (Status: Accepted)

University of Malaysia